S-N/99205--102

STOLLER-NAVARRO

Phase I Contaminant Transport Parameters for the Groundwater Flow and Contaminant Transport Model of Corrective Action Unit 99: Rainier Mesa/Shoshone Mountain, Nevada Test Site, Nye County, Nevada

Revision No.: 1

May 2008

Prepared for U.S. Department of Energy under Contract No. DE-AC52-03NA99205.

Available for public sale, in paper, from:

U.S. Department of Commerce
National Technical Information Service
5285 Port Royal Road
Springfield, VA 22161
Phone: 800.553.6847
Fax: 703.605.6900
Email: *orders@ntis.gov*
Online ordering: *http://www.ntis.gov/ordering.htm*

Available electronically at *http://www.osti.gov/bridge*

Available for a processing fee to U.S. Department of Energy and its contractors, in paper, from:

U.S. Department of Energy
Office of Scientific and Technical Information
P.O. Box 62
Oak Ridge, TN 37831-0062
Phone: 865.576.8401
Fax: 865.576.5728
Email: *reports@adonis.osti.gov*

S-N/99205--102

PHASE I CONTAMINANT TRANSPORT PARAMETERS FOR THE GROUNDWATER FLOW AND CONTAMINANT TRANSPORT MODEL OF CORRECTIVE ACTION UNIT 99: RAINIER MESA/SHOSHONE MOUNTAIN, NEVADA TEST SITE, NYE COUNTY, NEVADA

Contributors:

Stoller-Navarro Joint Venture
John S. Hand
Bill Fryer
Nathan Bryant
Jim Larentzos

National Securities Technologies, LLC
Lance Prothro
Sigmund L. Drellack

Lawrence Livermore National Laboratory
Qinhong Hu
Mavrik Zavarin

Comprehensive Volcanic Petrographics, LLC
Rick Warren

Revision No.: 1

May 2008

Stoller-Navarro Joint Venture
7710 W. Cheyenne, Building 3
Las Vegas, NV 89129

Prepared for U.S. Department of Energy under Contract No. DE-AC52-03NA99205.

PHASE I CONTAMINANT TRANSPORT PARAMETERS FOR THE GROUNDWATER FLOW AND CONTAMINANT TRANSPORT MODEL OF CORRECTIVE ACTION UNIT 99: RAINIER MESA/SHOSHONE MOUNTAIN, NEVADA TEST SITE, NYE COUNTY, NEVADA

Approved by: Sam Marutzky Date: 5/06/2008

Sam Marutzky, UGTA Project Manager
Stoller-Navarro Joint Venture

ACKNOWLEDGEMENT

We thank the many individuals who assisted in the creation of this report and especially appreciate the efforts of the document production staff for their support in preparing this document for publication. We also thank Greg Ruskauff for his contributions and thorough review.

TABLE OF CONTENTS

TABLE OF CONTENTS (CONTINUED)

TABLE OF CONTENTS (CONTINUED)

TABLE OF CONTENTS (CONTINUED)

TABLE OF CONTENTS (CONTINUED)

TABLE OF CONTENTS (CONTINUED)

LIST OF FIGURES

LIST OF FIGURES (CONTINUED)

LIST OF PLATES

NUMBER **TITLE**

LIST OF TABLES

LIST OF ACRONYMS AND ABBREVIATIONS

3-D	Three-dimensional
A-D	Anderson-Darling
bgs	Below ground surface
CADD	Corrective Action Decision Document
CAI	Corrective Action Investigation
CAIP	Corrective Action Investigation Plan
CAP	Corrective Action Plan
CAS	Corrective Action Site
CAU	Corrective Action Unit
CDF	Cumulative distribution function
CG	Characterization group
cm	Centimeter
CML	Carboxylate-modified latex
CR	Closure Report
CV	Coefficient of variation
DCE	Diffusion cell experiment
DDE_F	Data documentation evaluation flag
DEM	Digital elevation model
DFBA	Difluorobenzoic acid
DNA	Defense Nuclear Agency
DOE	U.S. Department of Energy
DQE_F	Data quality evaluation flag
DRI	Desert Research Institute
DTRA	Defense Threat Reduction Agency
DVD	Digital video disc
DWE	Diffusion water experiment
ECDF	Empirical cumulative distribution function
ERP	Environmental Restoration Project
FAI	Formation access interval
FF	Frenchman Flat
FFACO	*Federal Facility Agreement and Consent Order*
FGE	Forced-Gradient Experiment
ft	Foot

LIST OF ACRONYMS AND ABBREVIATIONS (CONTINUED)

FY	Fiscal year
g/cm^3	Grams per cubic centimeter
gpm	Gallons per minute
HFM	Hydrostratigraphic framework model
HGU	Hydrogeologic unit
hr	Hour
HST	Hydrologic source term
HSU	Hydrostratigraphic unit
ID	Identification
K-S	Kolmogorov-Smirnov
K	Hydraulic conductivity
K_d	Distribution coefficient
km	Kilometer
kt	Kiloton
Lpm	Liters per minute
LANL	Los Alamos National Laboratory
LLNL	Lawrence Livermore National Laboratory
m	Meter
m^2	Square meter
m^2/s	Square meters per second
meq/L	Milliequivalents per liter
mg/L	Milligrams per liter
mi	Mile
mL/g	Milliliters per gram
MWAT-TT	Multiple-well aquifer test-tracer test
N/A	Not applicable
NA	Not available
NAD	North American Datum
NC-EWDP	Nye County Early Warning Drilling Program
NDEP	Nevada Division of Environmental Protection
nm	Nanometer
NNSA/NSO	U.S. Department of Energy, National Nuclear Security Administration Nevada Site Office
NQA	Nuclear Quality Assurance

LIST OF ACRONYMS AND ABBREVIATIONS (CONTINUED)

NR	Not reported
NSTec	National Security Technologies, LLC
NTS	Nevada Test Site
pdf	Portable Document Format
PFBA	Pentafluorobenzoic acid
PGG	Petrographic, Geochemical, and Geophysical
PMOV	Pahute Mesa/Oasis Valley
QAPP	Quality Assurance Project Plan
RELAP	Reactive Transport LaPlace Inversion code
REV	Representative elementary volume
RMC	Reactive mineral category
RMSM	Rainier Mesa/Shoshone Mountain
RMU	Reactive mineral unit
RNM	Radionuclide Migration
RST	Radiologic source term
SD	Standard deviation
SNJV	Stoller-Navarro Joint Venture
SNL	Sandia National Laboratories
TDD	Transport data document
TFBA	Trifluorobenzoic acid
TNT	Trinitrotoluene
UGTA	Underground Test Area
USGS	U.S. Geological Survey
UTM	Universal Transverse Mercator
WIPP	Waste Isolation Pilot Plant
XRD	X-ray diffraction
YFCM	Yucca Flat/Climax Mine
YMP	Yucca Mountain Project
°C	Degrees Celsius
µm	Micrometer

LIST OF SYMBOLS FOR ELEMENTS AND COMPOUNDS

Am	Americium
Br^-	Bromide
C	Carbon
Ca	Calcium
Cl^-	Chloride
Cl	Chlorine
CO_2	Carbon dioxide
CO_3^{2-}	Carbonate
Cs	Cesium
Eu	Europium
F^-	Fluoride
HCO_3^-	Bicarbonate
I	Iodine
K	Potassium
Li	Lithium
Mg	Magnesium
Na	Sodium
Ni	Nickel
NO_3^-	Nitrate
Np	Neptunium
Pb	Lead
PO_4^{3-}	Phosphate
Pu	Plutonium
S	Sulfur
SiO_2	Silica
Sm	Samarium
Sn	Tin
SO_4^{2-}	Sulfate
Sr	Strontium
Th	Thorium
U	Uranium
Zr	Zirconium

LIST OF STRATIGRAPHIC UNIT ABBREVIATIONS AND SYMBOLS

AA	Alluvial aquifer
ARG	Argillic
ATICU	Ammonia Tanks intrusive confining unit
ATCU	Argillic tuff confining unit
BA	Benham aquifer
BFCU	Bullfrog confining unit
BRA	Belted Range aquifer
BRCU	Belted Range confining unit
CA	Carbonate aquifer
CC	Reactive mineral category for carbonate rocks
CCU	Clastic confining unit
CFCM	Crater Flat composite unit
CHCU	Calico Hills composite unit
CHICU	Calico Hills intrusive confining unit
CHVTA	Calico Hills vitric-tuff aquifer
CHZCM	Calico Hills zeolitized composite unit
DMP	Devitrified mafic-poor
DMR	Devitrified mafic-rich
FCCM	Fortymile Canyon composite unit
GCU	Granite confining unit
IICU	Intra-caldera intrusive confining unit
KA	Kearsarge aquifer
LCA	Lower carbonate aquifer
LCA3	Lower carbonate aquifer-thrust plate
LCCU	Lower clastic confining unit
LFA	Lava-flow aquifer
LPCU	Lower Paintbrush confining unit
LTCU	Lower tuff confining unit
LVTA	Lower vitric-tuff aquifer
MGCU	Mesozoic granite confining unit
ML	Mafic lava
OSBCU	Oak Spring Butte confining unit
PCM	Paintbrush composite unit
PLFA	Paintbrush lava-flow aquifer

LIST OF STRATIGRAPHIC UNIT ABBREVIATIONS AND SYMBOLS (CONTINUED)

PRETBG	Pre-Grouse Canyon Tuff lava-flow aquifer
PVTA	Paintbrush vitric-tuff aquifer
RMBCU	Rainier Mesa breccia confining unit
RMICU	Rainier Mesa intrusive confining unit
RVA	Redrock Valley aquifer
RVBCU	Redrock Valley breccia confining unit
RVICU	Redrock Valley intrusive confining unit
SC	Reactive mineral category for silicic rocks
SCICU	Silent Canyon intrusive confining unit
SCVCU	Subcaldera volcanic confining unit
SWA	Stockade Wash aquifer
SWNVF	Southwestern Nevada Volcanic Field
TCA	Tiva Canyon aquifer
TCU	Tuff confining unit
TCVA	Thirsty Canyon volcanic aquifer
TMA	Timber Mountain aquifer
TMCM	Timber Mountain composite unit
TM-LVTA	Timber Mountain lower vitric-tuff aquifer
TM-UVTA	Timber Mountain upper vitric-tuff aquifer
TM-WTA	Timber Mountain welded-tuff aquifer
TPA	Twin Peaks aquifer
TSA	Topopah Spring aquifer
TUBA	Tub Spring aquifer
UCA	Upper carbonate aquifer
UCCU	Upper clastic confining unit
UPCU	Upper Paintbrush confining unit
UTCU	Upper tuff confining unit
VA	Volcanic aquifer
VMP	Vitric mafic-poor
VMR	Vitric mafic-rich
VTA	Vitric-tuff aquifer
WTA	Welded-tuff aquifer
YMCHLFA	Yucca Mountain Calico Hills lava-flow aquifer
ZEOL	Zeolitic

1.0 INTRODUCTION

This document presents a summary and framework of available transport data and other information directly relevant to the development of the Rainier Mesa/Shoshone Mountain (RMSM) Corrective Action Unit (CAU) 99 groundwater transport model. Where appropriate, data and information documented elsewhere are briefly summarized with reference to the complete documentation.

1.1 Role of the Transport Data Document in the FFACO Process

The U.S. Department of Energy (DOE), National Nuclear Security Administration Nevada Site Office (NNSA/NSO) initiated the Underground Test Area (UGTA) Project to assess and evaluate the effects of the underground nuclear weapons tests on groundwater beneath the Nevada Test Site (NTS) and vicinity. The framework for this evaluation is provided in Appendix VI, Revision No. 2, of the *Federal Facility Agreement and Consent Order* (FFACO) [1]. Section 3.0 of Appendix VI "Corrective Action Strategy" of the FFACO describes the process that will be used to complete corrective actions specifically for the UGTA Project. The objective of the UGTA corrective action strategy is to define contaminant boundaries for each UGTA CAU where groundwater may have become contaminated from the underground nuclear weapons tests. The contaminant boundaries are determined based on modeling of groundwater flow and contaminant transport. Figure 1-1 outlines the FFACO process. This document fits within the "Develop CAU Flow and Transport Model" block of the diagram.

1.2 Role of the Transport Data Document in CAU-Scale Modeling

The RMSM Phase I transport parameters document is one of several documents produced as part of the modeling process. The transport parameters document identifies sources of data and analyses of data for use in transport modeling. The RMSM hydrologic data document is being produced concurrently with the RMSM contaminant transport parameters document. The hydrologic data document is similar to the contaminant transport parameters document, but contains data and analysis related directly to flow modeling and is applicable to transport modeling through the flow models. The RMSM modeling approach strategy document is also currently in development and will be released soon after this document. The modeling approach strategy document describes the modeling process that will be used for RMSM.

Modeling groundwater flow and transport in an area as complex as the RMSM CAU is a difficult process. In past UGTA CAUs, model sensitivity analysis has shown some parameters to be far more important than others, and the important parameters are not always consistent among models. An iterative approach to modeling works best, whereby datasets are refined to fill gaps and correct inconsistencies discovered during the modeling process. As such, the data and data characterizations used in this document are not final and are subject to revision during the modeling process. The

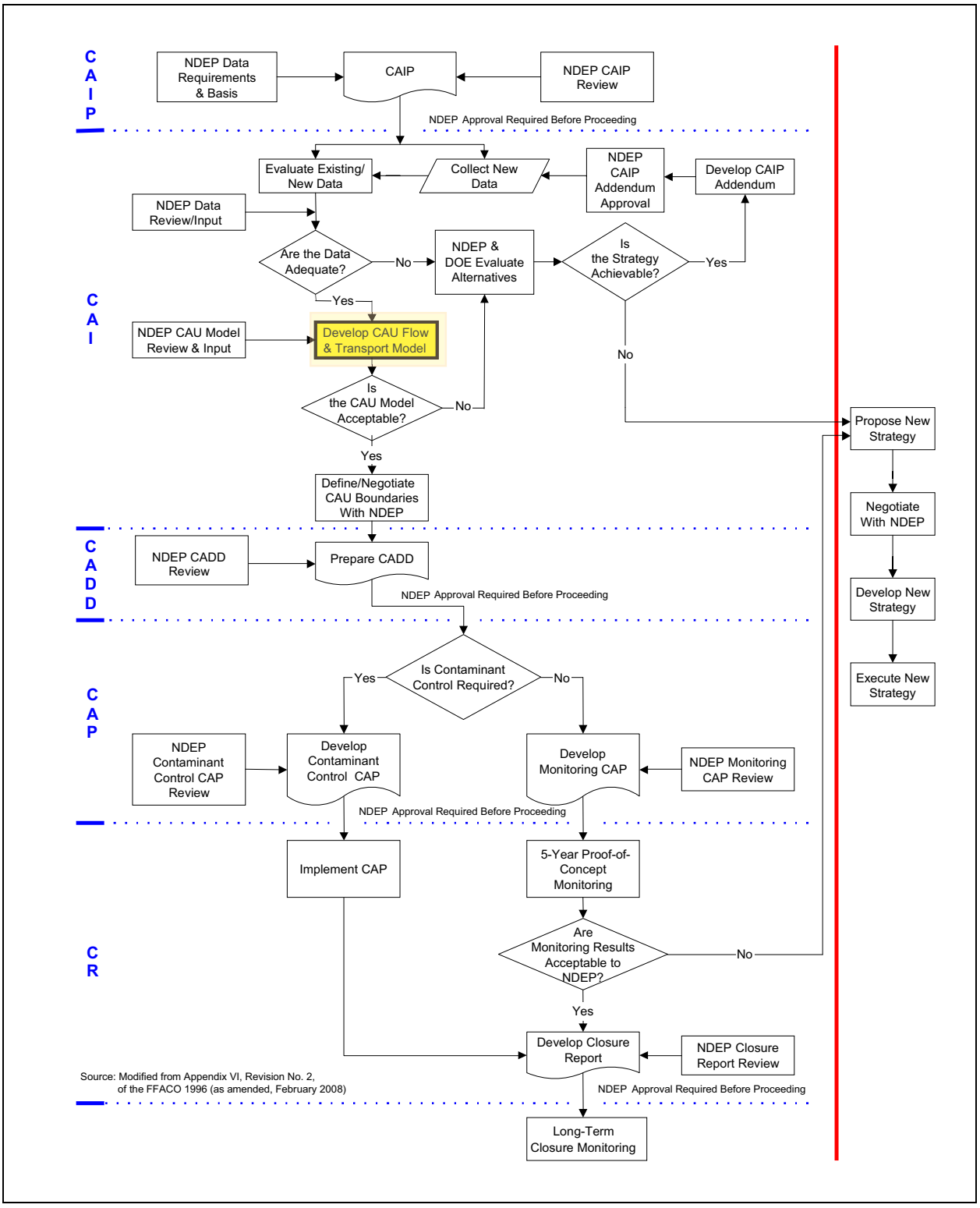

Figure 1-1
Underground Test Area Corrective Action Units Process Flow Diagram

emphasis for this document is to compile, describe, and evaluate basic datasets rather than to perform exhaustive analyses of all possible parameters, many of which will prove to be superfluous during modeling.

1.3 Underground Nuclear Testing in RMSM

Plate 1 is an overview of the RMSM model area with a digital elevation model (DEM) hillshade that shows physiography. Physiographic features are labeled in dark gray lettering. The RMSM CAU includes two distinct areas of nuclear testing, as outlined on Plate 1. The northern area in Area 12 where the majority of the RMSM tests are located includes all of Rainier Mesa and a small portion of Aqueduct Mesa to the northeast. The entire northern testing area is commonly referred to as Rainier Mesa, despite the inclusion of the portion of Aqueduct Mesa. The southern area in Area 16 is located beneath Tippipah Point, which is at the northeastern edge of the topographically high area generally referred to as Shoshone Mountain. Between 1957 and 1992, a total of 68 underground nuclear detonations were conducted in tunnels and shafts in this CAU. These tests included 62 detonations in the Rainier Mesa area and 6 detonations in Shoshone Mountain [2]. Cavities resulting from underground nuclear detonations are designated as corrective action sites (CASs) in the FFACO [1]. Multiple simultaneous detonations at one location are assigned to a single CAS. There are 60 CASs in Rainier Mesa and 6 in Shoshone Mountain for a total of 66 in the CAU. Section 5.0 contains a list of the underground nuclear tests and related test information. The location of the CASs, tunnel complexes, and UGTA wells in the RMSM CAU are shown in Plate 1.

Announced test yields for the RMSM CAU range from zero to 200 kilotons (kt), and the depths of burial range from 30 to 545 meters (m) below ground surface (bgs) [2]. Nuclear devices were emplaced in the Tertiary volcanics in Rainier Mesa and Shoshone Mountain. All detonations were conducted above the regional water table; however, some of the cavities have filled with perched groundwater in Rainier Mesa. Transport in the groundwater flow system is the primary avenue by which contaminants can move away from the test areas.

1.4 Supporting Documents

The NTS and surrounding areas have been the subject of intensive scientific study for more than half a century by a constellation of projects, programs, and organizations. A large body of literature and data supports a variety of activities at the NTS, much of which is useful to illuminate conditions and processes that affect radionuclide transport at the site. Table 1-1 lists documents that either provide a regional framework of the area around the NTS or document a variety of different types of information specific to the RMSM CAU. Each section of this report contains of references that are generally more specific to individual phenomena as well.

Table 1-1
Major Supporting Documents

Title	Description
Hydrogeologic and Hydrochemical Framework, South-Central Great Basin, Nevada-California, with Special Reference to the Nevada Test Site [3]	The first report published on the regional groundwater flow system in southern Nevada, specifically focused on the NTS area. It provides comprehensive background information describing data and information on the regional flow system as well as detailed information on the NTS.
Summary of Hydrogeologic Controls on Ground-Water Flow at the Nevada Test Site, Nye County, Nevada [4]	Summarizes what is known and inferred about groundwater flow throughout the UGTA region. Major controls on groundwater flow are identified, some uncertainties about groundwater flow are highlighted, and technical needs are prioritized and identified relative to the Environmental Restoration Project (ERP).
Corrective Action Investigation Plan for Corrective Action Unit 99: Rainier Mesa/Shoshone Mountain, Nevada Test Site, Nevada [5]	An FFACO [1] requirement that summarizes the historical data for the RMSM CAU. Describes the characterization activities that will be implemented to evaluate the extent of contamination in groundwater due to underground nuclear testing and support the development of groundwater flow and transport models to predict the contaminant boundary.
Value of Information Analysis for Corrective Action Unit 99: Rainier Mesa/Shoshone Mountain, Nevada Test Site, Nevada [6]	Describes the evaluation of the sufficiency of existing information to support the corrective action investigation (CAI) and identifies the major problems anticipated in developing the geologic, flow, and transport models. Potential data collection activities to improve characterization data are evaluated for potential benefit and prioritization.
Death Valley Regional Ground-Water Flow System, Nevada and California - Hydrogeologic Framework and Transient Ground-Water Flow Model [7]	Presents an updated regional flow model that was developed by the U.S. Geological Survey (USGS) in collaboration with the Yucca Mountain Project (YMP) and the UGTA Project.
A Hydrostratigraphic Model and Alternatives for the Groundwater Flow and Contaminant Transport Model of Corrective Action Unit 99: Rainier Mesa-Shoshone Mountain, Nye County, Nevada [8]	Presents the hydrostratigraphic framework model (HFM) for the RMSM CAU that will be used for Phase I groundwater flow and contaminant transport modeling.
Groundwater Flow Model Documentation Package (Phase I Data Analysis Documentation, Volume VI) [9]	Presents the original UGTA regional groundwater flow model.

1.5 References

FFACO, 1996; as amended, February 2008, see [1].

1. *Federal Facility Agreement and Consent Order.* 1996 (as amended). Agreed to by the State of Nevada; U.S. Department of Energy, Environmental Management; U.S. Department of Defense; and U.S. Department of Energy, Legacy Management.

2. U.S. Department of Energy, Nevada Operations Office. 2000. *United States Nuclear Tests, July 1945 through September 1992*, DOE/NV--209, Rev. 15. Las Vegas, NV.

3. Winograd, I.J., and W. Thordarson. 1975. *Hydrogeologic and Hydrochemical Framework, South-Central Great Basin, Nevada-California, with Special Reference to the Nevada Test Site,* Professional Paper 712-C. Washington, DC: U.S. Geological Survey.

4. Laczniak, R.L., J.C. Cole, D.A. Sawyer, and D.A. Trudeau. 1996. *Summary of Hydrogeologic Controls on Ground-Water Flow at the Nevada Test Site, Nye County, Nevada,* WRIR-96-4109. Carson City, NV: U.S. Geological Survey.

5. U.S. Department of Energy, National Nuclear Security Administration Nevada Site Office. 2004. *Corrective Action Investigation Plan for Corrective Action Unit 99: Rainier Mesa/Shoshone Mountain, Nevada Test Site*, DOE/NV--1001. Las Vegas, NV.

6. Stoller-Navarro Joint Venture. 2004. *Value of Information Analysis for Corrective Action Unit 99: Rainier Mesa/Shoshone Mountain, Nevada Test Site, Nevada.* Las Vegas, NV.

7. Belcher, W.R., J.B. Blainey, F.A. D'Agnese, C.C. Faunt, M.C. Hill, R.J. Laczniak, G.M. O'Brien, C.J. Potter, H.M. Putnam, C.A. San Juan, and D.S. Sweetkind. 2004. *Death Valley Regional Ground-Water Flow System, Nevada and California - Hydrogeologic Framework and Transient Ground-Water Flow Model,* Scientific Investigations Report 2004-5205. U.S. Geological Survey.

8. National Security Technologies, LLC. 2007. *A Hydrostratigraphic Model and Alternatives for the Groundwater Flow and Contaminant Transport Model of Corrective Action Unit 99: Rainier Mesa-Shoshone Mountain, Nye County, Nevada,* DOE/NV/29546--146. Las Vegas, NV.

9. IT Corporation. 1997. *Groundwater Flow Model Documentation Package (Phase I Data Analysis Documentation, Volume VI).* Prepared for the U.S. Department of Energy, Nevada Operations Office. Las Vegas, NV.

2.0 GEOLOGIC AND HYDROLOGIC SETTING

Geologic and hydrologic descriptions in this section are largely derived from discussions in Sections 1.4.3, 1.4.4, and 1.4.5 of the RMSM HFM report [1]. The report is distributed on the digital video disc (DVD) accompanying this document and should be consulted for more detail.

Rainier Mesa is a high volcanic plateau dissected by drainages. The mesa is preserved by the presence of a thick caprock of welded tuff, which overlies much less resistant bedded tuff layers. The top of the mesa is relatively flat, though incised in some areas by deep canyons. Ground-level elevations on Rainier Mesa are generally over 2,225 m (7,300 feet [ft]) above mean sea level, and average about 2,286 m (7,500 ft). The highest point on the NTS, 2,341 m (7,679 ft), is on Rainier Mesa. Aqueduct Mesa has slightly rougher and lower terrain, generally above 1,920 m (6,300 ft) in elevation. The edges of the mesas drop off abruptly on the west, south, and east sides.

Shoshone Mountain is a topographically high area located west of Yucca Flat, approximately 17 kilometers (km) (10.5 miles [mi]) due south of Rainier Mesa. Ground-level elevations at Shoshone Mountain range from 1,707 to 2,073 m (5,600 to 6,800 ft), but are generally above 1,830 m (6,000 ft). Tippipah Point, located at the northeast end of Shoshone Mountain and above the U16a Tunnel, has an elevation of 2,015 m (6,612 ft). The lowest region within the RMSM area is Mid Valley in the southeast portion of the model area at approximately 1,400 m (4,600 ft).

2.1 Geologic Overview of Rainier Mesa

Rainier Mesa consists of a layered volcanic rock sequence, with each layer exhibiting different physical and mechanical properties. The geology of the mesa can be briefly summarized as a thick sequence of relatively young Tertiary-age volcanic tuffs draped over an irregular substrate of much older Paleozoic sedimentary and Mesozoic intrusive rocks. The lower bedded tuffs have undergone significant *in situ* zeolitic alteration as a result of water percolating through them. In most places, the lower zeolitized section is overlain by a section of vitric bedded tuff, which lies just below the welded tuff caprock [2].

The geologic structure of the volcanic rocks of Rainier Mesa is well documented. Several high-angle normal faults have been mapped in the volcanic rocks; however, faults with greater than about 30 m (100 ft) of displacement are notably absent. The structure of the pre-Tertiary section is poorly known, though some geologists speculate that the trace of the Belted Range thrust fault is present in the pre-Tertiary rocks beneath Rainier Mesa. A broad synclinal feature mapped at the surface [3, 4] and in the tuffs of Rainier and Aqueduct Mesas may reflect a paleo-topographic low beneath the tuffs, but the exact character of this feature is unknown. It may be a “strike valley” related to the Belted Range thrust fault.

The structure of the pre-Tertiary rocks is complex and poorly known, but it is important because the pre-Tertiary section is very thick and extensive, and includes units that form regional aquifers. The main pre-Tertiary structures in the RMSM model area are related to the east-vergent Belted Range thrust fault, which placed Late Proterozoic to Cambrian-age rocks over rocks as young as Late Mississippian [5, 6]. In several places along the western margin of Yucca Flat, east-vergent structures related to the Belted Range thrust were deformed by younger west-vergent structural activity [6]. This west-vergent deformation is related to the CP thrust fault, which also placed older Paleozoic-age carbonate rocks over younger Paleozoic-age rocks (commonly the Eleana formation or Chainman shale) [7].

More recent large-scale extensional faulting in the NTS area is significant because the resulting faults have profoundly affected the hydrogeology of the Tertiary volcanic units by controlling to a large extent their alteration potential and final geometry. In addition, the faults themselves may facilitate flow of potentially contaminated groundwater from sources in the younger rocks into the underlying regional aquifers. The major Tertiary-age faults trend largely north-northeast consistent with the modern maximum compressive stress direction. Rainier Mesa is not as heavily faulted as central Pahute Mesa to the west.

2.2 Geologic Overview of Shoshone Mountain

The U16a Tunnel complex, the only tunnel complex at Shoshone Mountain used for nuclear testing, is located in zeolitized ash-fall and ash-flow tuffs [8], similar in age and physical properties to the rocks that are found at the southern end of Rainier Mesa (e.g., U12g and U12e Tunnels). A simplified description of the geologic section at U16a includes from the top of the mesa:

- A welded tuff “caprock” of Tiva Canyon tuff approximately 15 m (50 ft) thick; moderately to densely welded and related bedded tuff of the Topopah Spring tuff about 150 m (450 ft) thick;
- A sequence of bedded, vitric ash-fall tuffs related to the Calico Hills formation, approximately 38 m (125 ft) thick; and another 335-m (1,100-ft)-thick sequence of zeolitized ash-fall and interbedded welded ash-flow tuffs related to the Tunnel formation and older tuffs [10, 10].

The pre-Tertiary section in the vicinity of Shoshone Mountain consists of up to 300 m (1,000 ft) of Tippipah limestone overlying several hundred to perhaps 1,000 m of Eleana formation/Chainman shale. The Eleana formation/Chainman shale conformably overlies the thick section of Paleozoic carbonate rocks that form the lower carbonate aquifer (LCA).

The structural geology of the U16a area is quite complex, with many faults and fractures found throughout the tunnel system. Fault displacements range from a few centimeters to more than 30 m (100 ft). The strata strike generally north-south, and dip to the west. The dip of bedding measured along the tunnels ranges from about 8 to 18 degrees, with an average dip of approximately 15 degrees. This general attitude is mirrored in the gravity-postulated pre-Tertiary surface, which also dips gently toward the west.

Several faults have been mapped at Shoshone Mountain but, in general, the structure is less well known there than at Rainier Mesa. Shoshone Mountain is located at the northern limit of more extended terrain to the south and adjacent to the Mine Mountain basin. This area is more disrupted by basin-range faulting than the Rainier Mesa area, and there is evidence that Shoshone Mountain is more heavily faulted as well. The tunnel complex is cut by several faults with more than 30 m (100 ft) of displacement, and the strikes of the larger-displacement faults are more variable in orientation.

A conservative interpretation of the large-displacement faults found at tunnel level would indicate at least the potential for additional surface faulting, and a large displacement fault was logged near the 152 m (500 ft) depth in core from UE16a#1, which can be easily projected to the surface. Also, post-test surface mapping following the last underground test in the U16a Tunnel complex revealed a rather lengthy north-south striking fault with up to 1.0 m (3.3 ft) of displacement.

2.3 Hydrologic Setting

The hydrologic character of the NTS and vicinity reflects the arid climatic conditions and complex geology of the region [11]. The hydrology of the NTS has been extensively studied for more than 50 years [12], and numerous scientific reports and large databases are available. The following subsections present an overview of the hydrologic setting of the NTS and vicinity.

2.3.1 Surface Water

The NTS is located within the Great Basin, a closed hydrographic province that includes numerous closed hydrographic basins. In general, rivers and streams on the NTS are ephemeral and flow only in response to precipitation events or snowmelt. The runoff is conveyed through normally dry washes towards playa lakes in flats such as Yucca Flat and Frenchman Flat, where it evaporates. With the exception of a few infrequent, short-duration flash floods in Fortymile Canyon, Fortymile Wash, and Topopah Wash, long-distance surface water flow has not been observed on the NTS [13].

A few minor springs emanate from local perched groundwater systems in the foothills surrounding the Rainier and Aqueduct Mesa. Most water discharged from springs travels only a short distance from the source before evaporating or infiltrating into the ground.

2.3.2 Groundwater

The NTS is located within the Death Valley regional groundwater flow system, one of the major hydrologic subdivisions of the southern Great Basin [14, 15]. Groundwater in southern Nevada is conveyed within several flow-system sub-basins in the Death Valley regional flow system. A groundwater sub-basin is defined as the area that contributes water to a major surface discharge area [15]. Three principal groundwater sub-basins, named for their downgradient discharge areas, have been identified within the NTS region: the Ash Meadows, Oasis Valley, and Alkali Flat-Furnace Creek Ranch sub-basins [14]. Rainier Mesa lies along the boundary between the Ash Meadows and the Alkali Flat-Furnace Creek Ranch groundwater sub-basins. Shoshone Mountain is thought to lie

within the western portion of the Ash Meadows groundwater sub-basin [14]; however, it is close to the sub-basin boundary, which is somewhat uncertain.

The groundwater-bearing rocks at the NTS have been classified into several aquifers and confining units, of which the most extensive is the LCA, a thick sequence of Paleozoic carbonate rock. This unit extends throughout the subsurface of central and southeastern Nevada, and is considered to be a regional aquifer [15-17]. Various volcanic and alluvial aquifers are also locally important as water sources. Groundwater chemistry ranges from a sodium-potassium-bicarbonate type to a calcium-magnesium-carbonate type, depending on the mineralogical composition of the aquifer source [18].

The depth to groundwater in wells at the NTS varies from about 210 m (690 ft) below the land surface under the Frenchman Flat playa in the southeastern NTS, to more than 760 m (2,500 ft) below the land surface, beneath Shoshone Mountain at ER-16-1 [19]. Perched groundwater (isolated lenses of water lying above the regional groundwater level) occurs locally throughout the NTS, mainly within the volcanic rocks.

Recharge areas for the Death Valley groundwater system are the higher mountain ranges of central and southern Nevada, where there can be significant precipitation and snowmelt. Groundwater flow is generally from these upland areas to natural discharge areas in the south and southwest. Groundwater at the NTS is also derived from underflow from basins upgradient of the area [20]. The direction of groundwater flow may locally be influenced by structure, rock type, or other geologic conditions. Existing water-level data [21-23] and results of modeling groundwater flow [11, 17] indicate that the general groundwater flow direction within major water-bearing units beneath the NTS is to the south and southwest.

Most of the natural discharge from the Death Valley flow system is via transpiration by plants or evaporation from soil and playas in the Amargosa Desert and Death Valley rather than overland flow. Groundwater discharge at the NTS is minor, consisting of small springs that drain perched water lenses and artificial discharge at a limited number of water supply wells [16, 22].

2.4 References

1. National Security Technologies, LLC. 2007. *A Hydrostratigraphic Model and Alternatives for the Groundwater Flow and Contaminant Transport Model of Corrective Action Unit 99: Rainier Mesa-Shoshone Mountain, Nye County, Nevada*, DOE/NV/29546--146. Las Vegas, NV.

2. Sargent, K.A., and P.P. Orkild. 1973. "Geologic Map of the Wheelbarrow Peak-Rainier Mesa Area, Nye County, Nevada." U.S. Geological Survey Miscellaneous Geologic Investigations Map 1-754, scale 1:48,000. Washington, DC.

3. U.S. Department of Energy, National Nuclear Security Administration Nevada Site Office. 2006. *Completion Report for Well ER-12-3*, DOE/NV/11718--1182. Prepared by Bechtel Nevada, Las Vegas, NV.

4. U.S. Department of Energy, National Nuclear Security Administration Nevada Site Office. 2006. *Completion Report for Well ER-12-4*, DOE/NV--1128. Prepared by Bechtel Nevada, Las Vegas, NV.

5. Cole, J.C. 1997. *Major Structural Controls on the Distribution of Pre-Tertiary Rocks, Nevada Test Site Vicinity, Southern Nevada*. U.S. Geological Survey Open-File Report 97-533, scale 1:100,000, 19 pp. Denver, CO.

6. Cole, J.C., and P.H. Cashman. 1999. *Structural Relationships of Pre-Tertiary Rocks in the Nevada Test Site Region, Southern Nevada*. U.S. Geological Survey Professional Paper 1607.

7. Caskey, S.J., and R.A. Schweickert. 1992. "Mesozoic Deformation in the Nevada Test Site and Vicinity: Implications for the Structural Framework of the Cordilleran Fold and Thrust Belt and Tertiary Extension North of Las Vegas." In *Tectonics*, v. 11, No. 6, pp. 1314-1331.

8. Davis, R.E. 1962. *Preliminary Report on the Geology of the U16a Tunnel, Nevada Test Site. U.S. Geological Survey Technical Letter: Marshmallow-4.*

9. Orkild, P.P. 1963. *Geologic Map of the Tippipah Spring Quadrangle, Nye County, Nevada*. U.S. Geological Survey, Quadrangle Map GQ-213, scale 1:24,000. Washington, DC.

10. Slate, J.L., M.E. Berry, P.D. Rowley, C.J. Fridrich, K.S. Morgan, J.B. Workman, O D. Young, G.L. Dixon, V.S. Williams, E.H. McKee, D.A. Ponce, T.G. Hildenbrand, W.C. Swadley, S.C. Lundstrom, E.B. Ekren, R.G. Warren, J.C. Cole, R.J. Fleck, M.A. Lanphere, D.A. Sawyer, S.A. Minor, D.J. Grunwald, R.J. Laczniak, C.M. Menges, J.C. Yount, and A.S. Jayko. 1999. *Digital Geologic Map of the Map of the Nevada Test Site and Vicinity, Nye, Lincoln, and Clark Counties, Nevada and Inyo County, California*. U.S. Geological Survey Open-File Report 99B554BA, scale 1:120,000.

11. D'Agnese, F.A., C.C. Faunt, A.K. Turner, and M.C. Hill. 1997. *Hydrogeologic Evaluation and Numerical Simulations of the Death Valley Regional Groundwater Flow System, Nevada and California.* U.S. Geological Survey Water-Resources Investigations Report 96-4300, 133 pp. Denver CO: U.S. Geological Survey.

12. U.S. Department of Energy, Nevada Operations Office. 1996. *Final Environmental Impact Statement for the Nevada Test Site and Off-site Locations in the State of Nevada*, DOE/EIS-0243. Las Vegas, NV.

13. U.S. Geological Survey. 2001. *Flooding in the Amargosa River Drainage Basin, February 23–24, 1998, Southern Nevada and Eastern California, including the Nevada Test Site*. U.S. Geological Survey Fact Sheet 036–01. April. Las Vegas, NV.

14. Waddell, R.K., J.H. Robison, and R.K. Blankennagel. 1984. *Hydrology of Yucca Mountain and Vicinity, Nevada-California Investigative Results through Mid-1983*. U.S. Geological Survey Water-Resources Investigation Report 84-4267, 72 pp. Denver, CO.

15. Laczniak, R.J., J.C. Cole, D.A. Sawyer, and D.A. Trudeau. 1996. *Summary of Hydrogeologic Controls on the Ground-water Flow at the Nevada Test Site, Nye County, Nevada*. U.S. Geological Survey Water-Resources Investigation Report 96-4109. Carson City, NV.

16. Winograd, I.J., and W. Thordarson. 1975. *Hydrogeologic and Hydrochemical Framework, South-Central Great Basin, Nevada-California, with Special Reference to the Nevada Test Site.* U.S. Geological Survey Professional Paper 712-C, 126 pp. Washington, DC.

17. IT Corporation. 1996. *Regional Geologic Model Data Documentation Package (Phase I, Data Analysis Documentation, Volume I, Parts 1 and 2),* ITLV/10972--181. Las Vegas, NV.

18. Chapman, J.B. 1994. *Classification of Groundwater at the Nevada Test Site*. Desert Research Institute Report 45069, DOE/NV/10384-28.

19. U.S. Department of Energy, National Nuclear Security Administration Nevada Site Office. 2003. *Completion Report for Well ER-16-1 Corrective Action Unit 99: Rainier Mesa - Shoshone Mountain*. DOE/NV--1180. Las Vegas, NV.

20. Harrill, J.R., J.S. Gates, and J.M. Thomas. 1988. *Major Groundwater Flow Systems in the Great Basin Region of Nevada, Utah and Adjacent States*. Hydrological Investigation Atlas HA-694-C, scale 1:1,000,000. Denver CO: U.S. Geological Survey.

21. IT Corporation. 1996. *Potentiometric Data Task Documentation Package (Phase I, Data Analysis Documentation, Volume II),* ITLV/10972--181. Las Vegas, NV.

22. Reiner, S.R., G.L. Locke, and L.S. Robie. 1995. *Ground-Water Data for the Nevada Test Site and Selected Other Areas in South-Central Nevada 1992-1993.* U.S. Geological Survey Open-File Report 95-160.

23. U.S. Department of Energy, National Nuclear Security Administration Nevada Site Office. 2003. *Routine Radiological Environmental Monitoring Plan,* DOE/NV/11718--804. Prepared by Bechtel Nevada, Las Vegas, NV.

24. Hansen, D.J., P.D. Greger, C.A. Wills, and W.K. Ostler. 1997. *Nevada Test Site Wetlands Assessment*. Las Vegas, NV: Bechtel Nevada.

3.0 DATA CHARACTERIZATION OVERVIEW

This section presents an overview of the RMSM data compilation and characterization for the subject areas, and discussion of the variation in types of data evaluation and characterization presented in the subject chapters.

3.1 Characterization

Table 3-1 provides overview information about the data compilation, evaluation, and analysis for each of the transport parameters presented in this report. This information relates to requirements in the UGTA Quality Assurance Project Plan (QAPP) [1] and UGTA data transferability document [2] for data handling and analysis. The table provides a guide to the nature of the data for each parameter and categorizes the way in which data evaluation for each parameter was handled for characterization. Detailed information regarding the handling of various requirements is presented in the individual chapters in a variety of ways because the nature or situation for each parameter was sufficiently different to require substantially different approaches in presenting the material. This document builds upon the YFCM transport data document (TDD) [3] for background information, discussions of methodology, and supporting data where possible, and familiarizes the reader with YFCM TDD content as a guide in locating the particular information of interest. The RMSM-specific data and data analysis are presented where available data were sufficient to provide CAU-specific characterization. More general characterization for parameters, for which sufficient data are not available for CAU-specific characterization, are discussed regarding applicability to RMSM. Table 3-1 categorizes the various parameters regarding the QAPP and the data transferability evaluations, indicating where these evaluations were conducted, and identifies evaluations that were conducted for the RMSM effort. Table 3-1 also shows that much of this work has been completed previously and is not explicitly included in this document.

3.2 Parameterization

The subjects covered in this document were parameterized using a variety of methods, depending upon the nature of the available data for the topic. For some subjects, the data are measurements of physical quantities, and their variability may be easily quantified. The parameters for each subject are generally presented as the data for the topic are compiled (i.e., found in data sources) and reconciled as much as possible to be consistent in representativeness. In other cases, the data are interpreted or derived parameter values for processes that are functions of the theoretical framework used for interpretation. The parameterization (nature of the parameters) and interpretation assumptions may not be consistent for different sources or for the method in which the process will be modeled. With this type of parameter, the parameter values cannot be combined to characterize variability, or the evaluation of variability that includes qualifications related to the different interpretations, from which the parameter values were determined.

Table 3-1
Overview of Data Compilation, Evaluation, and Analysis
(Page 1 of 2)

Section	Parameter	Type	Data Availability	Text	Data Transfer Basis	Justification for Application to RMSM	Data Documentation Evaluation	Data Quality Evaluation	Data Weighting or Multiplier	Data Characterization	Scaling	Appendix	Sources
Hydrostratigraphic Framework and HSU Mineralogy (Section 4.0)	HFM Model	Measurement	CAU-specific data	RMSM-specific	No	N/A [a]	N/A [b]	N/A [c]	N/A [d]	Reference	N/A [d]	Data Tables, Block Diagrams, Cross Sections	UGTA HFM Model
	HSU Mineralogy (see Geochemistry)	Measurement	CAU-specific data	RMSM-specific	No	N/A [a]	N/A [c]	N/A [c]	No	Description	N/A [d]	(see Geochemistry) Data Tables, Statistics	SNJV Database
	Reactive Mineral Categorization	Interpreted	CAU-specific data	RMSM-specific	No	N/A [a]	N/A [c]	N/A [c]	No	Identification/ Description by HSU	N/A [d]	Data Tables	NSTec, unpublished
Contaminant Sources (Section 5.0)	Nuclear Test Information	Measurement	CAU-specific data	RMSM-specific	No	N/A [a]	N/A [b]	N/A [d]	N/A [d]	Data Tables	N/A [d]	None	NNSA/NNSO supplemented by SNJV
	Radionuclide Inventory	Interpreted/ Computed	CAU-specific data	RMSM-specific	No	N/A [a]	N/A [b]	N/A [d]	N/A [d]	Data Tables	N/A [d]	None	Published, unpublished
	Tunnel Information	Measurement	CAU-specific data	RMSM-specific	No	N/A [a]	N/A [b]	N/A [d]	N/A [d]	Data Tables	N/A [d]	None	Published, unpublished
Matrix Porosity (Section 6.0)	Matrix Porosity	Measurement	CAU-specific data	RMSM-specific	No	N/A [a]	N/A [c]	N/A [c]	No	CDF, Statistics by HGU/HSU	Discussion	Data Tables, Statistics, Characterization Plots	USGS, SNJV
Effective Porosity (Section 7.0)	Effective Porosity	Interpreted	NTS Area data and General data (depending upon CG)	Summary of YFCM TDD	Yes	Yes [e]	Yes [e]	Yes [e]	Yes	Distribution	No	Data Tables	UGTA reports, published literature
Dispersivity (Section 8.0)	Horizontal Dispersivity vs. Scale Relationship	Interpreted	NTS Area and General data	RMSM-specific	Yes	Yes [e]	Yes [e]	Yes [e]	No	Relationship with Scale, not CG-specific	Relationship with Scale, not CG-specific	Data Tables	UGTA reports, published literature
	Transverse Dispersivity vs. Scale Evaluation	Interpreted	General data	RMSM-specific	Yes	Yes [e]	Yes [e]	Yes [e]	No	Graph of Data	Discussion	Data Tables	UGTA reports, published literature
Matrix Diffusion (Section 9.0)	Tortuosity vs. Matrix Porosity Relationship	Interpreted	NTS Area and General data	Summary of YFCM TDD	Yes	Yes [e]	N/A [b]	Yes [e]	Yes	Graph, Relationship	Discussion	Data Tables	UGTA reports, published literature
	Tortuosity	Computed	CAU-specific data	RMSM-specific	No	N/A [f]	N/A [f]	N/A [f]	No	Statistics Graph, Table	Discussion	None	UGTA reports, published literature

Table 3-1
Overview of Data Compilation, Evaluation, and Analysis
(Page 2 of 2)

Section	Parameter	Type	Data Availability	Text	Data Transfer Basis	Justification for Application to RMSM	Data Documentation Evaluation	Data Quality Evaluation	Data Weighting or Multiplier	Data Characterization	Scaling	Appendix	Sources
Matrix Sorption Parameters (Section 10.0)	Mechanistic Model	Interpreted	CAU-specific, NTS Area, and General data	Summary of YFCM TDD	Yes	Yes [e]	N/A [b]	Yes [e]	No	Reference	N/A [d]	None	UGTA reports, published literature
	K_d -specific for individual radionuclides	Computed	CAU-specific data	RMSM-specific	No	N/A [f]	N/A [c]	Yes [e]	No	Graph of Statistics	Discussion	Data Tables	UGTA reports, published literature
Fracture Sorption (Section 11.0)	Mechanistic Model	Interpreted	NTS Area data	Summary of YFCM TDD	Yes	Yes [e]	N/A [b]	Yes [e]	No	Literature References	No	None	UGTA reports, published literature
	Retardation Factor	Computed	NTS Area data	RMSM-specific	Yes	Yes [e]	N/A [c]	Yes [e]	No	Data Tables	No	None	UGTA reports, published literature
Geochemistry (Section 12.0)	Water Chemistry	Measurement	CAU-specific data	RMSM-specific	No	N/A [a]	N/A [c]	N/A [c]	No	Description, Piper Diagrams	No	Data Tables, Statistics, Characterization Plots	SNJV Database
	Mineralogy	Measurement	CAU-specific data	RMSM-specific	No	N/A [a]	N/A [c]	N/A [c]	No	See Hydrostratigraphic Model, HSU Mineralogy	N/A [d]	Data Tables, Statistics, Characterization Plots	SNJV Database
Colloid-Facilitated Transport (Section 13.0)	Colloid Concentration, Size	Measurement	CAU-specific, NTS Area data	Summary of YFCM TDD	Yes	Yes [e]	N/A [c]	N/A [c]	No	Statistics, Distributions (by CG)	No	Data Tables	SNJV Database
	Transport Parameters	Interpreted	CAU-specific, NTS, and General data	Summary of YFCM TDD	Yes	Yes [e]	No	Yes [e]	No	Distribution (by CG)	No	Data Tables	UGTA, YMP literature
	Radionuclide K_d on colloids	Measurement	CAU-specific, NTS Area data	Summary of YFCM TDD	Yes	Yes [e]	N/A [b]	N/A [c]	No	Tables, Ranges (by CG)	No	Data Tables	UGTA, YMP literature

[a] Not applicable because no data transferred.
[b] Not applicable; source is published and data accepted as high quality.
[c] Not applicable; done for source material, source database.
[d] Not applicable to nature of data.
[e] General due to lack of CAU-specific data.
[f] Not applicable; computation is with CAU-specific data.

For all of these subjects, the use of these data for modeling will have to be considered within the model framework and representation of the parameters and processes for representativeness of properties and parameters. This document is a compilation, evaluation, and characterization of the data as they are available from sources, but does not characterize the data directly in the application framework for the transport model. This will require reconciliation during the modeling process. Consequently, the data characterization in this document does not provide or determine property or parameter values that specifically determine the property or parameter values for modeling.

3.3 References

1. U.S. Department of Energy, National Nuclear Security Administration, Nevada Site Office. 2003. *Underground Test Area Quality Assurance Project Plan, Nevada Test Site, Nevada,* DOE/NV--341-REV. 4. Las Vegas, NV.

2. Stoller-Navarro Joint Venture. 2004. *Transferability of Data Related to the Underground Test Area Project, Nevada Test Site, Nye County, Nevada*, Rev. 0, S-N/99205--020. Las Vegas, NV.

3. National Security Technologies, LLC. 2007. *A Hydrostratigraphic Model and Alternatives for the Groundwater Flow and Contaminant Transport Model of Corrective Action Unit 99: Rainier Mesa-Shoshone Mountain, Nye County, Nevada*, DOE/NV/29546--146. Las Vegas, NV.

4.0 RMSM HYDROSTRATIGRAPHIC FRAMEWORK AND HSU MINERALOGY

A three-dimensional (3-D) HFM and alternatives for the RMSM CAU were constructed in 2007 and are documented in the report *A Hydrostratigraphic Model and Alternatives for the Groundwater Flow and Contaminant Transport Model of Corrective Action Unit 99: Rainier Mesa-Shoshone Mountain, Nye County, Nevada* [1]. Overviews of the mineralogy of associated hydrostratigraphic units (HSUs) are provided in this section as background for the analyses presented in the later sections of this report. Detailed information about the HFM can be found in the original report.

4.1 RMSM HFM

The HFM provides the 3-D framework for flow and transport models. The base RMSM HFM incorporates numerous structural elements, including volcanic calderas, thrust faults, and 56 basin-and-range normal faults. The foundation of the HFM is the hydrostratigraphic system. The RMSM hydrostratigraphic classification system was developed through the rigorous evaluation and analysis of stratigraphic, lithologic, and alteration data from surface exposures and drill holes in and around the RMSM model area. The RMSM hydrostratigraphic system includes 44 HSUs that form individual 3-D volumes in the model.

The RMSM HFM consists of five models: a base HFM and four alternative HFMs. These alternative models are generally alternative structural interpretations of the geology and can contain HSUs not present in the base model.

4.1.1 Hydrogeologic and Hydrostratigraphic Units of the RMSM HFM

The RMSM HFM is based on a classification scheme that divides the rocks that make up the area two different ways: hydrogeologic units (HGUs) and HSUs. Descriptions of the HGUs and HSUs in the RMSM HFM are in Tables 4-3 and 4-4 of the HFM report [1] and in the RMSM_HFM.xls workbook in the Appendix\A folder on the accompanying DVD.

Hydrogeologic units are descriptive categories that indicate how water will flow through the rock and are based on hydrologic and lithologic properties of the rocks such as degree of consolidation, degree of fracturing, and secondary mineral alteration. Before the creation of the model, similar intervals of rock in boreholes in the model area are assigned HGUs based on properties determined from lithology logs and other borehole data. Because HGUs are descriptive, multiple non-continuous intervals in a single borehole are often assigned the same HGU.

The rocks of the RMSM model area are classified as one of the following nine HGUs: alluvial aquifer (AA), welded-tuff aquifer (WTA), vitric-tuff aquifer (VTA), lava-flow aquifer (LFA), tuff

confining unit (TCU), intra-caldera intrusive confining unit (IICU), granitic confining unit (GCU), clastic confining unit (CCU), and carbonate aquifer (CA).

Rocks of similar character are grouped into HSUs by HGU and stratigraphic position to facilitate mapping and 3-D model construction. For the RMSM model, most HSUs consist of a single HGU (e.g., the Timber Mountain lower vitric-tuff aquifer [TM-LVTA] essentially is 100% VTA). There are eight exceptions that may consist of several HGUs but are defined so a single general type of HGU dominates (e.g., mostly WTA). These exceptions are the Fortymile Canyon composite unit (FCCM), Timber Mountain upper vitric-tuff aquifer (TM-UVTA), Timber Mountain welded-tuff aquifer (TM-WTA), Timber Mountain composite unit (TMCM), Rainier Mesa breccia confining unit (RMBCU), Redrock Valley breccia confining unit (RVBCU), Stockade Wash aquifer (SWA), and Topopah Spring aquifer (TSA).

4.2 Reactive Mineral Characterization of Volcanic and Sedimentary Rocks

Most of the volcanic rocks in the RMSM model area are pyroclastic rocks composed of ash-flow tuffs and ash-fall deposits of rhyolitic composition. These silica-rich rocks can be composed of more than 80% glass when originally deposited (the remainder is a mixture of original phenocrysts and lithic fragments). Reactive minerals such as zeolite, clay, carbonate, mica, and hematite are rare in these vitric rocks. However, post-depositional processes such as welding, devitrification, zeolitization, and argillization can significantly alter the mineralogy of volcanic rocks. Volcanic units in the Southwestern Nevada Volcanic Field (SWNVF) show fairly consistent mineralogy that tends to vary only as a function of style and intensity of alteration [2].

Devitrification typically occurs in the inner portions of welded ash-flow tuffs and lavas shortly after deposition during cooling. Through devitrification, the original glass is converted to micro-crystalline quartz and feldspar, which is resistant to other post-depositional processes such as zeolitization and argillization. Devitrified welded ash-flow tuffs form important aquifers at the NTS (e.g., the TM-WTA).

Volcanic rocks that remain vitric after emplacement – such as nonwelded ash-flow tuffs, ash-fall deposits, and the outer portions of lavas – are susceptible to the diagenetic alteration processes of zeolitization and argillization. Zeolitization is the conversion of volcanic glass to the zeolite minerals and is common in tuffs on the NTS. Clinoptilolite is the most common zeolite on the NTS, but other zeolite minerals such as mordenite and analcime form at deeper depths. Because of the high percentage of glass in the original rocks, zeolitized volcanic rocks are composed predominantly of zeolite. Other reactive minerals such as carbonate, mica, and hematite are typically rare in zeolitic rocks. Clay, predominantly in the form of smectite, is usually a minor constituent. Large portions of the volcanic section in the RMSM model area are pervasively zeolitic and form important confining units (e.g., the lower tuff confining unit [LTCU]).

Unaltered volcanic rocks are also susceptible to argillization. In this post-depositional process, the original glass is converted to clay minerals such as smectite and lesser kaolinite. In portions of the RMSM model area, the basal portion of the volcanic section is commonly pervasively argillic and

forms a confining unit that directly overlies the regional carbonate aquifer (i.e., the argillic tuff confining unit [ATCU]).

Sedimentary rocks in the RMSM HFM include unconsolidated alluvium and much older carbonate and siliciclastic rocks. The mineralogy of alluvium can be quite diverse, reflecting the mineralogy of the constituent clasts. Carbonate rocks consist mineralogically of limestone and dolomite. Siliciclastic rocks include quartzite, sandstone, and siltstone that typically consist predominately of quartz grains. Siliciclastic rocks also include shale and argillite that predominately consist of clay minerals.

Relating the reactive minerals to geologic processes relevant to the rocks at the NTS yields several reactive mineral categories (RMCs), as shown in Table 4-1. The RMCs for NTS volcanic rocks are vitric mafic-poor (VMP), vitric mafic-rich (VMR), devitrified mafic-poor (DMP), devitrified mafic-rich (DMR), mafic lava (ML), zeolitic (ZEOL), and argillic (ARG). The RMCs for Paleozoic sedimentary rocks are calcic (CC) for the carbonate rocks, and silicic (SC) or ARG for the siliciclastic rocks. In general, the WTA-dominated HSUs relate to the DMR or DMP RMCs; the VTA-dominated HSUs relate to the VMR or VMP RMCs; and the TCU-dominated HSUs relate either to the ZEOL RMC or, in the case of the ATCU HSU, the ARG RMC. Granite belongs to the DMR RMC. The CA-dominated HSUs relate to the CC, and the siliciclastic confining units relate to the SC if mostly quartzite or the ARG if mostly shale. Mineralogical criteria used to establish RMCs for the RMSM HFM are provided in the RMSM_HFM.xls workbook in the Appendix\A folder on the accompanying DVD. The RMSM_HFM.xls workbook also provides the RMC assignments for each HSU in the RMSM HFM and includes reactive mineral unit (RMU) assignments used during construction of the reactive mineral model.

Table 4-1
RMSM HSUs with Corresponding RMUs and RMCs
(Page 1 of 3)

HSU	RMU	Dominant RMCs [a]
Alluvial aquifer (AA)	Alluvium upper vitric	VMP
Fortymile Canyon composite unit (FCCM)	Fortymile Canyon DMP	DMP
	Fortymile Canyon ML	ML, lesser ZEOL, SC
	Fortymile Canyon ZEOL	ZEOL lesser SC and VMP
Timber Mountain upper vitric-tuff aquifer (TM-UVTA)	Ammonia Tanks upper vitric	VMP, lesser VMR, minor VMP-Z, ZEOL
Timber Mountain welded-tuff aquifer (TM-WTA)	Ammonia Tanks DMP	DMP
	Timber Mountain zeolitic	ZEOL, lesser AR
	Rainier Mesa DMR	DMR
	Rainier Mesa DMP	DMP
Timber Mountain lower vitric-tuff aquifer (TM-LVTA)	Timber Mountain lower vitric	VMP, minor VMR, VMP-Z

Table 4-1
RMSM HSUs with Corresponding RMUs and RMCs
(Page 2 of 3)

HSU	RMU	Dominant RMCs [a]
Tiva Canyon aquifer (TCA)	Tiva Canyon DMP	DMP
Paintbrush vitric-tuff aquifer (PVTA)	Paintbrush VMP	VMP
Upper tuff confining unit (UTCU)	Upper tuff zeolitic	ZEOL
Topopah Spring aquifer (TSA)	Topopah Spring DMP	DMP
Lower vitric-tuff aquifer (LVTA)	Lower vitric	VMP, minor VMP-Z, DMP, ZEOL
Yucca Mountain Calico Hills lava-flow aquifer (YMCHLFA)	Yucca Mountain Calico Hills DMP	DMP
Calico Hills vitric-tuff aquifer (CHVTA)	Calico Hills VMP	VMP
Kearsarge aquifer (KA)	Kearsarge DMP	DMP
Upper tuff confining unit 2 (UTCU2)	Upper tuff zeolitic 2	ZEOL
Stockade Wash aquifer (SWA)	Stockade Wash DMP	DMP
Upper tuff confining unit 1 (UTCU1)	Upper tuff zeolitic 1	ZEOL
Lower vitric-tuff aquifer 2 (LVTA2)	Lower vitric 2	VMP
Bullfrog confining unit (BFCU)	Bullfrog zeolitic	ZEOL
Belted Range aquifer (BRA)	Belted Range DMP	DMP
Lower vitric-tuff aquifer 1 (LVTA1)	Lower vitric 1	VMP, minor VMP-Z, DMP, ZEOL
Belted Range confining unit (BRCU)	Belted Range zeolitic	ZEOL
Tub Spring aquifer (TUBA)	Tub Spring DMP	DMP
Lower tuff confining unit (LTCU)	TCU upper zeolitic	ZEOL
Oak Spring Butte confining unit (OSBCU)	Oak Spring Butte upper zeolitic	ZEOL, lesser DMR, lesser DMP
Redrock Valley aquifer (RVA)	Redrock Valley DMP	DMP
	Oak Spring Butte lower zeolitic	ZEOL
	Twin Peaks DMP	DMP, minor ZEOL
Redrock Valley breccia confining unit (RVBCU)	Redrock Valley breccia	ARG, lesser DMP
Lower tuff confining unit 1 (LTCU1)	Lower tuff zeolitic 1	ZEOL
Argillic tuff confining unit (ATCU)	Lower tuff argillic	ARG

Table 4-1
RMSM HSUs with Corresponding RMUs and RMCs
(Page 3 of 3)

HSU	RMU	Dominant RMCs [a]
Timber Mountain composite unit (TMCM)	Caldera-burying Ammonia Tanks DMR	DMR
	Caldera-burying Ammonia Tanks DMP	DMP
	Timber Mountain middle zeolitic	ZEOL
	Intra-caldera Rainier Mesa DMR	DMR
	Intra-caldera Rainier Mesa DMP	DMP
Rainier Mesa breccia confining unit (RMBCU)	Rainier Mesa breccia ZEOL	ZEOL, lesser ARG
Subcaldera volcanic confining unit (SCVCU)	Subcaldera-argillic	ARG, lesser DMP
Lower carbonate aquifer–thrust plate (LCA3-1)	Thrusted LCA3-1	CC
	(Alternative #4 only)	--
Upper clastic confining unit 1 (UCCU1)	Thrusted upper siliciclastic	SC
	(Alternative #4 only)	--
Lower clastic confining unit–thrust plate 1 (LCCU1)	Thrusted lower siliciclastic	SC
Lower carbonate aquifer–thrust plate (LCA3)	Thrusted LCA3	CC
Upper carbonate aquifer (UCA)	Upper carbonate aquifer	CC
Upper clastic confining unit (UCCU)	Upper siliciclastic	ARG, lesser SC
Silent Canyon intrusive confining unit (SCICU)	Silent Canyon intrusive DMP	DMP
Lower carbonate aquifer (LCA)	Lower carbonate aquifer	CC
Lower clastic confining unit (LCCU)	Lower siliciclastic	SC
Redrock Valley intrusive confining unit (RVICU)	Redrock Valley intrusive DMP	DMP
Mesozoic granite confining unit (MGCU)	Granitic unit DMR	DMR
Calico Hills intrusive confining unit (CHICU)	Calico Hills intrusive DMP	DMP
Rainier Mesa intrusive confining unit (RMICU)	Rainier Mesa intrusive DMR	DMR, lesser DMP
Ammonia Tanks intrusive confining unit (ATICU)	Ammonia Tanks intrusive DMR	DMR, lesser DMP

[a] See RMSM_HFM.xls workbook in the Appendix\A folder for RMC descriptions.

4.2.1 Alluvial Aquifer (AA)

The mineralogy of the alluvium mainly reflects the lithologic composition of the constituent clasts. Though typically tuffaceous, it may also contain a significant percentage of carbonate clasts (e.g., calcite and dolomite). Volcanic clasts contribute feldspars, quartz, and mafic minerals of biotite, hornblende, and magnetite, which may be oxidized to hematite. These mafic minerals are generally present in very small amounts, on the order of 1%. The alluvium is typically composed of 10 to 20% zeolite and clay minerals. Some portion of the clay minerals may be of sedimentary origin. Disseminated calcite from alluvial, eolian, and diagenic processes is also common.

Mineralogy of the alluvium varies laterally and vertically, reflecting the lithologic composition of the source rocks surrounding the basin, and the depositional processes associated with the formation of alluvial fans. In general, the deeper, older alluvium tends to be more tuffaceous. The upper portion of the alluvium in areas near Paleozoic-age carbonate outcrops may be carbonate-rich with up to 25% calcite and/or dolomite.

No mineralogical analyses are available for the AA in the RMSM model area. Based on analyses from AA in nearby Yucca Flat, the AA in the RMSM model area can be classified as a VMP RMC reflecting relatively low percentages of the reactive minerals zeolite, clay, and mica.

4.2.2 Fortymile Canyon Composite Unit (FCCM)

The FCCM in the RMSM HFM is subdivided into three RMCs based on the distribution of lithologic facies. The FCCM exposures in the southwestern portion of the model area are composed of rhyolitic lava (Tfs in the Slate et al. geologic map) (DMP RMC) [3].

Surface geologic relationships in the southeastern portion of the Timber Mountain caldera complex show the DMP section overlies a rather thick section of basaltic lava [4] (Tfd in the Slate et al. geologic map) (ML RMC) [3].

Information from drill holes ER-30-1 [5] and UE-18t [6] located just west of the model area boundaries suggests the mafic lavas pinch out northward beneath alluvial cover, and the FCCM in the northeastern portion of the caldera complex likely consists mostly of zeolitic bedded and nonwelded tuff (ZEOL RMC).

No x-ray diffraction (XRD) analyses are available for the FCCM in the RMSM model area. Several drill holes to the west of the RMSM model area encountered the FCCM, and mineralogical analyses from the FCCM in these holes may be applicable to the FCCM within the RMSM model area.

4.2.3 Timber Mountain Upper Vitric-Tuff Aquifer (TM-UVTA)

The reactive minerals zeolite, clay, carbonate, and biotite mica typically occur in low percentages in the TM-UVTA, reflecting the unaltered, glass-rich, and mafic-poor character of these volcanic rocks. Based on the low percentages of the reactive minerals zeolite, clay, carbonate, and mica, and the

abundance of glass, the TM-UVTA is categorized as a VMP RMC. No mineralogical analyses exist for the TM-UVTA within the RMSM model area. Mineralogical data for the TM-UVTA in the Yucca Flat model area can be assumed to be applicable to the TM-UVTA in the RMSM model area.

4.2.4 Timber Mountain Welded-Tuff Aquifer (TM-WTA)

Reactive minerals within the TM-WTA are typically rare, reflecting the devitrified welded-tuff lithology that results in a rock composed almost entirely of micro-crystalline quartz and feldspar.

The HSU is subdivided into four RMCs based on the degree of welding and associated devitrification, abundance of mafic minerals, and stratigraphic position. Welded devitrified tuff that forms most of the TM-WTA, includes two RMCs: an upper mafic-rich member (DMR RMC) and a thicker mafic-poor member (DMP RMC).

The overlying welded mafic-poor Ammonia Tanks tuff is categorized as a DMP RMC. This RMC is found in Mid Valley, where it composes the upper 15 m (50 ft) of the TM-WTA, and in the northeastern corner of the Timber Mountain caldera complex, where it forms virtually all of the TM-WTA. The overlying vitric nonwelded and bedded tuff that occurs between the Ammonia Tanks and Rainier Mesa tuffs is categorized as a VMP RMC. This RMC is only split in Mid Valley, where it is saturated and approximately 3 m (10 ft) thick.

Only one mineralogical analysis is available for TM-WTA within the RMSM model area. However, mineralogical analyses for TM-WTA from Yucca Flat are applicable for the TM-WTA in the RMSM model area.

4.2.5 Timber Mountain Lower Vitric-Tuff Aquifer (TM-LVTA)

Reactive minerals are typically rare in the TM-LVTA owing to its unaltered glass-rich character and general scarcity of biotite (RMSM_HSU_Mineralogy.xls). Consequently, the HSU is categorized as a VMP RMC.

4.2.6 Timber Mountain Composite Unit (TMCM)

The TMCM is designated a composite unit because of the possibility that hydrothermal alteration within this deep intra-caldera setting has altered the hydraulic properties of the rocks; in particular, filling fractures with secondary minerals such as quartz.

The TMCM is subdivided into five RMCs. The two dominant formations that make up the TMCM, the Ammonia Tanks and Rainier Mesa tuffs, are subdivided into DMR and DMP RMCs based on their devitrified and welded tuff lithology, and the presence of both mafic-rich and mafic-poor members of both formations. The thin interval of zeolitic nonwelded and bedded tuff that separates the two dominant formations is categorized as a ZEOL RMC. No mineralogical analyses are available for the TMCM within the RMSM model area. Several drill holes to the west of the RMSM

model area encountered the TMCM, and any mineralogical analyses from the TMCM in these holes are applicable to the TMCM within the RMSM model area.

4.2.7 Rainier Mesa Breccia Confining Unit (RMBCU)

The unit consists mostly of angular volcanic blocks within a tuffaceous matrix that is likely argillic at depth. There are no XRD analyses specifically of the RMBCU rocks in any of the UGTA CAU datasets. However, based on outcrop descriptions, this unit would be classified as an ARG RMC.

4.2.8 Sub-Caldera Volcanic Confining Unit (SCVCU)

If the SCVCU exists beneath the Timber Mountain caldera complex at the depths depicted in the model, then the rocks comprising the HSU are likely to be highly altered, so the unit is classified as an ARG RMC.

4.2.9 Tiva Canyon Aquifer (TCA)

The TCA contains few reactive minerals due to the high degree of devitrification, creating a rock predominantly composed of felsic minerals in the form of micro-crystalline quartz and feldspar. Within the model area, biotite is uncommon in the unit; therefore, the TCA is categorized as a DMP RMC. No XRD analyses are available for the TCA within the RMSM model area. However, data for the TCA in Yucca Flat can be assumed to be directly applicable for the TCA in the RMSM area.

4.2.10 Paintbrush Vitric-Tuff Aquifer (PVTA)

The vitric character and general scarcity of biotite in the stratigraphic units of the PVTA should result in rocks that are low in reactive minerals, so the unit is categorized as a VMP RMC. The XRD data from the TM-LVTA within the RMSM model area should be applicable to the PVTA because of the lithologic and mineralogical similarity between the two HSUs.

4.2.11 Upper Tuff Confining Unit (UTCU)

Because the UTCU is pervasively zeolitic, it is categorized as a ZEOL RMC. No XRD analyses are available for the UTCU in the RMSM model area; however, data for the unit in Yucca Flat can be assumed to be directly applicable to the RMSM model area.

4.2.12 Topopah Spring Aquifer (TSA)

The TSA contains few reactive minerals due to the high degree of devitrification, creating a rock predominantly composed of felsic minerals in the form of micro-crystalline quartz and feldspar. Within the model area, biotite is uncommon in the unit; therefore, the TSA is categorized as a DMP RMC. No XRD analyses are available for the TSA within the RMSM model area. However, data for the unit in Yucca Flat can be assumed to be directly applicable in the RMSM area.

4.2.13 Lower Vitric-Tuff Aquifer (LVTA)

Reactive minerals are typically rare in the LVTA because of its vitric character and the low abundance of mafic minerals in the included stratigraphic units. The HSU is categorized as a VMP RMC. Only five XRD analyses from one drill hole are available from the LVTA in the RMSM model area. The analyses show high mafic/mica content for the LVTA, which is inconsistent with the VMP designation. However, three of the five analyses are from relatively thin mafic-rich beds comprising only a small fraction of the LVTA.

4.2.14 Calico Hills Vitric-Tuff Aquifer (CHVTA)

There are no XRD analyses specifically of the CHVTA rocks in the RMSM dataset. However, a portion of the TM-LVTA contains similar unaltered stratigraphic units, so the dominant RMC is categorized as VMP. Chemistry and mineralogy attributes for the TM-LVTA may be used as a first approximation for the CHVTA.

4.2.15 Yucca Mountain Calico Hills Lava-Flow Aquifer (YMCHLFA)

No XRD analyses are available for the YMCHLFA in the RMSM model area. Because the YMCHLFA is generally unaltered, reactive minerals are rare in the HSU. Consequently, the YMCHLFA is categorized as a DMP RMC.

4.2.16 Kearsarge Aquifer (KA)

Although the KA is mostly devitrified, the top and basal portions are glassy to zeolitic. The KA is categorized overall as a DMR, but the top and basal portions may consist locally of VMR and ZEOL.

4.2.17 Upper Tuff Confining Unit 2 (UTCU2)

No XRD analyses are available for the UTCU2 in the RMSM model area. However, because zeolitic rocks are typically dominated by zeolite minerals, the UTCU2 is categorized as a ZEOL RMC.

4.2.18 Stockade Wash Aquifer (SWA)

No XRD analyses are available for the SWA. Because the Stockade Wash partially welded ash-flow tuff is typically devitrified and mafic-poor, it is categorized as a DMP RMC.

4.2.19 Lower Vitric-Tuff Aquifer 2 (LVTA2)

There are no XRD analyses specifically of the LVTA2 rocks in the RMSM dataset. Mineralogical data for the TM-LVTA (RMSM_HSU_Mineralogy.xls) may be used as a first approximation for the LVTA2, and the dominant RMC is VMP.

4.2.20 Bullfrog Confining Unit (BFCU)

The BFCU is zeolitic nonwelded ash-flow tuff and is categorized as a ZEOL RMC. No XRD analyses are available for the BFCU.

4.2.21 Upper Tuff Confining Unit 1 (UTCU1)

The UTCU1 averages 53% zeolite (RMSM_HSU_Mineralogy.xls). Other reactive minerals are relatively low in abundance. Because of the dominance of zeolite minerals in the UTCU1, it is categorized a ZEOL RMC.

4.2.22 Belted Range Aquifer (BRA)

Most of the rocks that compose the BRA are devitrified and mafic-poor; thus, the BRA is categorized overall as a DMP RMC. The occurrence of zeolitic tuff and lava results in some zones better characterized as ZEOL RMC. However, the distribution of these zeolitic zones is very poorly constrained, and the zones are not split. No XRD analyses are available for the BRA.

4.2.23 Lower Vitric-Tuff Aquifer 1 (LVTA1)

The LVTA1 is categorized as a VMP based on the unaltered (i.e., glassy) and general mafic-poor character of the constituent rocks. Although there are no XRD analyses specifically of the LVTA1 rocks in the RMSM dataset, a portion of the TM-LVTA contains similar unaltered stratigraphic units.

4.2.24 Belted Range Confining Unit (BRCU)

The BRCU averages 40% zeolite (RMSM_HSU_Mineralogy.xls) and thus is categorized as a ZEOL RMC.

4.2.25 Tub Spring Aquifer (TUBA)

The TUBA is categorized as a DMP RMC based on the devitrified and mafic-poor character of this welded tuff. There are no XRD analyses available for the TUBA within the RMSM model area. However, two XRD analyses of TUBA are available from Yucca Flat, and they are consistent with a DMP RMC designation.

4.2.26 Lower Tuff Confining Unit (LTCU)

Zeolite is the major mineral component of the LTCU (RMSM_HSU_Mineralogy.xls). Other reactive minerals are typically rare. Because of the high zeolite content, the LTCU is categorized as a ZEOL RMC.

4.2.27 Oak Spring Butte Confining Unit (OSBCU)

Lithologically, the OSBCU includes bedded tuff, non- to partially welded ash-flow tuff, tuffaceous sandstone, and tuffaceous paleocolluvium. The lithologic diversity of the OSBCU results in a more diverse mineralogy that may have important ramifications for radionuclide sorption and ion exchange processes [6].

Because some of the ash-flow tuff units within the OSBCU appear to be devitrified, there was little glass available to be altered later to zeolite. The OSBCU addresses the hydrogeologic and mineralogic variability these older, devitrified ash-flows may impart to an otherwise zeolitic interval. The OSBCU generally correlates to the felsic zone of Prothro [7].

The OSBCU has a relatively high zeolite content of 32% (RMSM_HSU_Mineralogy.xls) and is therefore categorized, like the LTCU, as a ZEOL RMC. The presence of several weakly zeolitized to devitrified ash-flow tuffs within the OSBCU, however, results in an overall zeolite content lower than that in the LTCU. The clay content of the unit is about 12%, and other reactive minerals are generally rare. The intercalated ash-flow tuffs consist predominately of felsic minerals and thus are categorized as DMP or DMR, depending on the mafic content of each ash-flow tuff unit. In summary, the diverse lithologies included in the OSBCU are manifested by the presence of several RMCs in the dataset, primarily ZEOL with lesser DMR, and DMP representing the older ash-flow tuffs.

4.2.28 Redrock Valley Aquifer (RVA)

The RVA is subdivided into three RMCs. The upper and lower portions of the RVA consist of thick, generally mafic-poor welded tuff, categorized as DMP RMC. The upper portion has a lateral extent the same as RVA. The lower DMP RMC correlates to the Twin Peaks aquifer (TPA), an HSU developed exclusively for the No Redrock Valley Caldera alternative model (see Section 4.5.27 in [1]), the lateral extent of the RMC is the same as that for the TPA. The upper and lower DMP RMCs within the RVA are separated by a relatively thin interval of zeolitic nonwelded tuff that is categorized as a ZEOL RMC. This RMC has a lateral extent the same as the lower DMP RMC. Only two XRD analyses are available for the RVA (RMSM_HSU_Mineralogy.xls), and both are from the upper DMP interval. These analyses indicate that the upper RMC within the RVA is best categorized as a DMP RMC, which is consistent with the devitrified and mafic-poor character of the stratigraphic units elsewhere.

4.2.29 Redrock Valley Breccia Confining Unit (RVBCU)

The unit is thought to mostly consist of breccia blocks within an argillic matrix, so it is designated as a confining unit and an ARG RMC.

4.2.30 Lower Tuff Confining Unit 1 (LTCU1)

The LTCU1 is non-welded and zeolitized. Because of the high zeolite content, the LTCU1 is categorized as a ZEOL RMC. No XRD analyses are available for the LTCU1.

4.2.31 Twin Peaks Aquifer (TPA)

The tuffs thought to make up the TPA are welded and mafic-poor, so the unit is categorized as a DMP RMC.

4.2.32 Argillic Tuff Confining Unit (ATCU)

The ATCU is characterized mineralogically by an abundance of clay, moderate amounts of felsic minerals, and a general absence of zeolites [7]. Consequently, the ATCU is categorized as an ARG RMC. Although no XRD analyses are available for the ATCU within the RMSM model area, XRD analyses for the ATCU in Yucca Flat are available and are suitable for use in the RMSM area.

4.2.33 Caldera-Related Intrusive Confining Units

Intrusive confining units cool much slower than extruded volcanic tuffs and lack the volcanic glass and, in turn, zeolites found in tuffs. The main reactive mineral found in these units is biotite, which is dependent on the mafic content of the rock. Mafic content of the rock is generally inferred from the composition of tuffs related to these intrusives. The four caldera-related intrusive confining units in the RMSM model area are:

- **Ammonia Tanks Intrusive Confining Unit (ATICU)**
  The ATICU should be classified as either a DMR or DMP RMC.
- **Rainier Mesa Intrusive Confining Unit (RMICU)**
  The RMICU should be classified as either a DMR or DMP RMC.
- **Redrock Valley Intrusive Confining Unit (RVICU)**
  The RVICU should be classified as either a DMR or DMP RMC.
- **Silent Canyon Intrusive Confining Unit (SCICU)**
  The SCICU should be classified as a DMP RMC.

4.2.34 Calico Hills Intrusive Confining Unit (CHICU)

Based on its inferred granitic composition, the CHICU is categorized as either a DMP or DMR RMC.

4.2.35 Mesozoic Granite Confining Unit (MGCU)

The mineralogy of the MGCU includes plagioclase, potassium feldspar, quartz, and biotite, with a trace of pyrite, sphene, zircon, apatite and iron oxides [8]. Based on this mineralogy, the MGCU is classified as a DMR RMC. No XRD analyses are available for the MGCU within the RMSM model area. However, XRD data for the Climax stock in northern Yucca Flat may be used.

Fracture-filling minerals in the MGCU, as reported in various lithologic logs, include calcite, quartz, secondary feldspars, clay, chlorite, pyrite, epidote, and iron oxides [8].

4.2.36 Upper Carbonate Aquifer (UCA)

There are no XRD data for the UCA in the RMSM HFM area. However, based on detailed lithologic descriptions, the UCA is predominately a CC RMC and, as noted here, there could be rare SC due to the presence of mudstone and siltstone interbeds.

Fracture-filling minerals in the UCA, as reported in various lithologic logs, include mostly calcite and iron-staining and lesser clay [9, 10].

4.2.37 Upper Clastic Confining Unit (UCCU)

The mineralogy of the UCCU varies with lithology. Rocks associated with the Eleana formation are generally siltstone and sandstones composed mainly of quartz and chert grains. The Eleana formation also contains several bioclastic limestones. The Chainman shale is mostly shale and argillite. Based on lithologic composition, the portion of the UCCU composed of the Eleana formation is categorized as an SC RMC, while the Chainman shale portion is categorized as an ARG RMC. No XRD analyses are available for the UCCU in the RMSM model area.

Fracture-filling minerals in the UCCU, as reported in various lithologic logs, include quartz, calcite, clay, and rare pyrite and trace pyrolusite [11-13].

4.2.38 Lower Carbonate Aquifer (LCA and LCA3)

The upper 30% of the LCA is predominately dolomite, while the lower 60% is mostly limestone. Relatively thin intervals of siliciclastic rocks such as the Eureka quartzite (125 m [400 ft] thick) and Dundenberg shale (70 m [225 ft] thick) occur within the HSU. Virtually all of the LCA is classified as a CC RMC, with only a few percent of the total thickness being an SC (e.g., Eureka quartzite) and an ARG (e.g., Dunderberg shale).

Detailed information about fracture geometry and fracture-filling minerals in LCA core samples from Wells ER-6-1 and ER-6-2 in southern Yucca Flat is presented by IT Corporation [14]. IT Corporation found the fractures in the LCA rocks were filled or lined with three types of minerals: iron oxides (limonite and hematite), including scarce pyrolusite carbonaceous clays; and carbonate minerals consisting almost always of calcite with rare occurrences of dolomite [14]. They also noted that silica cements are rare and restricted to fractures in quartzite lithologies. Another observation made was most of the fractures are lined or filled with a combination of two or more of these materials. Many of the fractures within the upper 15 m (50 ft) of the LCA are typically filled with tuffaceous clay [11].

A single XRD analysis of LCA3 from Well ER-12-3 showed 72% calcite and 2% mafic minerals. The mafic minerals are probably related to metamorphism associated with the nearby Gold Meadows stock.

4.2.39 Lower Clastic Confining Unit (LCCU, LCCU1, and LCCU2)

Fracture-filling minerals in the LCCU, LCCU1, and LCCU2, as reported from outcrop descriptions and a few lithologic logs, include quartz, calcite, and rare clay. Nearly all the LCCU is an SC RMC with lesser CC representing carbonate interbeds and the Noonday dolomite. The XRD analyses of the LCCU1 within the RMSM model area show an average of 30% mafic minerals, reflecting the micaceous character typical of many of the older siliciclastic rocks.

4.3 References

1. National Security Technologies, LLC. 2007. *A Hydrostratigraphic Model and Alternatives for the Groundwater Flow and Contaminant Transport Model of Corrective Action Unit 99: Rainier Mesa-Shoshone Mountain, Nye County, Nevada*, DOE/NV/29546--146. Las Vegas, NV.

2. Warren, R.G., D.A. Sawyer, F.M. Byers, Jr., and J.C. Cole. 2003. *A Petrographical, Geochemical and Geophysical Database and Framework for the Southwestern Nevada Volcanic Field.* Los Alamos National Laboratory Report LA-UR-03-1503.

3. Slate, J.L., M.E. Berry, P.D. Rowley, C.J. Fridrich, K.S. Morgan, J.B. Workman, O.D. Young, G.L. Dixon, V.S. Williams, E.H. McKee, D.A. Ponce, T.G. Hilderbrand, W.C. Swadley, S.C. Lundstrom, E.B. Ekren, R.G. Warren, J.C. Cole, R.J. Fleck, M.A. Lanphere, D.A. Sawyer, S.A. Minor, D.J. Grunwald, R.J. Laczniak, C.M. Menges, J.C. Yount and A.S. Jayko. 1999. *Digital Geologic Map of the Map of the Nevada Test Site and Vicinity, Nye, Lincoln, and Clark Counties, Nevada and Inyo County, California.* U.S. Geological Survey Open-File Report 99B554BA, scale 1:120,000.

4. Crowe, B.M. 1990. "Basaltic Volcanic Episodes of the Yucca Mountain Region." In *High-Level Radioactive Waste Management: Proceedings of the First Annual International Conference, Las Vegas, NV, April 8-12*. pp. 65-73. American Nuclear Society, La Grange Park, IL.

5. U.S. Department of Energy, Nevada Operations Office. 1995. *Completion Report for Well ER-30-1*, DOE/NV--407. Las Vegas, NV.

6. Byers, F.M., Jr., W.L. Hawkins, and D.C. Muller. 1981. *Geology of Drill Hole UE18t and Area 18 Timber Mountain Caldera Moat, Nevada Test Site*. U.S. Geological Survey Report USGS-474-312. Denver, CO.

7. Prothro, L.B. 2005. *Mineralogic Zonation Within the Tuff Confining Unit, Yucca Flat, Nevada Test Site*, DOE/NV/11718--995. Bechtel Nevada, Las Vegas, NV.

8. Maldonado, F. 1977. *Summary of the Geology and Physical Properties of the Climax Stock, Nevada Test Site*. U.S. Geological Survey Open-File Report 77-356, 25 pp. Denver, CO.

9. Hodson, J.N., and D.L. Hoover. 1978. *Geologic and Lithologic Log for Drill Hole UE17a, Nevada Test Site*. U.S. Geological Survey Open-File Report USGS-1543-1. 17 pp. Denver, CO.

10. Metcalf, J.G., H.E. Huckins-Gang, B.M. Allen, and M.J. Townsend. 1999. Written communication. Subject: *Geology and Rock Mass Character of U16b Tunnel and Vicinity, Nevada Test Site, Nye County, Nevada*. Bechtel Nevada, Las Vegas, NV.

11. U.S. Department of Energy, National Nuclear Security Administration Nevada Site Office. 2004. *Completion Report for Well ER-12-2*, DOE/NV/11718--846. Prepared by Bechtel Nevada, Las Vegas, NV.

12. Russell, C.E., D. Gillespie, J.C. Cole, S.L. Drellack, L.B. Prothro, P.H. Thompson, R.L. McCall, G.A. Pawloski, and R. Carlson. 1996. *Completion Report for Well ER-12-1*, DOE/NV/10845-36. Prepared for U.S. Department of Energy Nevada Operations Office, Las Vegas, NV.

13. Fernald, A.T., F.M. Byers, and J.P. Ohl. 1975. *Lithologic Logs and Stratigraphic Units of Drill Holes and Mined Shafts in Areas 1 and 6, Nevada Test Site.* U.S. Geological Survey Open-File Report 474-206, 61 pp. Denver, CO.

14. IT Corporation. 1996. *Regional Geologic Model Data Documentation Package (Phase I, Data Analysis Documentation, Volume I, Parts 1 and 2*), ITLV/10972--181. Las Vegas, NV.

5.0 CONTAMINANT SOURCES

Nuclear testing in the RMSM CAU was primarily in mined tunnels. Information on the tunnels, particularly regarding the hydrogeologic character of the formations in which the tunnels are located and the relationship of the tunnels with groundwater, is discussed as background for evaluating mobility of contaminants from the tests. The radiologic source term (RST) of a test is the inventory (or quantity) of radionuclides in existence after the test detonation, associated with that test, regardless of form and distribution of the radionuclides. Today, the RST for the RMSM CAU comprises only 0.67% of the entire NTS RST. The hydrologic source term (HST), the amount of radioactivity that is available for transport in groundwater, is a subset of the RST and will be addressed in a future document.

5.1 Overview of Testing in the RMSM CAU

Within the RMSM CAU, nuclear tests were conducted at 60 underground locations at Rainier Mesa between 1957 and 1992, and at 6 locations at Shoshone Mountain between 1962 and 1971 [1]. Nearly all (65) of the 67 nuclear tests (68 detonations) within the RMSM CAU were detonated in mined tunnels. The other two tests, CLEARWATER (U12q) and WINESKIN (U12r), were detonated in shafts at Rainier Mesa. Data for the RMSM tests are in Table 5-1, and their locations are shown on Plate 1 [1-3].

Table 5-1
Nuclear Detonations Conducted at RMSM CAU
(Page 1 of 3)

Detonation Name	Date	Location ID	Depth of Burial (ft)	Announced Yield [a]	Cavity Radius [b] (ft)
RAINIER	09/19/1957	U-12b	899	1.7 kt	57
TAMALPAIS	10/08/1958	U-12b.02	330	72 tons	26
EVANS	10/29/1958	U-12b.04	840	55 tons	19
FEATHER	12/22/1961	U-12b.08	812	150 tons	26
CHENA	10/10/1961	U-12b.09	838	Low	132
YUBA	06/05/1963	U-12b.10	796	3.1 kt	72
URANUS	03/14/1958	U-12c.01	114	< 1 ton	8
SATURN	08/10/1957	U-12c.02	128	0	0
NEPTUNE	10/14/1958	U-12c.03	98	115 tons	40
VENUS	02/22/1958	U-12d.01	100	< 1 ton	8
LOGAN	10/16/1958	U-12e.02	930	5 kt	81
ANTLER	09/15/1961	U-12e.03a	1,319	2.6 kt	60
BLANCA	10/30/1958	U-12e.05	987	22 kt	131

Table 5-1
Nuclear Detonations Conducted at RMSM CAU
(Page 2 of 3)

Detonation Name	Date	Location ID	Depth of Burial (ft)	Announced Yield [a]	Cavity Radius [b] (ft)
DORSAL FIN	02/29/1968	U-12e.10	1,345	< 20 kt	117
DIESEL TRAIN	12/05/1969	U-12e.11	1,375	< 20 kt	117
HUDSON MOON	05/26/1970	U-12e.12	1,386	< 20 kt	117
DIDO QUEEN	06/05/1973	U-12e.14	1,284	< 20 kt	119
DINING CAR	04/05/1975	U-12e.18	1,257	< 20 kt	119
HYBLA GOLD	11/01/1977	U-12e.20	1,263	< 20 kt	119
MERCURY	09/23/1958	U-12f.01	183	Slight	193
MARS	09/28/1958	U-12f.02	125	13 tons	18
MADISON	12/12/1962	U-12g.01	1,320	Low	118
RED HOT	03/05/1966	U-12g.06	1,330	< 20 kt	118
DOOR MIST	08/31/1967	U-12g.07	1,463	< 20 kt	115
CYPRESS	02/12/1969	U-12g.09	1,350	< 20 kt	117
CAMPHOR	06/29/1971	U-12g.10	1,390	< 20 kt	116
DES MOINES	06/13/1962	U-12j.01	660	2.9 kt	74
PLATTE	04/14/1962	U-12k.01	631	1.85 kt	64
MIDI MIST	06/26/1967	U-12n.02	1,237	< 20 kt	120
HUDSON SEAL	09/24/1968	U-12n.04	1,130	< 20 kt	123
MISTY NORTH	05/02/1972	U-12n.05	1,234	< 20 kt	120
DIANA MIST	02/11/1970	U-12n.06	1,319	< 20 kt	118
HUSKY ACE	10/12/1973	U-12n.07	1,364	< 20 kt	117
MING BLADE	06/19/1974	U-12n.08	1,272	< 20 kt	119
HYBLA FAIR	10/28/1974	U-12n.09	1,325	< 20 kt	118
MIGHTY EPIC	05/12/1976	U-12n.10	1,306	< 20 kt	118
DIABLO HAWK	09/13/1978	U-12n.10a	1,273	< 20 kt	119
MINERS IRON	10/31/1980	U-12n.11	1,278	< 20 kt	119
MINI JADE	05/26/1983	U-12n.12	1,244	< 20 kt	120
DIAMOND ACE, HURON LANDING	09/23/1982	U-12n.15	1,390/1,339	< 20 kt/< 20 kt	116/118
MISTY RAIN	04/06/1985	U-12n.17	1,275	< 20 kt	119
TOMME/MIDNIGHT ZEPHYR	09/21/1983	U-12n.18	1,328	< 20 kt	118
DIAMOND BEECH	10/09/1985	U-12n.19	1,326	< 20 kt	118
MILL YARD	10/09/1985	U-12n.20	1,217	< 20 kt	120
MIDDLE NOTE	03/18/1987	U-12n.21	1,308	< 20 kt	118
MINERAL QUARRY, RANDSBURG [c]	07/25/1990	U-12n.22 U-12n.22a	1,278	< 20 kt/< 20 kt	119/119
MISTY ECHO	12/10/1988	U-12n.23	1,312	< 150 kt	231

Table 5-1
Nuclear Detonations Conducted at RMSM CAU
(Page 3 of 3)

Detonation Name	Date	Location ID	Depth of Burial (ft)	Announced Yield [a]	Cavity Radius [b] (ft)
HUNTERS TROPHY	09/18/1992	U-12n.24	1,264	< 20 kt	119
MISSION CYBER	12/02/1987	U-12p.02	888	< 20 kt	130
DISKO ELM	09/14/1989	U-12p.03	857	< 20 kt	131
DISTANT ZENITH	09/19/1991	U-12p.04	865	< 20 kt	131
DIAMOND FORTUNE	04/30/1992	U-12p.05	774	< 20 kt	135
CLEARWATER	10/16/1963	U-12q	1,788	Intermediate	236
WINESKIN	01/15/1969	U-12r	1,700	20-200 kt	239
MINT LEAF	05/05/1970	U-12t.01	1,330	< 20 kt	118
DIAMOND SCULLS	07/20/1972	U-12t.02	1,391	< 20 kt	116
HUSKY PUP	10/24/1975	U-12t.03	1,076	< 20 kt	124
MIDAS MYTH/ MILAGRO	02/15/1984	U-12t.04	1,184	< 20 kt	121
MIGHTY OAK	04/10/1986	U-12t.08	1,294	< 20 kt	119
MISSION GHOST	06/20/1987	U-12t.09	1,054	< 20 kt	125
MARSHMALLOW	06/28/1962	U-16a	1,020	Low	132
GUM DROP	04/21/1965	U-16a.02	1,000	< 20 kt	133
DOUBLE PLAY	06/15/1966	U-16a.03	1,075	< 20 kt	130
MING VASE	11/20/1968	U-16a.04	1,010	< 20 kt	132
DIAMOND DUST	05/12/1970	U-16a.05	830	< 20 kt	139
DIAMOND MINE	07/01/1971	U-16a.06	873	< 20 kt	137

Source: Modified from [3].

[a] Yield is the total effective energy released in a nuclear explosion and is usually expressed in terms of equivalent tonnage of trinitrotoluene (TNT) required to produce the same energy release in an explosion (1 kt = 1,015 calories). From 1945 to 1963, a less-than-20-kt yield was defined as "low," while a 20- to 200-kt-yield range was referred to as "intermediate." In some cases, the term "slight" was used without amplification [1].

[b] The cavity radii are from Table 3-2 of [3], which are calculated using the highest value of the reported yield ranges and formula of $R_c=[70.2W^{1/3}] / [(\tilde{n}h)^{1/4}]$, where R_c is the cavity radius (m), W is the test yield (kt), ñ is the average overburden density (g/cm^3), and h is the depth of the working point from the surface (m). For the "low" and "slight" announced yields, 20 kt was used for the cavity radius calculation. For the "intermediate" announced yield, 200 kt was used for the cavity radius calculation.

[c] Mineral Quarry and Randsburg were separate detonations conducted simultaneously in separate. However, they were assigned to a single CAS.

Townsend et al. compiled, reviewed, and summarized post-test data gathered from all the tests conducted by the Defense Nuclear Agency ([DNA], now Defense Threat Reduction Agency [DTRA]), and Sandia National Laboratories (SNL) at Rainier Mesa [4]. Re-entry (mine-back and/or drill-back) data were analyzed with respect to cavity/chimney dimensions, cavity/chimney physical characteristics, micro-failure (microscopic-scale damage caused to the tuff by the passage of the shock wave), macro-failure (discrete, measurable motion along a planar surface caused by the energy of the explosion), radiation, and water-related observations [4]. Lawrence Livermore National Laboratory (LLNL) summarized the sampling history of radioactive liquids, post-test distributions of radionuclides, temperatures and fractures for eight nuclear tests (including RAINIER, LOGAN, RED HOT, NEPTUNE) at Rainier Mesa [5].

5.2 Tunnels and Shafts

Six large and several smaller tunnel complexes (herein referred to as tunnels) were constructed at Rainier Mesa for underground nuclear testing starting in the 1950s and continuing through the early 1990s (Plate 1). Nuclear tests were also conducted in vertical shafts U12r (WINESKIN) and U12q (CLEARWATER) on Rainier Mesa. In addition, the U16a Tunnel (DIAMOND DUST and DIAMOND MINE) at Shoshone Mountain was also used to conduct similar tests in vertical shafts during the 1960s and early 1970s.

5.2.1 Rainier Mesa Tunnels

There are six major tunnels and several smaller tunnels in Rainier Mesa (Plate 1) [6]. Many of the tunnels drain to ponds located outside the portals. The drainage includes water inflows from fractures and faults intersected by the tunnel. During mining, the drainage also included water used for the mining process. Some ponds continue to receive drainage from unsealed tunnels.

5.2.1.1 B-Tunnel

The U12b Tunnel, in north-central Rainier Mesa, was constructed between 1956 and 1963, and consists of 4,903.3 m (16,087 ft) of mined drifts. Six nuclear tests were conducted in B-Tunnel. The vertical U12b.07 shaft that was mined down from tunnel level a distance of 151.8 m (498 ft) and short drift that was mined horizontally north from the base of the shaft were abandoned for operational reasons that included significant water inflow from faults and fractures encountered during mining. The geologic and hydrogeologic setting of B-Tunnel are somewhat different from the other three nearby tunnels because of the higher portal elevation (2,016.3 m [6,615 ft]). The portal is in the upper portion of Tunnel formation, Tunnel 4 Member, and the tunnel was driven up-section through both the lower and upper portions of the Grouse Canyon formation with the majority of the tunnel within the pre-Rainier/post-Grouse Canyon section. Some portions of the tunnel penetrate the upper level of pervasive zeolitization, a situation only encountered elsewhere in the U12p Tunnel.

Little water was encountered during the initial mining or re-entry mining of the B-Tunnel drifts, with the exception of the U12b.07 vertical shaft mentioned above. The relatively high stratigraphic position of the tunnel openings, and the resultant low fault and fracture frequency are probably

responsible for the dryness of the U12b Tunnel. This tunnel was sealed some distance back from the portal with a shotcrete bulkhead in 1987.

5.2.1.2 E-Tunnel

The U12e horizontal tunnel, in the east-central part of Rainier Mesa, was constructed between 1957 and 1977, and comprises 15,149.2 m (49,702 ft) of mined drifts. Nine underground tests were conducted in E-Tunnel. The portal is located at 1,865.7 m (6,121 ft) above sea level and is currently closed. Mining of the access tunnel began in Paleozoic-age dolomite and progressed stratigraphically up-section through tunnel beds 1 and 2, Tub Spring tuff, and Tunnel formation, Tunnel 3 and 4 Members. All rocks within the tunnel are zeolitized ash-fall tuff and nonwelded ash-flow tuff of Tertiary age with the exception of the dolomite encountered at the portal.

Water was present during all phases of construction of the U12e Tunnel. The volumes of water ranged from seeps to flows of 18.9 to 75.7 liters per minute (Lpm) (5 to 20 gallons per minute [gpm]). No single source of water was identified in the E-Tunnel area. The tunnel is not sealed, and the collective complex continues to produce water at rates of 30.3 to 56.8 Lpm (8 to 15 gpm) [6].

5.2.1.3 G-Tunnel

The U12g horizontal tunnel, in the southernmost portion of Rainier Mesa, was constructed between 1961 and 1989 and was used for five underground tests. The G-Tunnel consists of 11,667.1 m (38,278 ft) of mined drifts. The tunnel portal is 1,863.5 m (6,114 ft) above sea level and is currently open. After the last underground test in G-Tunnel (1971), several organizations used the drift complex as an underground laboratory, where high-explosive tests, rock mechanics experiments, and many other types of non-nuclear experiments were performed. The tunnel was mined entirely within zeolitized bedded tuff and nonwelded ash-flow tuff of Tertiary-age tunnel bed 2, Tunnel 3 and 4 Members of the Tunnel formation, and the bedded Grouse Canyon formation.

No large-volume (> 3.8 Lpm [1 gpm]) sources of water were encountered during mining and drilling in the G-Tunnel. However, small amounts of water were found in several faults and fractures within the welded rocks of the Grouse Canyon formation located considerably above tunnel level, and some water continues to flow from this source.

5.2.1.4 N-Tunnel

The U12n horizontal tunnel, in north-central Rainier Mesa, was constructed between 1961 and 1993, and 25,146 m (82,500 ft) of tunnels were mined to conduct 21 low-yield nuclear tests and one 1.07-kt chemical explosion. The portal of the U12n Tunnel is 1,835.8 m (6,023 ft) above sea level. The tunnel was mined entirely in zeolitized bedded tuff and nonwelded ash-flow tuffs of the Tertiary-age Tunnel formation, the bedded Grouse Canyon formation, Tub Spring tuff, and tunnel beds 1 and 2.

Small volumes of water (< 3.8 Lpm [1 gpm]) were infrequently encountered on fault and fracture planes during mining, and more significant volumes (18.9 to 75.7 Lpm [5 to 20 gpm]) were present

during the drilling of several horizontal exploratory holes. A large volume of water was encountered in the mining of the U12n.03 drift in the northeastern portion of N-Tunnel. Water issued from a fracture system exposed in the drift at a rate of 208.2 Lpm (55 gpm) initially, and continued to flow at lesser rates for many years. In February 1994, the tunnel was sealed at the portal using the existing 5.5 m (18 ft) thick plug of concrete (designed for containment during the execution of underground nuclear tests), thereby eliminating the discharge of radioactive effluent to the unlined ponds. There are similar additional seals further back in the tunnel. At the time the tunnel was sealed, approximately 117.3 Lpm [31 gpm] was flowing from the portal. The tunnel behind the portal has been filling with groundwater since it was sealed, and analysis of time-pressure data through 2002 shows the open tunnel immediately behind the portal has probably filled with groundwater [7]. The extent of filling of sections of the tunnel behind the additional seals is not known. There are data for the analysis of samples from sampling ports in the outer seal. However, the water quality determined for these samples is not necessarily indicative of the water quality of drainage from the tunnel before it was sealed. The filling of the tunnels and inundation of the test cavities has altered the environment of the tunnels.

5.2.1.5 P-Tunnel

The U12p Tunnel is located in the northeastern portion of Aqueduct Mesa. Mining of the tunnel began in 1962, when a single drift was driven 610.8 m (2,004 ft) into the mesa. However, no additional mining occurred at the site until 1984, when it was reactivated for four underground tests (1987 to 1992). The P-Tunnel consists of 7,192.4 m (23,597 ft) of mined drifts, including one partially constructed test site. The portal of the U12p Tunnel is located at an elevation of 1,676.4 m (5,500 ft) above sea level and is currently open. Stratigraphically, the tunnel is located entirely within pre-Rainier/post-Grouse Canyon units. The upper level of pervasive zeolitization is at or slightly below tunnel level in the northeastern portion of the tunnel and a few feet above tunnel level in the western area.

Free water was rarely present during the construction of the U12p Tunnel, presumably because of the lack of faults and fractures. As with the U12b Tunnel, the tunnel position relative to the upper level of zeolitization is probably a factor in the low fracture frequency and insignificant occurrence of perched water in the otherwise saturated tuff.

5.2.1.6 T-Tunnel

The U12t horizontal tunnel was constructed between 1968 and 1988 in Aqueduct Mesa. The tunnel system, where six underground tests were conducted, consists of 10,642 m (34,913 ft) of drifts. The presently closed portal is 1,707 m (5,600 ft) above sea level, and the overburden thickness at the test locations ranges from 348 to 424 m (1,143 to 1,391 ft), varying with the surface topography. The tunnel was mined entirely within the Tertiary-age volcanic rocks of the Tunnel 3 and 4 Members of the Tunnel formation, Tub Spring tuff, and tunnel bed 2. These rocks are zeolitized ash-fall and nonwelded ash-flow tuff.

Significant volumes of water were encountered during mining of the T-Tunnel at only two locations: one in the main access drift, approximately 610 m (2,000 ft) from the portal, and the other near the terminus of the bypass drift in the U12t.03 Tunnel. However, large volumes of water (> 1,514 Lpm [400 gpm]) were present during the drilling of several horizontal exploratory holes located northwest of the drifts. The water was flowing from fractures and faults located entirely beyond the open drifts, which were interconnected over distances of greater than 30 m (100 ft). The water flow diminished over time, but stabilized and continued to flow until the holes were sealed. The U12t Tunnel was closed in September 1993, has been filling with groundwater, and analysis of time-pressure data through 2002 indicates the tunnel is probably completely filled [7]. The status of sections of the tunnel behind additional seals and stemming is not known.

5.2.1.7 Other Tunnels

The U12a Tunnel, also known as the USGS Tunnel, was mined in 1956 in support of planning for the impending RAINIER nuclear experiment and consisted of an access drift and two test drifts at right angles (186.8 m [613 ft] in total length). The U12a Tunnel is located in zeolitized tuff. Two high-explosives tests (chemical explosives) were conducted in this tunnel.

The U12c Tunnel is located adjacent to and just south of B-Tunnel, but at a higher elevation of 2,045.8 m (6,712 ft), with 91.4 m (300 ft) of mined drifts. Three underground tests were conducted there in 1957 and 1958. Mining of C-Tunnel began in the lower (bedded) Grouse Canyon formation and progressed up-section through a thin welded zone, into the lower part of the pre-Rainier/post-Grouse Canyon.

The U12d Tunnel was driven from the same portal area as U12c and U12f (elevation 2,049.8 m [6,725 ft]), and consisted of a single drift 67.1 m (220 ft) long. This site was used for the underground test code-named VENUS in 1958. The geology is essentially the same as at C- and F-Tunnels, which are located within approximately 61.0 m (200 ft) of D-Tunnel.

The U12f Tunnel, located adjacent to the U12c Tunnel, was constructed at the same portal elevation, and consisted of 350.5 m (1,150 ft) of drifts with four test areas. However, only two underground tests (MERCURY and MARS) were conducted in F-Tunnel. The geologic setting of F-Tunnel is similar to that of C-Tunnel.

The U12i, U12j, and U12k Tunnels, driven from the same portal facility in 1959, are located in the southeastern portion of Aqueduct Mesa. Each tunnel consists of approximately 762.0 m (2,500 ft) of mined drifts (portal elevations all 1,717.5 m [5,635 ft]), but only U12k and U12j were used for nuclear tests (PLATTE and DES MOINES, respectively), conducted in 1962 [1]. The I-Tunnel was abandoned as mined because of the containment failures in the two adjacent tunnels. These three tunnels were constructed in the vitric (non-zeolitized) portion of the pre-Rainier/post-Grouse Canyon and were dry.

5.2.1.8 Groundwater at Rainier Mesa

The working points for most tests conducted at Rainier Mesa (not including Aqueduct Mesa) were within the zeolitized tuffs of the Tunnel formation, a Tertiary bedded tuff composed principally of rhyolitic air-fall tuff and non-welded ash-flow tuff. A few early tests in B-Tunnel were conducted in the upper vitric rocks. The relatively impermeable nature of the zeolitized ash-fall tuff and relatively high recharge rate (7 to 8% of the 12.53 inches per year [31.8 centimeters per year] average precipitation rate) have produced perched saturated zone(s) in the vicinity of several tunnels in Area 12, N- and T-Tunnels in particular, but not B-Tunnel [7]. Static water levels in two nearby piezometers (ER-12-3 and ER-12-4) completed almost to full depth in the volcanic section are above the level of all but B-Tunnel. However, the permeability of the saturated zeolitized tuff is extremely low, and there is no appreciable flow of water from interstitial porosity into the tunnels, except through fractures and faults or silicified horizons within the tuffs. Groundwater movement through fractures in the tuff is thought to be limited because the fractures are poorly connected. Flows from fractures usually diminish with time after being exposed during mining, although there are some persistent flows. The N- and T-Tunnels have been closed and subsequently are filling with groundwater [3, 7]. Beneath the Rainier Mesa tunnels, thrust blocks of LCA (designated LCA3) comprise an aquifer system that may receive recharge from the overlying volcanic tuffs. The Rainier Mesa tests were located approximately 365 to 715 m (1,200 to 2,345 ft), depending on the elevation of the particular tunnel, above the water table located in underlying pre-Tertiary rocks [3, 7].

5.2.2 Shoshone Mountain Tunnel

The Shoshone Mountain tunnel (U16a) is located in Area 16, about 20 km (12 mi) south of Rainier Mesa. The U16a Tunnel was constructed between 1961 and 1971 by the U.S. Department of Defense, with additional exploratory work continuing through 1973. Six low-yield nuclear tests were conducted in the U16a Tunnel. The underground portions of the testing area have been inactive since 1973.

The U16a Tunnel is located at an elevation of about 1,649 m (5,410 ft) above sea level, in zeolitized ash-fall and ash-flow tuffs, similar in age and physical properties to the rocks that are found at the southern end of Rainier Mesa (e.g., U12g and U12e Tunnels). There is approximately 1,105 m (3,625 ft) of mined tunnel. Available mining records suggest no significant quantities of water were encountered during mining or exploratory drilling. The Shoshone Mountain underground tests are approximately 893 m (2,930 ft) above the water table, which is located in Paleozoic carbonate rocks [6].

5.2.3 Radiologic Source Term

The total RST for the RMSM CAU was reported in an unclassified report wherein the RST associated with underground nuclear tests at the NTS was subdivided into five principal geographic test centers. For each geographic test center, a total unclassified RST was calculated based on the sum of the classified inventories of individual tests. The RMSM CAU comprises one of the test centers (Plate 1) [8].

A Los Alamos National Laboratory (LANL) report [8] compiled a list of radionuclides for RMSM CAU tests, with inventories corrected to September 23, 1992 (date of the last underground nuclear test at the NTS), as shown in Table 5-2. The tests conducted at RMSM have relatively low yields, with the majority being less than 20 kt (Table 5-1). Consequently, the percentage of the total NTS RST in the RMSM CAU (0.67%), is only a bit larger than that of the Frenchman Flat CAU (0.14%) and much smaller than that of the Pahute Mesa (60.6%) and Yucca Flat (38.6%) CAUs.

Table 5-2
Radionuclide Inventory for the RMSM CAU [a]
(Page 1 of 2)

Radionuclide	Atoms	Curies	Ratio: RMSM/NTS (%) [b]
Tritium	1.59E+25	7.65E+05	0.61
Carbon-14	1.06E+24	1.10E+02	3.88
Aluminum-26	5.44E+20	4.55E-04	0.42
Chlorine-36	5.73E+24	1.13E+01	1.84
Argon-39	1.66E+22	3.66E+01	1.14
Potassium-40	1.98E+28	9.23E+00	1.14
Calcium-41	1.23E+25	7.06E+01	1.59
Nickel-59	2.59E+23	2.02E+00	1.78
Nickel-63	3.57E+22	2.12E+02	1.66
Krypton-85	2.44E+22	1.34E+03	0.76
Strontium-90	7.72E+23	1.59E+04	0.73
Zirconium-93	2.02E+24	7.99E-01	1.05
Niobium-93m	7.23E+19	2.67E+00	0.02
Niobium-94	3.12E+22	9.25E-01	0.23
Technetium-99	2.81E+24	7.82E+00	1.37
Palladium-107	1.27E+24	1.16E-01	3.40
Cadmium-113m	6.04E+20	2.55E+01	1.32
Tin-121m	1.00E+22	1.08E+02	1.51
Tin-126	2.19E+23	5.20E-01	1.57
Iodine-129	7.72E+23	2.92E-02	1.66
Cesium-135	3.47E+24	8.97E-01	1.50
Cesium-137	1.91E+24	3.77E+04	1.32
Samarium-151	2.94E+23	1.94E-03	0.00
Europium-150	1.25E+17	2.06E-03	0.00
Europium-152	3.89E+22	1.70E+03	1.13
Europium-154	1.32E+22	9.09E+02	0.86
Holmium-166m	6.78E+21	3.35E+00	2.28
Thorium-232	1.59E+28	6.76E-01	1.15
Uranium-232	1.08E+20	9.19E-01	0.13
Uranium-233	2.97E+24	1.11E+01	2.37

Table 5-2
Radionuclide Inventory for the RMSM CAU [a]
(Page 2 of 2)

Radionuclide	Atoms	Curies	Ratio: RMSM/NTS (%) [b]
Uranium-234	2.29E+24	5.52E+00	1.42
Uranium-235	2.04E+26	1.72E-01	2.00
Uranium-236	5.85E+24	1.48E-01	1.58
Uranium-238	5.21E+27	6.92E-01	1.56
Neptunium-237	2.17E+23	6.03E-02	0.12
Plutonium-238	3.93E+23	2.66E+03	6.73
Plutonium-239	4.41E+26	1.09E+04	6.78
Plutonium-240	3.05E+25	2.76E+03	6.59
Plutonium-241	1.05E+24	4.32E+04	7.30
Plutonium-242	2.50E+23	3.96E-01	2.45
Americium-241	1.86E+24	2.56E+03	6.89
Americium-243	9.81E+21	7.90E-01	11.2
Curium-244	1.51E+21	4.96E+01	0.66
Total	4.16E+28	8.87E+05	0.67

[a] Total inventory decay corrected to September 23, 1992 (date of last underground nuclear test); Source: Modified from [8].
[b] Ratio based on radioactivity (curies).

Radionuclides listed in Table 5-2 are the most relevant radionuclides for consideration [8]. These should not be considered an exhaustive list of all possible test-related radionuclides but, rather, those with sufficiently long half-lives and abundance to be of regulatory concern over the next 1,000 years [9]. It should be noted that the reported inventories of potassium (K)-40, thorium (Th)-232, uranium (U)-234, U-235, and U-238 include estimates of their natural (non-test-related) abundance that was incorporated in melt glass. With the exception of K-40, the amount of these radionuclides that is either natural or test-related in origin has not been determined. Note that K-40 is entirely of natural origin [8, 10].

Radionuclides measured directly are more accurately reported than those for which estimates had to be made based on device characteristics and performance [8]. There are also tests in the inventory for which little or no post-test information exists; estimates of radionuclide content for these tests are considerably more uncertain and increase the overall uncertainty for a given nuclide. The accuracy of the estimate of the radionuclide content is highly dependent on the source(s) of the radionuclide information. Therefore, LANL reported the accuracy of the reported inventory as a function of radionuclide groups depending on their source: fission products (~10 to 30%), unspent fuel materials (≤ 20%), fuel activation products (≤ 50%), residual tritium (≤ 300%), and activation products (~ a factor of 10) [8].

5.3 References

1. U.S. Department of Energy, Nevada Operations Office. 2000. *United States Nuclear Tests, July 1945 through September 1992*, DOE/NV-209, Rev. 15. Las Vegas, NV.

2. U.S. Department of Energy, Nevada Operations Office. 1997. *Shaft and Tunnel Nuclear Detonations at the Nevada Test Site: Development of a Primary Database for the Estimation of Potential Interactions with the Regional Groundwater System*.

3. U.S. Department of Energy, National Nuclear Security Administration Nevada Site Office. 2004. *Corrective Action Investigation Plan for Corrective Action Unit 99: Rainier Mesa/Shoshone Mountain, Nevada Test Site, Nevada*, DOE/NV--1031, Revision No.: 0. December. Las Vegas, NV.

4. Townsend, D.R., M. Townsend, and B.L. Ristvet. 2007. *A Geotechnical Perspective on Post-test Data from Underground Nuclear Tests Conducted in Rainier Mesa*, DTRIAC-SR-07-002, DOE/NV/25946-269. 192 p. Defense Threat Reduction Agency, Kirtland AFB, NM.

5. Hu, Q., and M. Zavarin. 2007. *Evaluation of the Rainier Mesa/Shoshone Mountain CAU HST Transport Parameters Based on Solid and Water Sampling*, UCRL-MI-234814, pp. 62. Livermore, CA: Lawrence Livermore National Laboratory.

6. National Security Technologies, LLC. 2007. *A Hydrostratigraphic Model and Alternatives for the Groundwater Flow and Contaminant Transport Model of Corrective Action Unit 99: Rainier Mesa-Shoshone Mountain, Nye County, Nevada*, DOE/NV/29546--146. Las Vegas, NV.

7. Russell, C.E., R.H. French, R.A. Nicholson, J.S. Miller, and S. Benner. 2003. *Letter Report: Evaluation of Monitoring Data from Impounded Water within U12n and U12t Tunnel – Rainier and Aqueduct Mesas, Nevada Test Site.* Division of Hydrologic Sciences, Desert Research Institute, University and Community College System of Nevada. Las Vegas, NV.

8. Bowen, S.M., D.L. Finnegan, J.L. Thompson, C.M. Miller, P.L. Baca, L.F. Olivas, C.G. Geoffrion, D.K. Smith, W. Goishi, B.K. Esser, J.W. Meadows, N. Namboodiri, and J.F. Wild. 2001. *Nevada Test Site Radionuclide Inventory, 1951-1992*, LA-13859-MS. Los Alamos, NM: Los Alamos National Laboratory.

9. Kersting, A.B., D. Finnegan, B. Esser, A. Thompson, D. Smith, M. Zavarin, C. Bruton, and G. Pawloski. Date Unknown. *Radionuclide Decay and In-Growth Technical Basis Document*, UCRL-ID-153798. Los Alamos, NM: Los Alamos National Laboratory.

10. Tompson, A.F.B., M. Zavarin, C.J. Bruton, and G.A. Pawloski. 2004. *Methods for Calculating a Simplified Hydrologic Source Term for Frenchman Flat Sensitivity Studies of Radionuclide Transport Away from Underground Nuclear Tests, UCRL -TR-201817*. Livermore, CA: Lawrence Livermore National Laboratory.

6.0 MATRIX POROSITY

The matrix porosity of a geologic medium is a component of the medium's total porosity. The total porosity is the proportion of void space within the total unit volume of the medium at a representative elementary scale. The porosity of geologic material can be of two types: primary (or interstitial) and secondary. Primary porosity is due to the soil or rock matrix (i.e., matrix porosity), and secondary porosity is due to secondary changes to the rock, such as solution or fracture development (i.e., fracture porosity). If the medium is porous, the matrix porosity can be considered to be approximately equivalent to the total porosity of the medium. In fractured rock, fracture porosity and matrix porosity differ, and matrix porosity becomes a distinct component of the total porosity.

6.1 Role of Matrix Porosity in Contaminant Transport

In unfractured rock, water flows through the rock matrix. In a fractured rock, a dual-porosity conceptualization is typically assumed, where most flow and transport take place through the fractures while diffusive exchange between secondary and primary rock porosity allows the matrix to act as storage for some of the solutes being transported from the fractures into the matrix or from the matrix into the fractures. For most fractured geologic systems, the volume occupied by fractures is a small percentage of the total rock volume; the matrix comprises the majority of the rock volume. In this case, the total porosity and matrix porosity are nearly equivalent. The large reservoir of water in the matrix can be extremely important to radionuclide migration. When matrix pores are well connected through diffusive pathways, a higher radionuclide concentration in fracture water causes the migration of the radionuclide into the matrix, effectively slowing the rate of transport relative to groundwater flow. The matrix porosity, coupled with the matrix diffusion coefficient, controls the rate of diffusion into and out of the matrix.

A large portion of the data used to determine matrix porosity represents total porosity. In most fractured rock aquifers, the total porosity is the sum of matrix porosity and effective or fracture porosity. Fracture porosities are typically less than 1%, whereas matrix porosity may be 25% or more. The total porosity is, therefore, a good estimator of the matrix porosity of fractured rocks in most cases. In the case of unfractured rocks, matrix porosity can be reasonably assumed to be equivalent to total porosity.

Porosity measurement methods for core data typically involve the measurement of dry bulk density, grain density, and saturated water content in the laboratory [1].

6.2 Data Sources and Availability

The matrix porosity data are from 8,088 tunnel and borehole core samples in the RMSM HFM area from the USGS Rock-Property Database [2]. The data are current to the end of fiscal year (FY) 2007 and are presented in Appendix B.

6.3 Data Compilation

The matrix porosity dataset is from the USGS Rock-Property Database generated as part of the FY 2007 data integration task for the UGTA Project [2]. The USGS compiled interval-specific rock-property data for nearly 600 holes drilled or mined on and around the NTS. Rock-property data were taken from reports and historical paper files located at the USGS Las Vegas office, and the USGS Core Library and Data Center in Mercury, Nevada. Records were compiled from a combination of sources, including field notes and forms, memorandums and other internal correspondence, unpublished draft manuscripts and tables, and published reports. Because record reviews ranged from cursory to thorough, some data are preliminary and may be subject to revision. All data used in the quantitative analyses are from the RMSM HFM area; see Appendix B and associated datasets referenced in Section B.2.0.

6.4 Data Analysis

The data consist of measurements of porosity collected since the early 1970s as part of the underground testing containment program. Hydrostratigraphic units were assigned to each porosity value using a query of the RMSM HFM. For sample locations not categorized by HSU, placement within the EarthVision model framework determined the assignments. The basis of the HGU assignments for each porosity value is provided in Table 6-1.

Linear regression plots of HGU porosity as a function of depth in Appendix B show no clear reduction of porosity with depth. Part of the RMSM CAU-scale flow and transport model input parameter selection involves the assignment of the matrix porosity parameters from a probability distribution. To derive the HGU and HSU porosity data probability distributions, cumulative distribution functions (CDFs) were fit to the sample data. The fitting algorithm uses Maximum Likelihood Estimation, a statistical method used to make inferences about parameters of the underlying probability distribution of a given dataset [3]. The fitted distribution parameters do not always exactly reproduce the measured data statistics so the fitted distributions are ranked based on either their chi-squared statistic, Anderson-Darling (A-D) statistic, or Kolmogorov-Smirnov (K-S) statistic. A CDF for the data is chosen based on the most suitable fit statistic for the fitted distribution. Box and whisker plots of the HGU and HSU values are presented in Figures 6-1 and 6-2, and the sample summary statistics with distributions are listed in Table 6-2. Histograms and CDFs of matrix porosity for the RMSM HGUs and HSUs are in the Appendix\B folder on the accompanying DVD.

Table 6-1
HSU to HGU Assignments

HSU	HGU
AA	AA
LCA	CA
LCA3	
UCA	
LCCU	CCU
LCCU1	
UCCU	
MGCU	GCU
RVICU	IICU
KA	LFA
PRETBG	
YMCHLFA	

HSU	HGU
FCCM	LFA, TCU
BFCU	TCU
BRCU	
LTCU	
LTCU1	
OSBCU	
RBCU	
RMBCU	
UTCU	
UTCU1	
UTCU2	

HSU	HGU
CHVTA	VTA
LVTA	
LVTA1	
LVTA2	
PVTA	
TM-LVTA	
TM-UVTA	
BRA	WTA
RVA	
SWA	
TCA	
TMCM	
TM-WTA	
TSA	
TUBA	

6.5 Limitations

Core-derived measurements usually provide the best estimates of matrix porosity in both porous and fractured media if the sample is at least as large as the matrix representative elementary volume (REV). However, the scale of the REV is not generally known. In unconsolidated media (e.g., alluvium), grain size may range from microns to meters (boulders), assumptions about representativeness must be specified, and sample volume will be too small to accurately measure representative matrix porosity. Consequently, estimates of matrix porosity in alluvium may be highly, spatially variable depending on the degree of grain size heterogeneity and anisotropy. Other sources of uncertainty related to laboratory measurement for porosity of core samples are incomplete saturation of the sample (underestimate of matrix porosity) and unconsolidation of the sample resulting from both physical disturbance and reduced lithostatic confining pressure in the laboratory (overestimate of matrix porosity). Site-specific spatial geologic variations, common with volcanic units, were not considered due to the lack of appropriate data. Furthermore, samples collected for the underground testing containment program were not necessarily random but located to specifically sample features of interest for containment studies. Consequently, the resulting distributions based on this data are most likely conservatively biased.

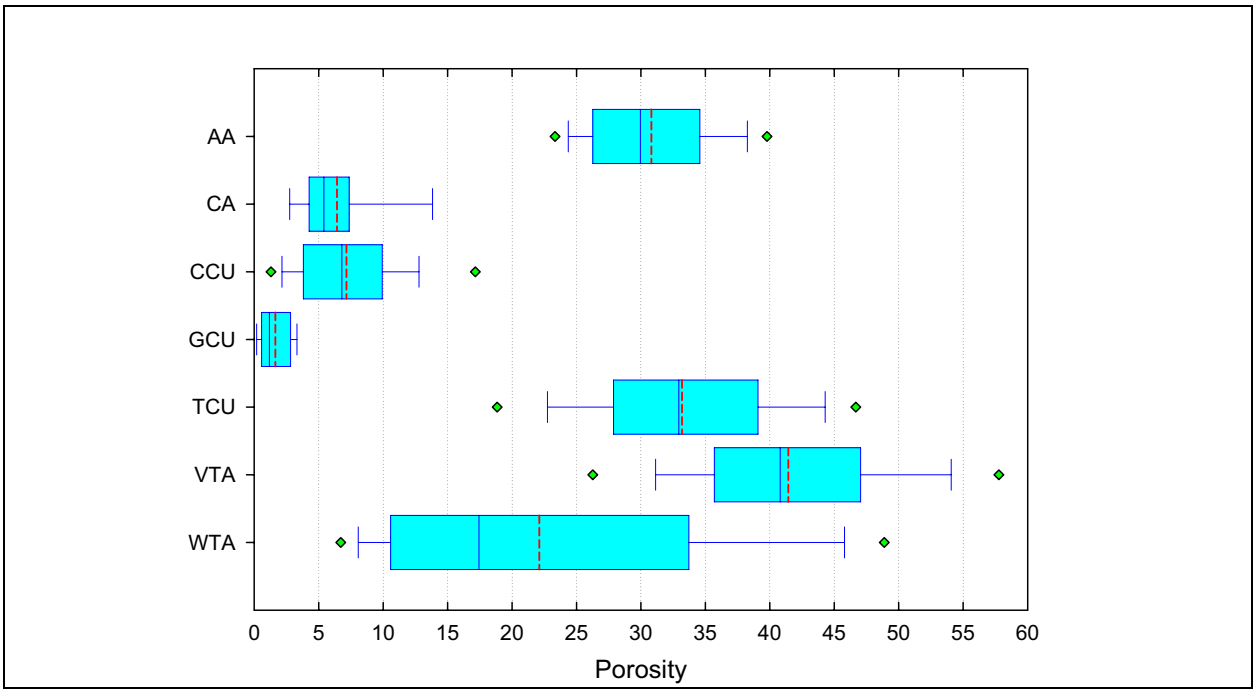

Figure 6-1
Rainier Mesa/Shoshone Mountain HGU Porosity Values

MEAN: Red vertical dashed line; MEDIAN: Blue vertical line in box; 1ST QUARTILE: Left box side; 3RD QUARTILE: Right box side; 10TH PERCENTILE: Left whisker; 90TH PERCENTILE: Right whisker; 5TH PERCENTILE: Left green diamond; 95TH PERCENTILE: Right green diamond

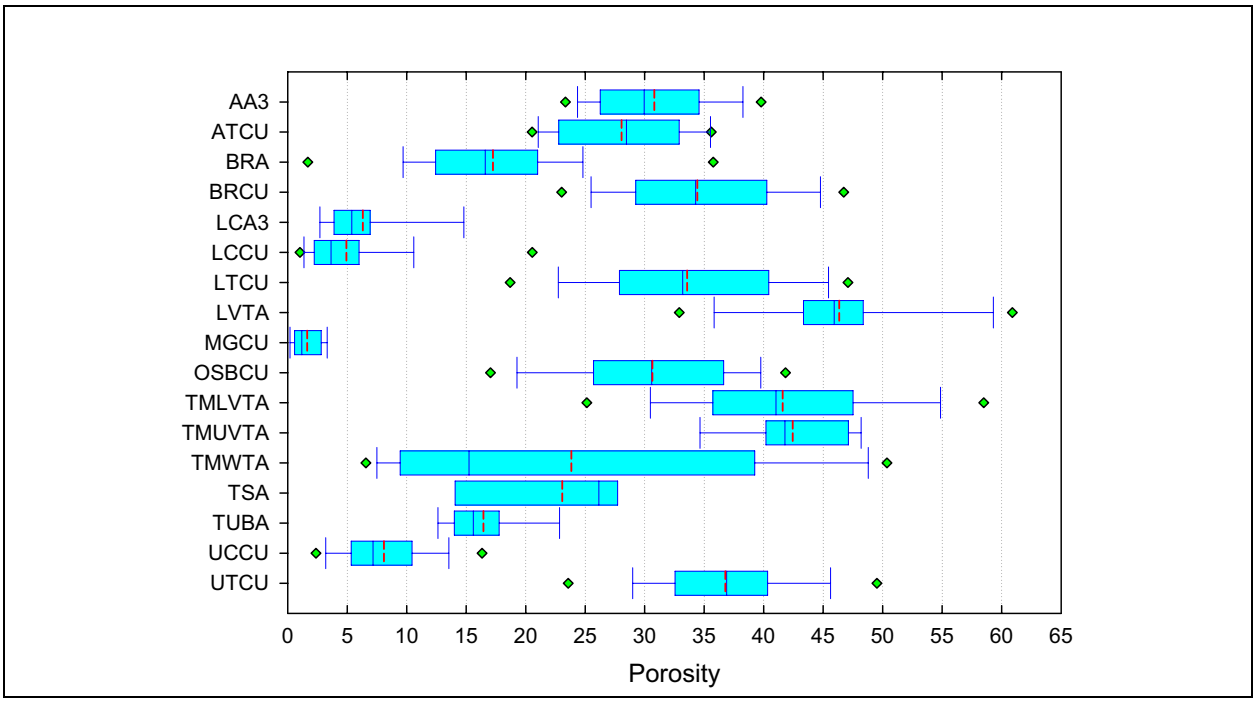

Figure 6-2
Rainier Mesa/Shoshone Mountain HSU Porosity Values

Table 6-2
Sample Summary Statistics for Matrix Porosity

Unit	Mean	Distribution	N	Range	Minimum	Maximum	Median	SD	CV
Hydrogeologic Units									
AA	30.9	Lognormal	100	35.2	21.0	56.2	30.0	5.7	18.6%
CA	6.4	--	14	15.1	2.6	17.7	5.7	--	--
CCU	7.3	Lognormal	77	22.3	0.7	23.0	6.9	4.5	62.0%
GCU	1.3	--	18	3.3	0.0	3.3	1.1	--	--
TCU	35.2	Normal	6467	55.7	2.3	58.0	35.7	6.2	17.5%
VTA	41.3	Normal	852	69.9	0.8	70.8	40.7	9.5	23.0%
WTA	20.5	Triangular	171	52.4	1.7	54.1	15.9	13.1	63.8%
Hydrostratigraphic Units									
AA3	30.9	Lognormal	100	35.2	21.0	56.2	30.0	5.7	18.6%
ATCU	28.1	--	20	15.1	20.5	35.6	28.5	--	--
BRA	17.6	Lognormal	41	45.1	1.7	46.7	16.4	8.1	45.8%
BRCU	35.6	Normal	946	45.3	6.0	51.3	36.2	6.0	16.8%
LCA3	6.4	--	14	15.1	2.6	17.7	5.7	--	--
LCCU1	5.5	Exponential	28	22.0	1.0	23.0	3.8	5.5	100.4%
LTCU	35.5	Normal	4607	55.7	2.3	58.0	35.9	5.9	16.8%
LVTA	46.6	Lognormal	38	28.2	32.8	61.0	46.0	6.8	14.7%
MGCU	1.3	--	18	3.3	0.0	3.3	1.1	--	--
OSBCU	32.3	Normal	657	38.1	12.9	51.0	33.3	6.7	20.8%
TM-LVTA	41.0	Normal	799	69.9	0.8	70.8	40.3	9.6	23.4%
TM-UVTA	42.4	--	15	15.8	33.2	49.0	41.8	--	--
TM-WTA	21.9	Normal	110	48.4	5.7	54.1	15.2	15.2	69.4%
TSA	23.1	--	8	20.8	11.0	31.8	26.1	--	--
TUBA	16.3	--	12	10.3	12.6	22.9	15.3	--	--
UCCU	8.4	Lognormal	49	16.8	0.7	17.6	7.2	3.5	42.3%
UTCU1	36.7	Normal	237	40.0	13.6	53.6	36.6	6.6	18.0%

N = Population size
SD = Standard deviation
CV = Coefficient of variation

6.6 References

1. Stoller-Navarro Joint Venture. 2004. *Transferability of Data Related to the Underground Test Area Project, Nevada Test Site, Nye County, Nevada*, S-N/99205-020. Las Vegas, NV.

2. U.S. Geological Survey. 2007. Mercury Core Library & Data Center Rock-Property Information Rock-Property Database. As accessed at http://nevada.usgs.gov/mercury/rock.html on 3 October. Mercury, NV.

3. Fisher, R.A. 1922. *On the Mathematical Foundations of Theoretical Statistics*. Philosophical Transactions of the Royal Society of London, Ser. A.

7.0 EFFECTIVE POROSITY

Porosity is defined as the total volume of voids per total volume of rock. In geologic material, not all voids transmit water. Therefore, the appropriate porosity for transport modeling is the effective porosity, which is defined as the volume of voids transmitting water (interconnected voids) per total volume of rock. Effective porosity is always less than or equal to total porosity due to the adhesion of water to solids, unconnected pores, and dead-end pores. An NTS-wide summary of effective porosity is compiled in Section 8.0 of the YFCM TDD [1]. The YFCM TDD is included on the accompanying DVD and referenced rather than repeated where practical. Tables containing the ranges of effective porosity are also included in the RMSM_Effective_Porosity.xls workbook in the Appendix\C folder on the accompanying DVD [1].

7.1 The Role of Effective Porosity in Contaminant Transport

The nature of fluid flux through a porous system was first outlined by French engineer Henri Darcy in 1856. Darcy's law states that the volumetric discharge of a porous flow system is equal to the hydraulic conductivity of the media multiplied by the hydraulic gradient and the cross-sectional area perpendicular to flow. The law is described by the equation [2]:

$$q = \frac{Q}{A} = -Ki \qquad (7\text{-}1)$$

where:
q = specific discharge (L/t)
Q = volumetric flow rate (L^3/t)
A = cross-sectional area perpendicular to flow (L^2)
K = hydraulic conductivity (L/t)
i = hydraulic gradient (dimensionless)

In Equation (7-1), the cross-sectional area is the entire surface area, not the surface area of the pore openings. Therefore, the specific discharge in Darcy's law must be divided by the effective porosity to obtain the actual groundwater velocity. The interstitial groundwater velocity is given by the equation [2]:

$$v = \frac{q}{\phi_e} = \frac{Q}{\phi_e A} = -\frac{K}{\phi_e} i \qquad (7\text{-}2)$$

where:
v = interstitial groundwater velocity (L/t)
ϕ_e = effective porosity (dimensionless)

The interstitial velocity is always greater than the specific discharge and decreases with increasing effective porosity. The groundwater velocity, and thus velocity of contaminant migration, in a porous media is governed by Equation (7-2). Therefore, consideration of the effective porosity of a porous media is essential for contaminant transport modeling.

The presence of fractures can have a large effect on the effective porosity of a flow system. Well-connected fractures generally have hydraulic conductivities much higher than the surrounding matrix, which creates preferential flow paths through the system. Typically, these systems are treated as dual-porosity systems in which all flow is assumed to be in the fractures with diffusive interaction with the matrix.

7.2 Data Compilation and Evaluation

Effective porosity is evaluated using framework of the HGU and HSU system of the RMSM HFM [3]. The HGUs categorize lithologic types by their ability to transmit water. The HSUs are groupings of contiguous stratigraphic units having a particular hydrogeologic character, such as an aquifer or confining unit. Most HSUs either consist of a single HGU or have one HGU dominating the composition. Details of the HFM system for RMSM are outlined in the RMSM HFM [3]. This document heavily references Section 8.0 of the YFCM TDD, which is included on the accompanying DVD. It is suggested that users familiarize themselves with the data and recommendations it contains. The fractured volcanic units data discussed are transferred from other locations on the NTS and also applicable to RMSM. Many of the other units in RMSM are analogous to those in Yucca Flat. Other sources of data are recommended in this section for units that are not directly comparable nor discussed in the YFCM TDD.

Effective porosities for RMSM are summarized here by HGU. The first step in investigating the effective porosity for an HGU is to assess whether it behaves as porous media or fractured media. If it behaves as porous media, the effective porosity for the HGU is assumed to be represented by a portion of the matrix porosity discussed in Section 6.0. The portion varies depending on the type of sediments, grain size, and cementation or welding as discussed in the introduction to Section 8.0 of the YFCM TDD [1]. If it behaved as fractured media, fracture porosities from available sources were compiled and evaluated, and a distribution developed. For fractured media, the effective porosity is assumed to be the same as the fracture porosity.

For most of the HGUs, there are multiple sources of effective porosity information. To assign an effective porosity to an HGU, the quality and suitability of the data sources for the unit is evaluated and compared to other sources. The HGU effective porosity estimates and uncertainty are recommended based on the associated strengths and weaknesses of different sources.

7.3 Effective Porosity for the Aquifer Hydrogeologic Units

The hydrostratigraphic model of RMSM has five HGU types (AA, WTA, VTA, LFA, and CA) classified as aquifers.

7.3.1 The Alluvial Aquifer Hydrogeologic Unit

The AA consists of unconsolidated to partially consolidated sandy gravel and gravelly sand. The source of these sediments is erosion of the surrounding mountains during basin development. Interspersed within these coarser-grained alluvial deposits are finer-grained eolian sands and silts. The AA HSU corresponds to the AA HGU in the RMSM area.

This loosely consolidated aquifer is not fractured; therefore, flow through it is diffuse, and the effective porosity is assumed to be a fraction of the matrix porosity. The recommended matrix porosity distribution for the AA HGU is discussed in Section 6.0. Because loosely consolidated sediments comprise this HGU, the effective porosity ranges from 80 to 100% of the matrix porosity [1, 4-8].

7.3.2 The Welded-Tuff Aquifer Hydrogeologic Unit

The WTA HGU is characterized by aquifers consisting predominately of welded tuffs [1, 3, 9]. In the RMSM area, the WTA HGU is the dominant composition of nine HSUs (TM-WTA, TMCM, TCA, TSA, SWA, BRA, TUBA, RVA, and TPA). The WTA HGU will be treated as a dual-porosity medium in the RMSM CAU flow and transport model due to its fractured nature. To appropriately represent the WTA HGU in the CAU-scale model, the recommended distribution for the effective porosity must be consistent with this conceptualization.

There are no new sources of effective porosity data for the WTA HGU, so the data sources evaluated and discussed for the evaluation of effective porosity in Section 8.0 of the YFCM TDD will be used for the RMSM CAU [1].

7.3.3 The Vitric-Tuff Aquifer Hydrogeologic Unit

The VTA HGU is characterized by aquifers consisting predominately of nonzeolitized, nonwelded ash-flow and bedded tuff [1, 3]. In the RMSM area, the VTA HGU is the dominant composition of seven HSUs (TM-UVTA, TM-LVTA, PVTA, LVTA, CHVTA, LVTA2, and LVTA1). Flow through the VTA is considered to be diffuse rather than fracture dominated due to the lack of open fractures and the high interstitial porosity. As a result, the effective porosity is considered to be a fraction of the matrix porosity for this HGU. Details regarding the recommended matrix porosity distribution for the VTA HGU at Yucca Flat are provided in Section 7.0 of the YFCM TDD [1]. The effective porosity of this HGU ranges from 80 to 100% of the matrix porosity because the VTA HGU is only slightly welded and has a soft, friable nature [1, 4-8].

7.3.4 The Lava-Flow Aquifer Hydrogeologic Unit

The LFA HGU is characterized by aquifers consisting predominately of lava flows [1, 3]. In the RMSM area, the LFA HGU is the dominant composition of three HSUs (FCCM, YMCHLFA, and KA). The LFA HGU will be treated as a double-porosity medium in the YFCM CAU flow and transport model due to its fractured nature. To appropriately represent the WTA HGU in the

CAU-scale model, the recommended distribution for the effective porosity must be consistent with this conceptualization.

A number of data sources are evaluated and discussed for the evaluation of effective porosity in Section 8.0 of the YFCM TDD [1]. There are no new sources of effective porosity data for the LFA HGU that have become available since the compilation of the YFCM TDD; thus, the data from the YFCM TDD will be used.

7.3.5 The Carbonate Aquifer Hydrogeologic Unit

The CA HGU consists of limestone and dolomite rocks having low interstitial porosities and form fractured aquifers [10]. In the RMSM area, the CA HGU is the dominant composition of three HSUs (LCA3, UCA, and LCA). The CA HGU will be treated as a dual-porosity medium in the flow and transport model of the RMSM CAU due to its fractured nature.

There are no new sources of effective porosity data for the CA HGU, so the data sources evaluated and discussed in detail for the evaluation of effective porosity in Section 8.5.5 of the YFCM TDD will be used [1].

7.4 Effective Porosity of the Confining Unit Hydrogeologic Units

There are four confining unit HGUs (TCU, CCU, GCU, and IICU) in the RMSM model area.

7.4.1 The Tuff Confining Unit

The TCU HGU consists predominately of zeolitized nonwelded tuffs. A distinguishing characteristic of the TCU HGU is the extensive zeolitization that substantially decreases the permeability of the unit. Zeolitization diagenesis also tends to decrease the overall porosity of the TCU HGU [11]. The TCU HGU is the dominant composition of 11 HSUs (RMBCU, SCVCU, UTCU, UTCU2, BFCU, UTCU1, BRCU, LTCU, OSBCU, LTCU1, and ATCU).

Although open fractures are present in the TCU HGU, the hydraulic connection is typically poor. Aquifer tests in the unit and discharge data from the tunnels in Rainier and Aqueduct Mesas show fractured zones initially yield more water than the surrounding matrix, but the yield of these zones decreases rapidly as fractures are depressurized. Flow through the unit is probably controlled by interstitial permeability rather than fracture transmissibility [10].

Because of the lack of fracture flow within the TCU HGU, the effective porosity for this HGU is assumed to be represented by a fraction of the matrix porosity. The recommended matrix porosity distribution for the TCU HGU is in Section 6.0. The effective porosity ranges from 50 to 80% of the matrix porosity due to the fine-grained nature and types of material present. Therefore, the recommended distribution for the effective porosity of the TCU HGU is 50 to 80% of the recommended matrix porosity distribution [1, 4-8].

7.4.2 The Clastic Confining Unit

The CCU HGU consists of siliciclastic sedimentary rocks, quartzite, and shale. Although some fractures are found within the CCU, they tend to be either healed or sealed. Winograd and Thordarson report that fractures observed in core from this HGU in a Yucca Flat well were "tightly sealed either by selvage minerals or by quartz or calcite veinlets, or by virtue of their never having been opened" [10]. They also state the porous, fine-grained rock (i.e., shale) found in the CCU typically deform plastically, which limits development of open fractures. These porous, fine-grained rocks will also tend to seal or isolate fractures developed in the dense quartzite [10]. Regional flow in this HGU is most likely controlled by small-scale fractures combined with interstitial permeability rather than fracture transmissibility [10]. There are three HSUs in the RMSM area having the CCU HGU as the dominant composition (UCCU, LCCU1, and LCCU).

The effective porosity of the CCU HGU is considered to be a fraction of the matrix porosity due to the lack of interconnected fractures. The matrix porosity for this HGU is in Section 6.0 with the distribution recommended for the CAU-scale model. Based on the types of sediments found in this HGU, the effective porosity ranges from 50 to 90% of the matrix porosity. Therefore, the recommended effective porosity distribution for the CCU HGU is 50 to 90% of the recommended matrix porosity distribution [1, 4-8].

7.4.3 The Granite Confining Unit

The GCU HGU consists of the granodiorite and quartz monzonite Climax and Gold Meadows stocks. A single HSU (MGCU) comprises the GCU that is saturated at depth and has low intergranular porosity and low permeability.

Although the unit has been studied extensively at the Climax Mine, little quantitative information was found about the aperture of fractures in the unit [12-18]. Total porosity is roughly estimated to average 0.9% with interstitial porosity accounting for less than 0.4% from borehole cores in the Climax stock [19].

Lee and Farmer show fracture porosity typically ranges from 0.0005% to 0.05% for clastic, metavolcanic, and crystalline rocks [20]. At the Stripa site, in Sweden, the flow porosity is in the range of 0.001% to 0.02% [21-24]. The Stripa site is the most thoroughly studied flow system in fractured crystalline rock that was found during the literature review.

7.4.4 The Intra-caldera Intrusive Confining Unit

The IICU HGU comprises rocks deep beneath the calderas on the western side of the HFM model. The HSUs composed of this HGU are not penetrated by drill hole and are not exposed in outcrop, so the nature of these units is conjectural. It is assumed the HGU is analogous to the GCU HGU, which also is intrusive crystalline rock.

Crystalline intrusive rocks have very low interstitial porosities and permeabilities, so flow through the unit is likely controlled by fracturing. The greater depth and corresponding increase in lithostatic pressure of these units could cause fracture behavior to differ from the GCU observations. Low effective porosities in the unit should be accompanied by low hydraulic conductivities as hydraulic conductivity is expected to be controlled by fracturing.

7.5 References

1. Stoller-Navarro Joint Venture. 2007. *Phase I Contaminant Transport Parameters for the Groundwater Flow and Contaminant Transport Model of Corrective Action Unit 97: Yucca Flat/Climax Mine, Nevada Test Site, Nye County, Nevada*, Revision No. 0, S-N/99205--096. Las Vegas, NV.

2. Domenico, P.A., and F.W. Schwartz. 1990. *Physical and Chemical Hydrogeology,* 2nd Edition New York, NY: John Wiley & Sons.

3. National Security Technologies, LLC. 2007. *A Hydrostratigraphic Model and Alternatives for the Groundwater Flow and Contaminant Transport Model of Corrective Action Unit 99: Rainier Mesa-Shoshone Mountain, Nye County, Nevada*, DOE/NV/29546--146. Las Vegas, NV.

4. de Marsily, G. 1986. *Quantitative Hydrogeology.* Orlando, FL: Academic Press Inc.

5. Bradley, H.B., Ed. 1992. *Petroleum Engineering Handbook.* Richardson, TX: Society of Petroleum Engineers.

6. Castany, G. 1967. *Traité Pratique des Eaux Souterraines.* Paris, France: Dunod.

7. van der Kamp, G., D.R. Van Stempvoort, and L.I. Wassenaar. 1996. "The Radial Diffusion Method 1. Using Intact Cores to Determine Isotopic Composition, Chemistry, and Effective Porosities for Groundwater in Aquitards." In *Water Resources Research,* Vol. 32 (6): 1815-1822.

8. Hudak, P.F. 1994. "Effective Porosity of Unconsolidated Sand; Estimation and Impact on Capture Zone Geometry." In *Environmental Geology,* Vol. 24(2): 140-143.

9. Winograd, I.J. 1971. "Hydrogeology of Ash Flow Tuff: A Preliminary Statement." In *Water Resources Research,* Vol. 7(4): 994-1006.

10. Winograd, I.J., and W. Thordarson. 1975. *Hydrogeologic and Hydrochemical Framework, South-Central Great Basin, Nevada-California, with Special Reference to the Nevada Test Site,* USGS-PP-712-C. Denver, CO: U.S. Geological Survey.

11. Moncure, G.K., R.C. Surdam, and H.L. McKague. 1981. "Zeolite Diagenesis Below Pahute Mesa, Nevada Test Site." In *Clays and Clay Minerals,* Vol. 29(5): 385-396. Washington, DC: The Clay Minerals Society.

12. U.S. Geological Survey. 1983. *Geological and Geophysical Investigations of Climax Stock Intrusive, Nevada*, USGS-OFR-83-377. Denver, CO: U.S. Geological Survey.

13. Wilder, D.G. 1986. *Influence of Stress-Induced Deformations on Observed Water Flow in Fractures at the Climax Granitic Stock*, Rev.1, UCRL-95539. Livermore, CA: Lawrence Livermore National Laboratory.

14. Isherwood, D., E. Raber, R. Stone, D. Lord, N. Rector, and R. Failor. 1982. *Engineering Test Plan for Field Radionuclide Migration Experiments in Climax Granite*, UCRL-53286. Livermore, CA: Lawrence Livermore National Laboratory.

15. Thorpe, R.K. 1984. *An Analysis of Fracturing In Hole UG-2, Spent Fuel Test - Climax.* Livermore, CA: Lawrence Livermore National Laboratory.

16. Wilder D.G., and J.L. Yow, Jr. 1981. *Fracture Mapping at the Spent Fuel Test-Climax*, UCRL-53201. Livermore, CA: Lawrence Livermore National Laboratory.

17. Yow, Jr., J.L. 1984. *Geologic Structure Mapping Database, Spent Fuel Test-Climax, Nevada Test Site.* Livermore, CA: Lawrence Livermore National Laboratory.

18. Maldonado, F. 1977. *Summary of the Geology and Physical Properties of the Climax Stock, Nevada Test Site*, USGS-OFR-77-356. Denver, CO: U.S. Geological Survey.

19. Walker, G.E. 1962. *Ground Water in the Climax Stock, Nevada Test Site, Nye County, Nevada*, USGS-TEI-813. Denver, CO: U.S. Geological Survey.

20. Lee, C.H., and I. Farmer. 1993. *Fluid Flow in Discontinuous Rocks.* London, UK: Chapman and Hall.

21. Neretnieks, I., H. Abelin, and L. Birgersson. 1989. "Some Recent Observations of Channeling in Fractured Rocks - Its Potential Impact on Radionuclide Migration." In *Proceedings of the Conference on Geostatistical, Sensitivity, and Uncertainty Methods for Ground-Water Flow and Radionuclide Transport Modeling*, held September 15-17, 1987. CONF-870971: 387-410. San Francisco, CA: Battelle Press.

22. Rasmuson, A., and I. Neretnieks. 1986. "Radionuclide Transport in Fast Channels in Crystalline Rock." In *Water Resources Research*, Vol 22, No 8, pp. 1247-1256. August.

23. Birgersson, L., L. Moreno, I. Neretnieks, H. Widén, T. Ågren. 1993. "A Tracer Migration Experiment in a Small Fracture Zone in Granite." In *Water Resources Research*, Vol 29, No 12, pp. 3867-3878. December.

24. Neretnieks, I., T. Eriksen, and P. Tahtinen. 1982. "Tracer Movement in a Single Fissure in Granitic Rock: Some Experimental Results and Their Interpretation." In *Water Resources Research*, Vol. 18(4): 849-858.

8.0 DISPERSIVITY

Conceptually, for modeling contaminant transport at field scale, dispersivity is not a characteristic property of the geologic system but rather is a modeling parameter that accounts for the unmeasured and/or unspecified variability in the hydraulic properties within the flow and transport model domain. Dispersivity is often observed to be scale-dependent (i.e., a function of mean travel distance of solutes). Representative dispersivity values (at specific transport scales) are typically derived from data collected during tracer tests, and from model calibration of contaminant plumes and geochemical or environmental isotope distributions in regional flow systems. For additional discussion on the role of dispersion in contaminant transport, refer to the technical basis document entitled, *The Role of Dispersion in Radionuclide Transport - Data and Modeling Requirements* [1].

8.1 Role of Dispersion in Contaminant Transport

Unlike molecular diffusion (see Section 9.0), an inherent property of a solute in water, mechanical dispersion arises from the complex and heterogeneous movement of water and solute particles through an intricate network of pores and fractures. In the simplest terms, dispersion is the process of spreading a solute over a volume that is larger than it would be predicted based on estimates of the mean groundwater velocity. Because, in practice, the results of mechanical dispersion and molecular diffusion are not easily separable, hydrodynamic dispersion is defined as a combined effect of both processes. Freeze and Cherry write the following general relationship for the hydrodynamic dispersion coefficient for one-dimension transport [2]:

$$D = \alpha V + D_d \qquad (8\text{-}1)$$

where:
D = hydrodynamic dispersion coefficient (L^2/t)
α = dispersivity (L)
V = average groundwater flow velocity (L/t)
D_d = coefficient of molecular diffusion (L^2/t) for the solute in the porous medium

A conceptual understanding of mechanical dispersion along individual conduits can enhance the understanding of the processes involved. At relatively small scales in porous media, mechanical dispersion is the result of the velocity distribution in the pore spaces, changes in direction of flow, and variation in mean velocity as fluid moves from one pore space to the next. Mechanical dispersion in fractured networks can grow complicated as mixing occurs in preferential pathways. One might visualize the complicated system of fractures where fractures with varying dip and strike, aperture thickness, and aperture surface roughness are encountered in geologic systems such as that of the RMSM CAU. At larger scales, dispersion is controlled by the spreading caused by the heterogeneous nature of the geologic system.

The effect of dispersion during transport of solutes in geologic systems is commonly quantified in terms of longitudinal and transverse dispersivities. Longitudinal dispersivity is defined relative to the direction of flow, whereas transverse dispersivity is defined relative to directions normal to the flow direction. Determination of appropriate values for these dispersivities is important for predicting contaminant concentrations in groundwater flow systems. These parameters affect the spreading of contaminants at a macroscopic scale. Theoretically, hydrodynamic dispersion is independent of the scale of measurement as long as the measurement is made within a representative elementary volume [3, 4]. However, in reality, the representative elementary volume changes with the size of the transport scale because the heterogeneity introduced in the expanded domain results in larger overall dispersivity values.

Dispersivities estimated from laboratory experiments are found to be much smaller that those determined for field conditions. Dispersivity values representative of field conditions are derived in the literature from data collected during tracer experiments or observations of plume migration, geochemical data, and environmental isotope data. Field-scale dispersion observed in large-scale plumes or geochemical/isotope data is generally accepted to be the result of the heterogeneous velocity field at scales smaller than the plume or scale of investigation. Heterogeneity at scales larger than the plume causes changes in the mean position of the plume; however, if the plume encompasses several heterogeneous domains, the result may appear as a larger dispersivity. The nature of heterogeneity differs from site to site. Dispersivity values may vary by orders of magnitude depending on the nature of the site and the transport scale of interest. Unless the transport properties of each of the domains are characterized in detail, a lumped dispersivity value may be used to simulate the plume.

Based on data from studies in a variety of geologic settings, dispersivity appears to be scale-dependent [5-12]. The scale/dispersivity relationship is not linear [13].

Field-scale tracer tests are typically limited to a few hundred meters in scale, so experimentally derived dispersivity values are available only for relatively short transport distances as compared to the transport distances of interest for predictions of long-term contaminant transport. Dispersivity data for larger scales have been determined at some sites through transport model calibration to observations of concentration distribution within contamination plumes. With a site as large and as varied as the RMSM CAU, it is impractical to conduct tracer tests in enough locations to accurately estimate dispersivity, particularly at a physical scale representative of transport for the 1,000-year period of interest. Tracer tests conducted at scales of a few tens to hundreds of meters will not yield dispersivity values appropriate at the CAU scale because of the apparent trends in dispersivity with scale. Time and budget constraints make it nearly impossible to perform a tracer test at the CAU scale. Thus, the appropriate dispersivity values to use for the CAU-scale modeling will depend on the expected distance of transport. As a result, it is helpful to know the expected distances of contaminant transport *a priori* to best assess the range of dispersivity values most appropriate for modeling efforts. Future RMSM CAU modeling activities will provide information about expected radionuclide transport paths and distances from source locations of interest. Based on the estimated distances, expected values and bounds of dispersivities may be estimated using the statistical relationships developed from this study. These bounds and statistical parameters will also be useful in uncertainty analysis for transport of contaminants.

8.2 Data Compilation and Transfer

Data from the YFCM HFM area and from other NTS CAUs, YMP, and Nye County were used for this analysis due to the unavailability of comprehensive data from the RMSM HFM area for all HGUs. All data locations used in quantitative analyses are identified in the dataset, and individual discussions of the applicability of the transferred data are provided for each HGU. There are limited data from the NTS area to determine a RMSM-specific distribution for the parameter values. Data from literature for locations worldwide were used to evaluate the NTS area data with respect to the general distribution of dispersivity and scale dependence. A quantitative assessment of the sensitivity of transport modeling to the uncertainty in this parameter cannot be provided before the transport model development. The parameter description discusses the importance of this parameter.

8.2.1 Data Types and Sources

Dispersivity values are derived from interpretation of tracer tests, studies of contaminant plume migration studies of geochemical data, or studies of environmental isotopes. The types of data used to document dispersivity include the location of the site, primary lithology of the rocks, identity of the tracer or contaminant that migrated, transport scale, data analysis method, dispersivity interpretation results, and data source.

Dispersivity data have been determined from one Radionuclide Migration (RNM) investigation (CAMBRIC) and several tracer tests conducted at or near the NTS. These studies were conducted at the following sites (Figure 8-1):

- CAMBRIC site, Frenchman Flat, NTS
- BULLION Forced-Gradient Experiment (FGE), Pahute Mesa, NTS
- C-holes Complex, Yucca Mountain
- Amargosa Tracer Calibration Site, Amargosa Desert, Nevada
- C-Well Site, Yucca Flat, NTS
- ER-6-1 Well Cluster, Yucca Flat, NTS
- Nye County Early Warning Drilling Program (NC-EWDP) Site 22, Fortymile Wash, NTS

Additional data available from non-NTS sites were obtained from the scientific literature. Gelhar et al. published a critical review of data on field-scale dispersion in aquifers, reporting data from 59 field sites [5]. The most recent literature summary of laboratory and field dispersivity data is compiled by Schulze-Makuch [12]. He states that he has summarized data from 109 authors, including those summarized in Gelhar et al. [5]. These sources and other investigations reported in the scientific literature were used to supplement the tracer test data from the NTS and vicinity to develop a dataset of dispersivity versus scale.

8.2.2 Data Documentation Evaluation

The data documentation evaluation flag (DDE_F) was assigned to the records based on the level of reliability and the amount of documentation available. An explanation of DDE_F is included in the RMSM_Dispersivity_Data.xls workbook in the Appendix\D folder on the accompanying DVD.

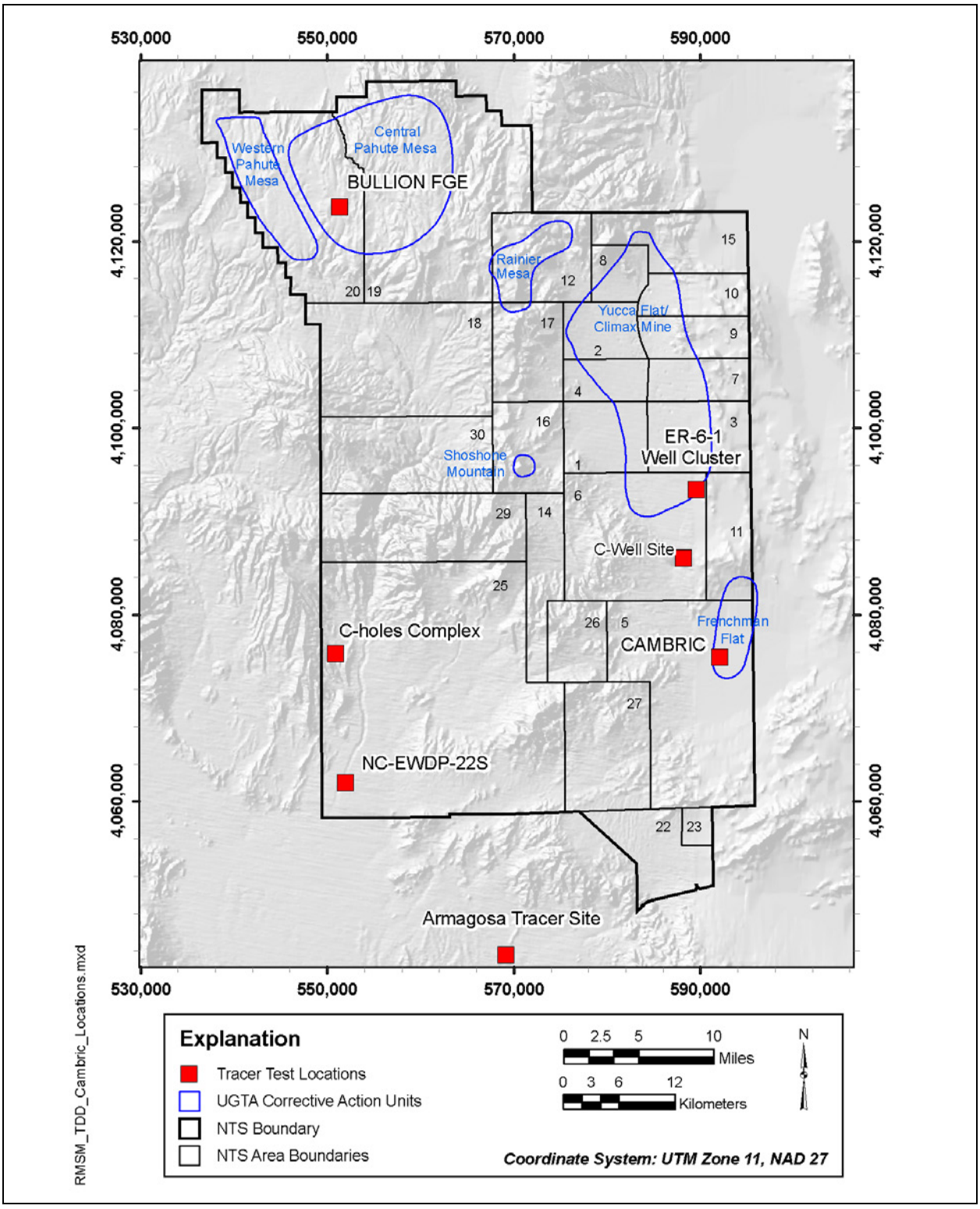

Figure 8-1
Locations of CAMBRIC Radionuclide Migration Experiment and Tracer Tests at NTS and Vicinity
Source: [14]

The BULLION FGE and the ER-6-1 Well Cluster multiple-well tracer tests are the only tracer tests conducted under the Environmental Restoration Project (ERP). These tests were conducted following an established quality assurance program, and the data were assigned a DDE_F of 1 because adequate documentation is available. Documentation of the experiments conducted at the CAMBRIC site and the C-holes Complex of Yucca Mountain were assigned a DDE_F of 1. At the Waste Isolation Pilot Plant (WIPP) site, the data were assigned a level of 3 as these tests were conducted outside of the ERP but are well documented under a Nuclear Quality Assurance (NQA)-1 program. The DDE_F for the tracer tests conducted at Amargosa Desert was assigned a level of 4 as the data were not documented under an NQA-1 program. All other data were assigned a DDE_F of 5 as sufficient documentation of the procedures and their application during field data collection and analysis are not readily available.

8.3 Data Evaluation

The data evaluation approach consisted of summarizing the existing NTS and vicinity studies, including the range of dispersivity values obtained by different investigators. Data from dispersivity studies available in the scientific literature were also incorporated to determine a range of values appropriate for the scales of interest for the RMSM CAU transport modeling effort. The dispersivity data derived from tracer tests and observations of plume migration, geochemical data, or environmental isotope data were compiled into a comprehensive dataset. The dataset includes 188 records for longitudinal dispersivity. A subset of the data sources reporting longitudinal dispersivity also provides transverse dispersivity data.

8.3.1 NTS and Vicinity Dispersivity Data

This subsection summarizes dispersivities obtained from the RNM experiment and tracer tests conducted to date at the NTS and vicinity. Results derived from the migration and tracer tests data using different interpretation approaches are included. The data for these experiments are summarized in Table 8-1. There are several differences between this table and the corresponding table presented in Table 9-1 of the YFCM TDD [14]. In several cases, original sources were found to contain slightly different values than the summary source referenced in that document. In other cases, the original range of values rather than average values are now reported. This supports the use of the geometric mean for analysis. Further information and discussion on the test sites, experimental methods, interpretation approaches, and interpreted dispersivity results for the CAMBRIC site, BULLION FGE, C-holes Complex, Amargosa Tracer Calibration Site, and C-Well Site were presented and discussed in detail in *Phase II Contaminant Transport Parameters for the Groundwater Flow and Contaminant Transport Model for Corrective Action Unit 98: Frenchman Flat, Nye County, Nevada* [13]. Summary descriptions and discussions for the tracer tests conducted more recently at the NC-EWDP Site 22 and ER-6-1 Well Cluster and their interpreted dispersivities were presented in *Phase I Contaminant Transport Parameters for the Groundwater Flow and Contaminant Transport Model for Corrective Action Unit 97: Yucca Flat/Climax Mine, Nye County, Nevada* [14].

Table 8-1
Dispersivity Information Summary from Studies at the Nevada Test Site and Vicinity
(Page 1 of 2)

Site Location	Test Site Geology	Scale of Test (m)	Test Method	Tracers	Analysis Method	Longitudinal Dispersivity (m)	Reference
CAMBRIC Test, Frenchman Flat, Nevada	Tuffaceous Alluvium	91	Radial converging	Nuclear test radionuclides: tritium	Sauty, 1980 [15]	2.0	[16]
				Nuclear test radionuclides: tritium	Sauty, 1980 [15]	9.1	[17]
				Nuclear test radionuclides: tritium	Sauty, 1980 [15]	15.1	[18, 19]
				Nuclear test radionuclides: Cl-36, tritium	Welty and Gelhar, 1989 [20]	3.1 - 9.6	[14, 21]
BULLION FGE, Pahute Mesa, Nevada	Fractured Lava-Flow Aquifer, Calico Hills Formation	130.2	Radial converging	PFBA, DFBA, I, CML, polystyrene microspheres	MODFLOWT calibration	10 (horizontal) 3 (horizontal transverse) 2 (vertical transverse)	[22]
		41.5 - 130.2			RELAP (Reimus and Haga, 1999) [23]	8.7 - 25.3	[22]
		88.7 - 130.2			Welty and Gelhar, 1989 [20]	3.9 - NA [a]	[14]
C-holes Complex, Yucca Mountain, Nevada	Prow Pass Tuff (fractured)	30	Unbalanced dipole	TFBA, I	Moench, 1989 [24]	0.27 [b]	[25]
				PFBA, Br^-, Cl^-, Li	RELAP (Reimus and Haga, 1999) [23]	0.3 - 33.3	[25]
				TFBA, PFBA, Cl^-	Welty and Gelhar, 1989 [20]	1.7 - 8.6	[14]
	Bullfrog Tuff (fractured)	30	Unbalanced dipole	PFBA, Br^-, Li	RELAP (Reimus and Haga, 1999) [23]	3.2 - 18.8	[25]
				PFBA	Welty and Gelhar, 1989 [20]	0.8 - 2.6	[14]
				DFBA	Moench, 1989 [24]	1.9 - 2.4	[25]
Amargosa Tracer Calibration Site, Amargosa Desert, Nevada	Cambrian Bonanza King Dolomite (fractured)	122.8	Doublet recirculating	tritium, S-25, Br^-	Grove, 1977 [26]	15 - 30.5	[27]

Table 8-1
Dispersivity Information Summary from Studies at the Nevada Test Site and Vicinity
(Page 2 of 2)

Site Location	Test Site Geology	Scale of Test (m)	Test Method	Tracers	Analysis Method	Longitudinal Dispersivity (m)	Reference
ER-6-1 Well Cluster	Fractured Limestone	NR	Radial converging	2,4,5-TFBA, I (lower zone)	RELAP (Reimus and Haga, 1999) [23]	34 - 36	[28]
		64.1		2,4,5-TFBA, I (lower zone)	Welty and Gelhar, 1989 [20]	3.0 - 11.1	[14]
		NR		PFBA (upper zone)	RELAP (Reimus and Haga, 1999) [23]	22	[28]
		64.1		PFBA (upper zone)	Welty and Gelhar, 1989 [20]	3.0 - NA [a]	[14]
NC-EWDP Site 22	Alluvium	18	Radial converging	2,4,5-TFBA, DFBA	RELAP (Reimus and Haga, 1999) [23]	2.7 - 5	[29]
					Moench, 1989 and 1995 [24, 30]	0.3 - 3	[31]
					Welty and Gelhar, 1989 [20]	0.8 - 3.6	[14]

[a] NA refers to case where falling limb of breakthrough curve was insufficient to allow calculation of dispersivity estimate using the equation from [20] that requires both rising and falling limbs of the breakthrough curve.

[b] The interpretation accounted for plume spreading by assuming a long, slow release of tracer from the injection well and, therefore, it was not necessary to invoke strong dispersion in the aquifer.

NR = Not reported

8.3.2 Non-NTS Dispersivity Data

Dispersivity data are available for many locations outside the NTS from the scientific literature [5, 12]. These references provide detailed tables summarizing dispersivities, scale of transport, and other relevant information describing studies for both tracer tests and contaminant or environmental tracer transport modeling investigations. In addition, dispersivity data interpreted and published in the scientific literature from other tracer tests and modeling studies have been included in the dataset for use in developing a relationship between dispersivity and scale of transport for the RMSM CAU.

Gelhar et al. reviewed dispersivity observations from 59 different field sites worldwide [5]. Their review included tabulated information on site location, description of aquifer material, average aquifer saturated thickness, hydraulic properties, effective porosity, mean pore velocity, flow configuration, dimensionality of monitoring network, tracer type, method of data interpretation, overall scale of observation, and longitudinal and transverse dispersivities from original sources. The dispersivity data were classified into three reliability classes corresponding to the data reliability evaluation flags described in Section 8.3.3. They found that, at a given scale, dispersivity varied over several orders of magnitude, with the higher-reliability data tending to be in the lower part of the dispersivity range. Neuman noted that part of the large scatter is due to experimental and interpretive errors [7]. An example of an interpretation issue that can lead to apparent scaling of dispersivity is discussed by Domenico and Robbins [32], where they present calculations showing that interpreted dispersivity will be scaled larger whenever an (*n-1*)-dimensional model is calibrated to describe transport in an *n*-dimensional system.

Analyses by various authors indicate a trend of systematic increase in the longitudinal dispersivity with increase in the observation scale. The longitudinal dispersivities reported by Gelhar et al. ranged from 10^{-2} to 10^{4} m for travel distances ranging from 10^{-1} to 10^{5} m; however, the largest distance with high-reliability data was only 250 m, and the largest high-reliability longitudinal dispersivity was only 4 m [5]. They concluded from the data that, overall, dispersivity values tended to scatter over a similar range for both porous and fractured media.

Schulze-Makuch [12] gathered data from additional sources and added to those data presented by Gelhar et al. [5]. He presents 184 additional dispersivity values from 39 authors in a similar fashion to that of Gelhar et al. [5]. An evaluation of some of the data summarized by Schulze-Makuch had revealed a number of discrepancies as discussed in the YFCM TDD [14]. The accuracy of the reported dispersivities and scales of transport tabulated in Gelhar et al. [5] and Schulze-Makuch [12] was examined for all those references that could be readily obtained and not already checked for the dispersivity dataset developed for the YFCM CAU, and the database was updated. Although included in the database for the YFCM CAU, data for studies where the interpreted longitudinal dispersivity was greater than the transport scale were removed from the database for the RMSM CAU. These very large longitudinal dispersivities are considered unrepresentative for modeling studies where some degree of the variability in hydraulic properties is incorporated in the transport model, as will be the case for the RMSM CAU flow and transport model.

8.3.3 Data Quality Evaluation

The dataset developed for the RMSM CAU includes a data quality evaluation flag (DQE_F) that corresponds to the levels of reliability defined by Gelhar et al. [5] and later adopted by Schulze-Makuch [12]. The reliability levels were defined using the following criteria:

- Level 1: Corresponds to "High Reliability," Level I of Gelhar et al. [5]. The tracer study meets the following criteria: (1) tracer test was either ambient flow, radial diverging flow, or two-well instantaneous pulse test without recirculation; (2) tracer input was well defined; (3) tracer was conservative; (4) spatial dimensionality of the tracer concentration measurements was appropriate; and (5) analysis of the tracer concentration data was appropriate and consistent with the measurements.
- Level 2: Corresponds to "Intermediate Reliability," Level II of Gelhar et al. [5]. The tracer study does not meet the criteria for high or low reliability.
- Level 3: Corresponds to "Low Reliability," Level III of Gelhar et al. [5]. The tracer study meets the following criteria: (1) two-well recirculating test with step input was used; (2) single-well, injection-withdrawal test where tracer monitoring at the single well was used; (3) tracer input was not clearly defined; (4) tracer breakthrough curve was assumed to be the superposition of breakthrough curves in separate layers; (5) measurement of tracer concentration in space was inadequate; and (6) equation used to obtain dispersivity was not appropriate for the data collected.

The "high-reliability" dispersivity values were considered to be accurate within a factor of two, and the "low-reliability" values were considered to be no more accurate than one to two orders of magnitude.

8.3.4 General Description of Dispersivity-Scale Dataset

8.3.4.1 Longitudinal Dispersivity

A log-log plot of the longitudinal dispersivity versus scale data developed from the NTS and non-NTS sources discussed above, including the reliability information (Levels 1, 2, or 3), is shown in Figure 8-2. The longitudinal dispersivity values in the dataset range from 5×10^{-3} to 910 m for field transport distances ranging from 1 to 5×10^{4} m. Longitudinal dispersivity varies from two to three orders of magnitude for a given scale of transport. The data show a systematic increase in longitudinal dispersivity with increasing transport scale which is consistent with findings by previous authors [5]. The largest scale with high-reliability data (Level 1) was only 266 m, with a longitudinal dispersivity of 0.55 m. The high-reliability dispersivity data tend to be somewhat smaller in magnitude than other data at any particular scale. Gelhar et al. noted that dispersivities in the lower half of the range are favored for a given scale [5]. At the larger transport scales (e.g., greater than 300 m), only lower-reliability data are available, which could lead to greater uncertainty in longitudinal dispersivity for large plumes or longer transport distances.

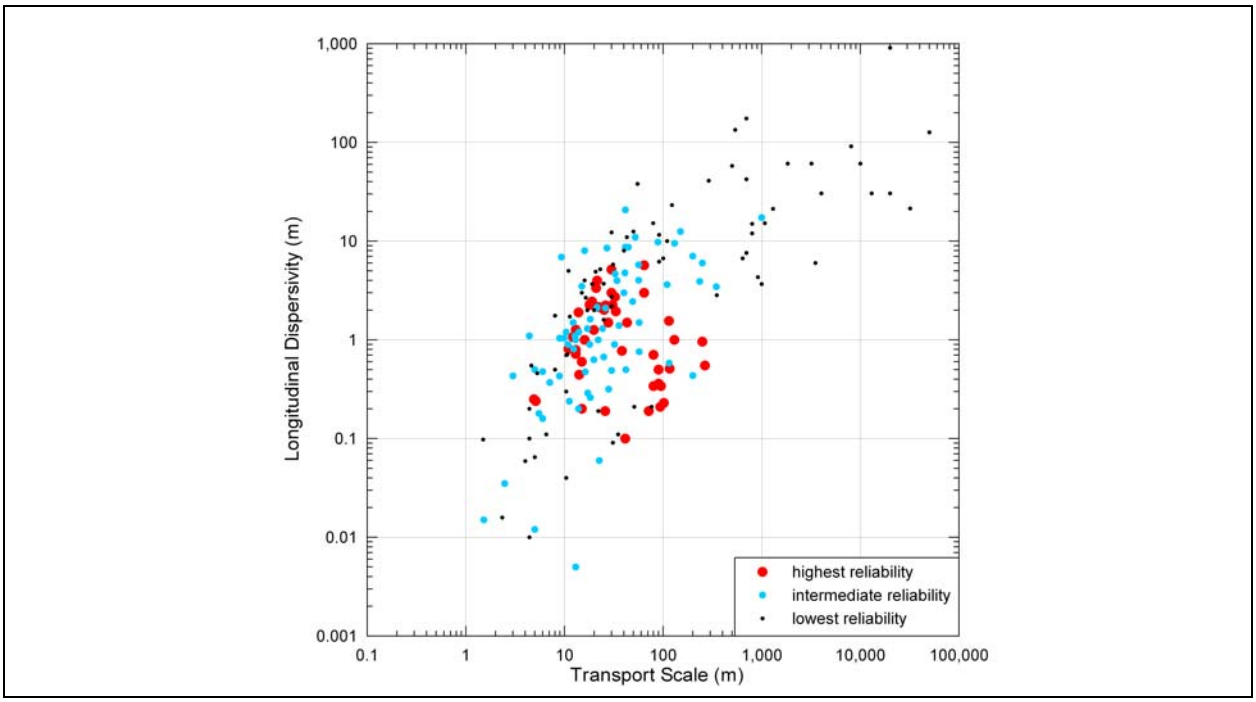

Figure 8-2
Log-Log Plot of Longitudinal Dispersivity as a Function of Transport Scale

The longitudinal dispersivity values determined from the NTS region are compared with the worldwide values in Figure 8-3. The longitudinal dispersivities from the NTS region range from 2.2 to 23.2 m (average values for individual flow paths) with transport scales ranging from 18 to 130 m. It can be seen that the longitudinal dispersivities determined from the contaminant migration experiment and the tracer tests conducted in the NTS and vicinity are consistent with those obtained from other studies in the literature at similar scales.

There are insufficient data across all transport scales for various rock types to allow for a meaningful assessment of whether the dispersivity-scale relationship is a function of rock type. Hence, the analysis to determine a dispersivity-scale relationship used the entire dataset lumped together using all rock types.

Cumulative probability distribution functions for scale and longitudinal dispersivity are shown in Figures 8-4 and 8-5, respectively. The median scale is about 29 m, and the median longitudinal dispersivity is about 2 m. For the scale data, 95% of the data fall between 4 and 10,975 m, and 75% are less than 91 m. For the longitudinal dispersivity data, 95% of the data fall between 0.03 and about 71 m, and 75% are less than 6 m. These figures show that the majority of the data are at a scale much less than that for the RMSM CAU model and that the majority of the determined longitudinal dispersivities are less than 10 m.

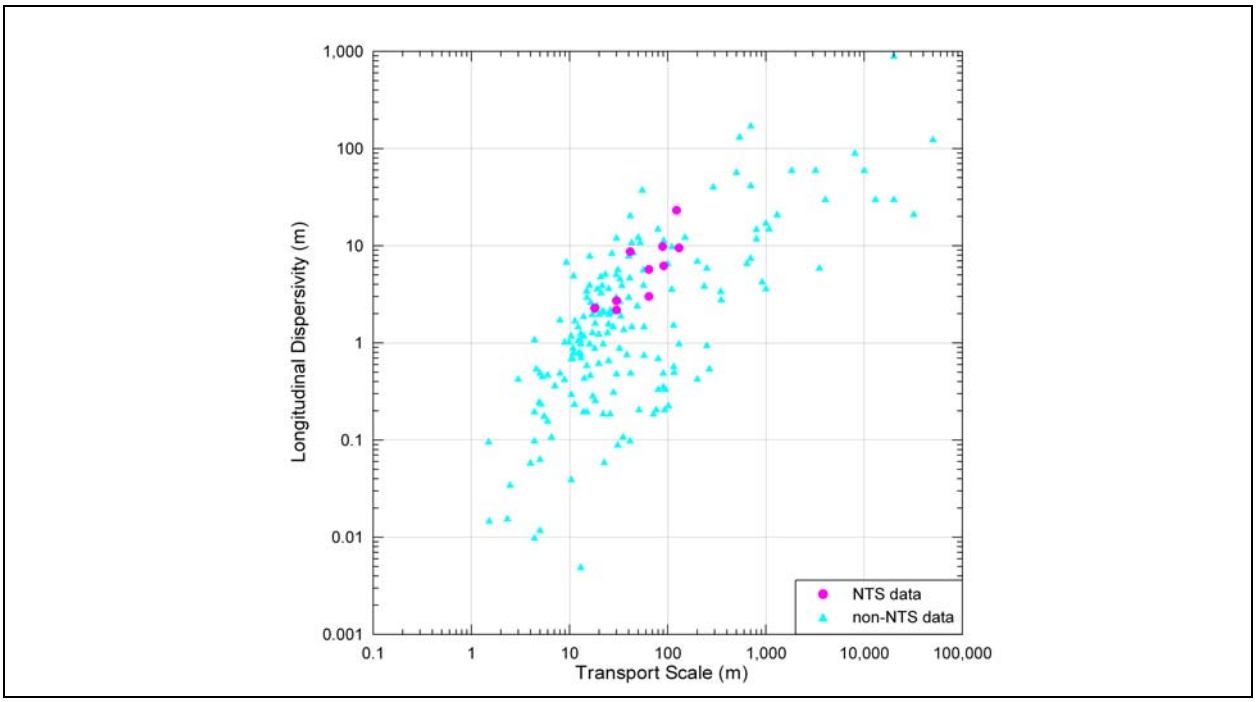

Figure 8-3
NTS and Non-NTS Dispersivity as a Function of Transport Scale

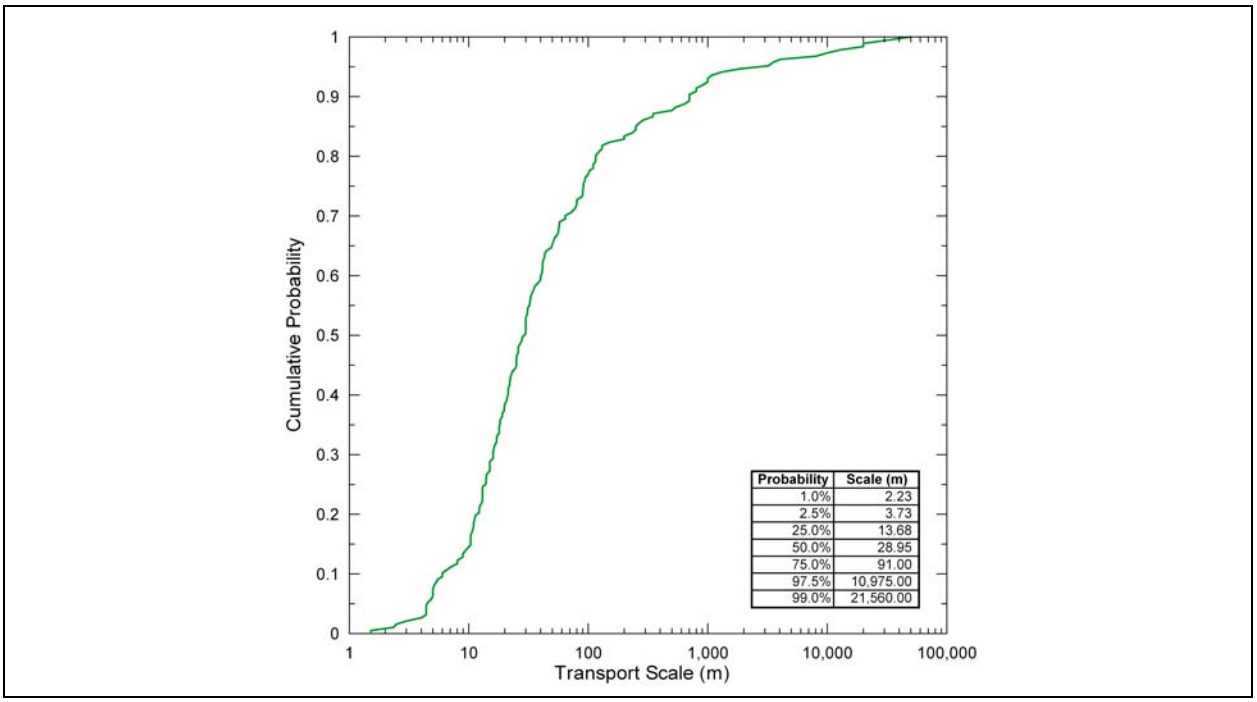

Figure 8-4
Cumulative Distribution Function for Scale

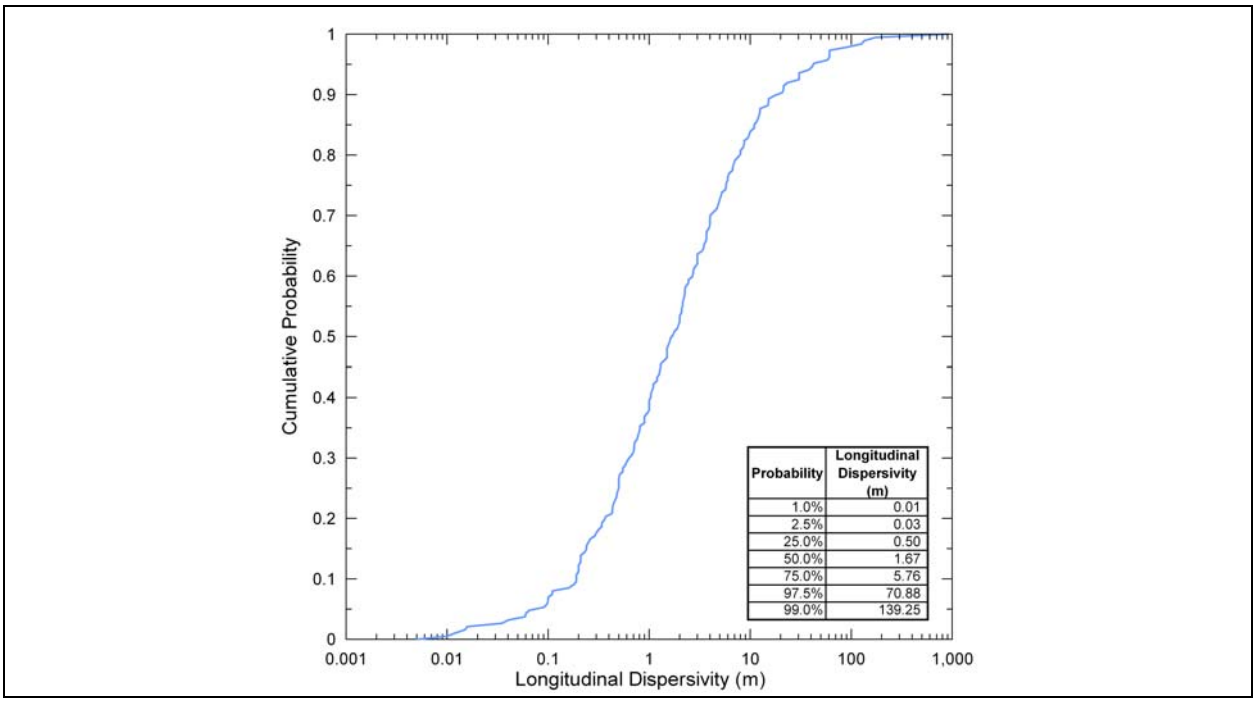

Figure 8-5
Cumulative Distribution Function for Longitudinal Dispersivity

8.3.4.2 Transverse Dispersivities

The data available for transverse horizontal dispersivity, or the spreading of solutes at right angles to the direction of horizontal groundwater flow, are shown in Figure 8-6(a). Transverse horizontal dispersivities up to 1,370 m have been reported. Although the data are much more sparse compared to that available for longitudinal dispersivity, the transverse horizontal dispersivity data exhibit the same pattern of increasing value with transport scale as does the longitudinal dispersivity. Although the low-reliability data show an increasing trend at larger scales, the intermediate- and high-reliability data show a trend of more constant transverse horizontal dispersivity values with scale. The ratio of longitudinal to transverse horizontal dispersivity is shown in Figure 8-6(b). The transverse horizontal dispersivity is, in general, a factor of 3 to 30 less than the longitudinal dispersivity. Gelhar et al. reported that, based on two high-reliability data points, transverse horizontal dispersivity is one order of magnitude less than longitudinal dispersivity [5]. Ratios of longitudinal to transverse horizontal dispersivity of about 10 are typically chosen when developing appropriate values of horizontal transverse dispersivity for use in regional transport models.

Figure 8-7(a) depicts the sparse data for transverse vertical dispersivity. Transverse vertical dispersivities up to 2 m have been observed. No trend of transverse vertical dispersivity with transport scale is apparent. The ratio of longitudinal to transverse vertical dispersivity is shown in Figure 8-7(b). The only significant observation is that the transverse vertical dispersivity is much less than either the longitudinal or horizontal transverse dispersivity. Gelhar et al. found that in all cases where both horizontal and vertical transverse dispersivities were measured, the values of vertical

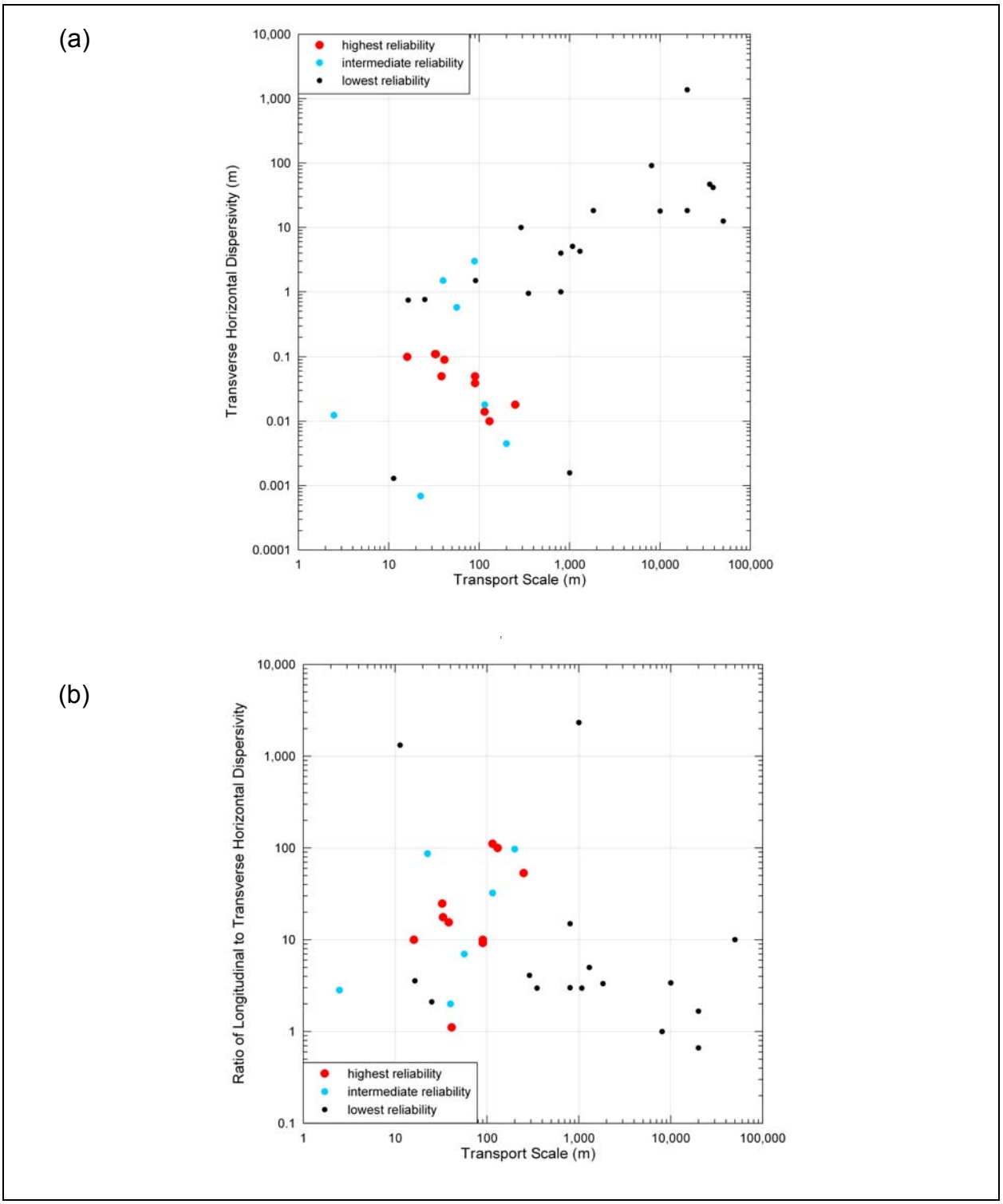

Figure 8-6
(a) Transverse Horizontal Dispersivity as a Function of Transport Scale and (b) Ratio of Longitudinal to Transverse Horizontal Dispersivity as a Function of Transport Scale

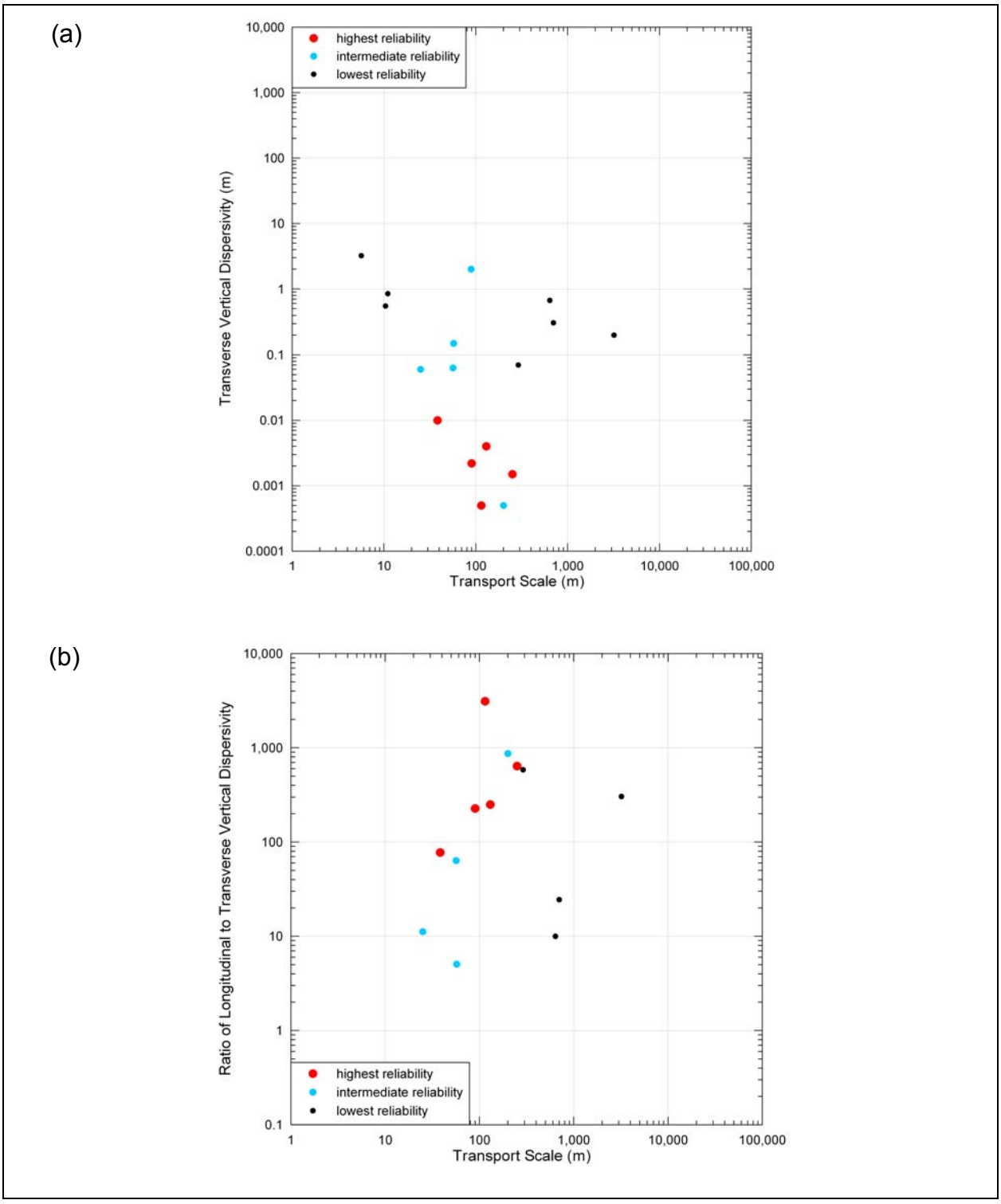

Figure 8-7
(a) Transverse Vertical Dispersivity as a Function of Transport Scale and (b) Ratio of Longitudinal to Transverse Vertical Dispersivity as a Function of Transport Scale

transverse dispersivity were one to two orders of magnitude less than those of the horizontal transverse dispersivity [5]. This reduction in spreading may be controlled mainly by the layering of the geologic materials, where less permeable layers will significantly reduce the ability of the tracer to disperse upward or downward.

8.3.4.3 Summary of Observations from Dispersivity Dataset Assessment

Several important observations related to the evaluation of dispersivity data in the literature have been previously summarized in SNJV documents based on the available information [1, 13, 14]. These observations generally are corroborated with the more recent data presented in this document and have been modified to reflect new information. The major observations are:

- Longitudinal dispersivity apparently increases with scale (distance from the contaminant source or the spacing between tracer-injection and monitoring wells).
- The ratio of longitudinal dispersivity to transverse horizontal dispersivity is generally in the range of 3 to 30, and the ratio of longitudinal dispersivity to transverse vertical dispersivity is generally in the range of 10 to 800. The transverse vertical dispersivity is typically one to two orders of magnitude smaller than the transverse horizontal dispersivity.
- As the density of information on hydraulic conductivity increases, the effect of dispersivity increasing with scale may be reduced. Dispersivity accounts for unmeasured and unspecified variability in the variations in hydraulic properties within the flow and transport model. As more of the variability is modeled explicitly, the appropriate dispersivity becomes smaller in magnitude.
- Whether the geologic media is porous or fractured appears to have no significant effect on dispersivity. In other words, dispersivities used for porous media can also be used in fractured media at similar scales.
- The longitudinal dispersivity data from NTS and vicinity studies fall within the range of values published in the scientific literature for other locations.

8.3.5 Evaluation of Scale Dependency of Dispersivity

8.3.5.1 Background and Previous Investigations of Scale Dependency

The scientific literature documents that longitudinal dispersivity representative of field conditions typically increases with the scale of measurement [5-12].

Pickens and Grisak developed a simple linear relationship between dispersivity and scale for transport in a stratified aquifer using a theoretical relationship based on the statistical properties of the aquifer [10]. For a stratified sandy aquifer, they developed a simple linear relationship where dispersivity equals 0.1 times the mean transport distance, and they found it to be consistent with results for a two-well tracer test conducted on a scale of 8 m. The authors recognized that dispersivity is unlikely to increase continually with scale but instead likely approaches some asymptotic value. They proposed a range of functional relationships between dispersivity and transport distance, including linear, exponential, and asymptotic [11].

Two studies graphically display large datasets of longitudinal dispersivity versus transport scale and fit dispersivity-scale power-law relationships (linear on a log-log graphical presentation of the dispersivity-scale data) of the form [7, 12]:

$$\alpha = cL^m \qquad (8\text{-}2)$$

where:
α = longitudinal dispersivity (L)
c = coefficient
L = transport scale of interest or mean travel distance (L)
m = scaling exponent (slope of the straight line fit on a log-log plot of the dispersivity-scale data)

These authors fit this relationship to the databases they had assembled for longitudinal dispersivity versus transport scales.

Neuman developed expressions using Equation (8-2) from regression of the dispersivity-scale data excluding the large-scale contaminant-transport model calibration cases and determined two linear regions on the log-log plot corresponding to scales less than 100 m (c = 0.0169 and slope m = 1.53) and greater than 100 m (c = 0.32 and slope m = 0.83) [7]. When he included the dispersivity-scale data corresponding to the large-scale contaminant-transport model calibrations, he determined the slope m to be about 0.5. Gelhar et al. caution against routinely adopting dispersivities from a linear regression through the data because examination of the underlying data favors the use of dispersivities from the lower half of the dispersivity range at any given scale [5].

Neuman concluded that dispersivities interpreted from calibration of numerical models to both hydraulic and concentration data tend to increase more slowly with increasing scale than those that are calibrated to concentration data alone [7]. This appears to occur because calibration often provides information about the spatial variation of hydraulic conductivities on scales exceeding the dimensions of model subregions (called "zones") within which they are kept constant or allowed to vary at a relatively slow rate. The calibrated dispersivities are associated with a reduced length scale L_r that depends on the dimensions of the zones rather than on the mean travel distance L_s of the plume. The regression analysis suggested that L_r increased with the mean travel distance at an average rate proportional to $L_s^{0.5}$. Neuman concluded the scale parameter controlling dispersivity in a transport model diminishes as the amount of detail on hydraulic heterogeneity increases [7].

Xu and Eckstein [33] developed dispersivity-scale relationships from the data presented in Gelhar et al. [5] using a weighted least-squares method where weights could be assigned to data points in accordance with their reliability. They presented results for three weighting schemes (1:1:1, 1:1.5:2, and 1:2:3) that were assigned according to weight value for the lowest-reliability, intermediate-reliability, and highest-reliability data, respectively. They also presented a graphical presentation of the data that shows linearization when plotted as log α versus log (log L) where α is longitudinal dispersivity and L is the transport scale of interest or mean travel distance. Using the

Gelhar et al. [5] data, Xu and Eckstein [33] developed the following relationship for the 1:1:1 weighting scheme:

$$\alpha = 1.20 (\log L)^{2.958} \quad (8\text{-}3)$$

As expected, this relationship exhibits a declining rate of change in dispersivity as transport scale increases.

Schulze-Makuch developed relationships for unconsolidated media and for various rock types (sandstones, carbonates, basalts, and granites) using Equation (8-2) [12]. The parameter *c* varied between approximately 0.01 and 0.8, and the scaling exponent *m* varied between 0.4 and 0.94. He obtained a mean scaling exponent of about 0.5 for his entire dataset, with no statistical difference between geologic media. This exponent of 0.5 is similar to that obtained by Neuman for his dataset when he included large scale plumes [7]. Because of the limited amount of data for each rock type and the data accuracy problems found when evaluating his summary table of dispersivity-scale data, the parameters from Schulze-Makuch are given here for comparison purposes only and should be considered with caution [12]. The relationships he developed for the various rock types should not be used because of the limited amount of data available across the range of scales for each rock type and the general large scatter in the data.

8.3.5.2 Determination of Dispersivity-Scale Relationships

For the dispersivity-scale analyses performed for the Frenchman Flat CAU [13] and the YFCM CAU [14], the nonweighted least squares analysis was deemed most appropriate for determining a dispersivity-scale relationship over the full range of transport scales because of the lack of any high-reliability data for scales greater than about 300 m. The dataset developed to support the RMSM CAU has the same limitation on data reliability at scales greater than 300 m. Therefore, a nonweighted least squares approach was adopted for the current analyses.

The log-log plot of longitudinal dispersivity versus scale for all rock types, shown in Figure 8-2, demonstrates a large amount of scatter in the data but also a consistent trend of increasing longitudinal dispersivity with transport scale. In addition, it is observed that the rate of increase in longitudinal dispersivity tends to decrease at larger transport scales (e.g., greater than 300 m). Regression analysis was performed using several types of dispersivity-scale relationships:

- Log-log linear (equivalent to relationship given in Equation [8-2])
- Log-log piecewise linear (1 line for < 300 m scale and 1 line for $\geq$ 300 m scale)
- Log-log quadratic
- Log-log asymptotic
- Log-log(log) linear

The dispersivity-scale data and regression lines for the log-log linear, log-log piecewise linear, log-log quadratic, and log-log asymptotic fits are shown in Figure 8-8. The linear fit to the data plotted as log dispersivity versus log (log scale) is presented in Figure 8-9a and the resultant regression line with the data plotted in log-log space is provided in Figure 8-9b [33]. The results of the regression analyses for the five dispersivity-scale relationships are summarized in Table 8-2.

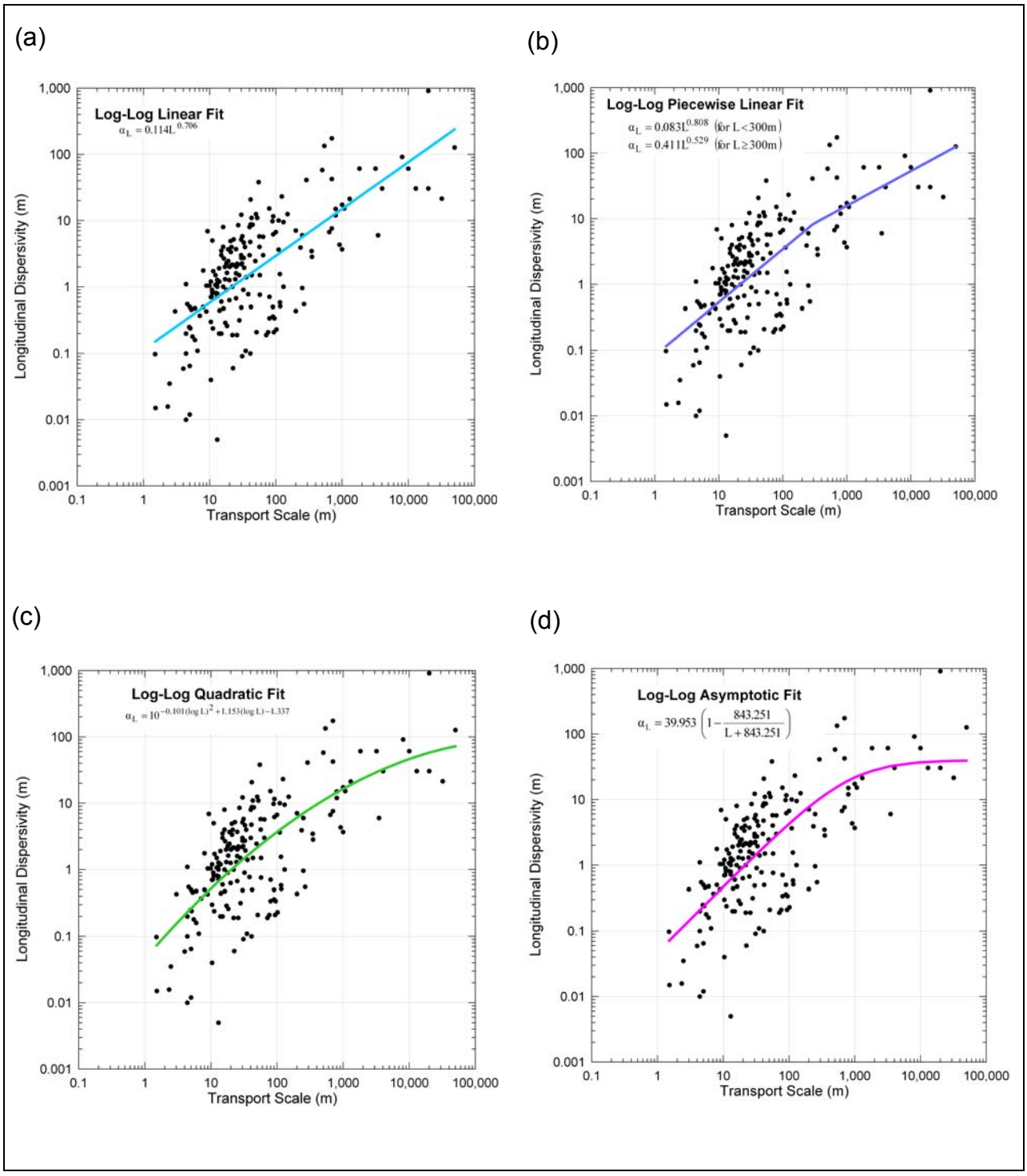

Figure 8-8
Dispersivity-Scale Relationships Determined from Regression Analyses: (a) Log-Log Linear, (b) Log-Log Piecewise Linear, (c) Log-Log Quadratic, and (d) Log-Log Asymptotic

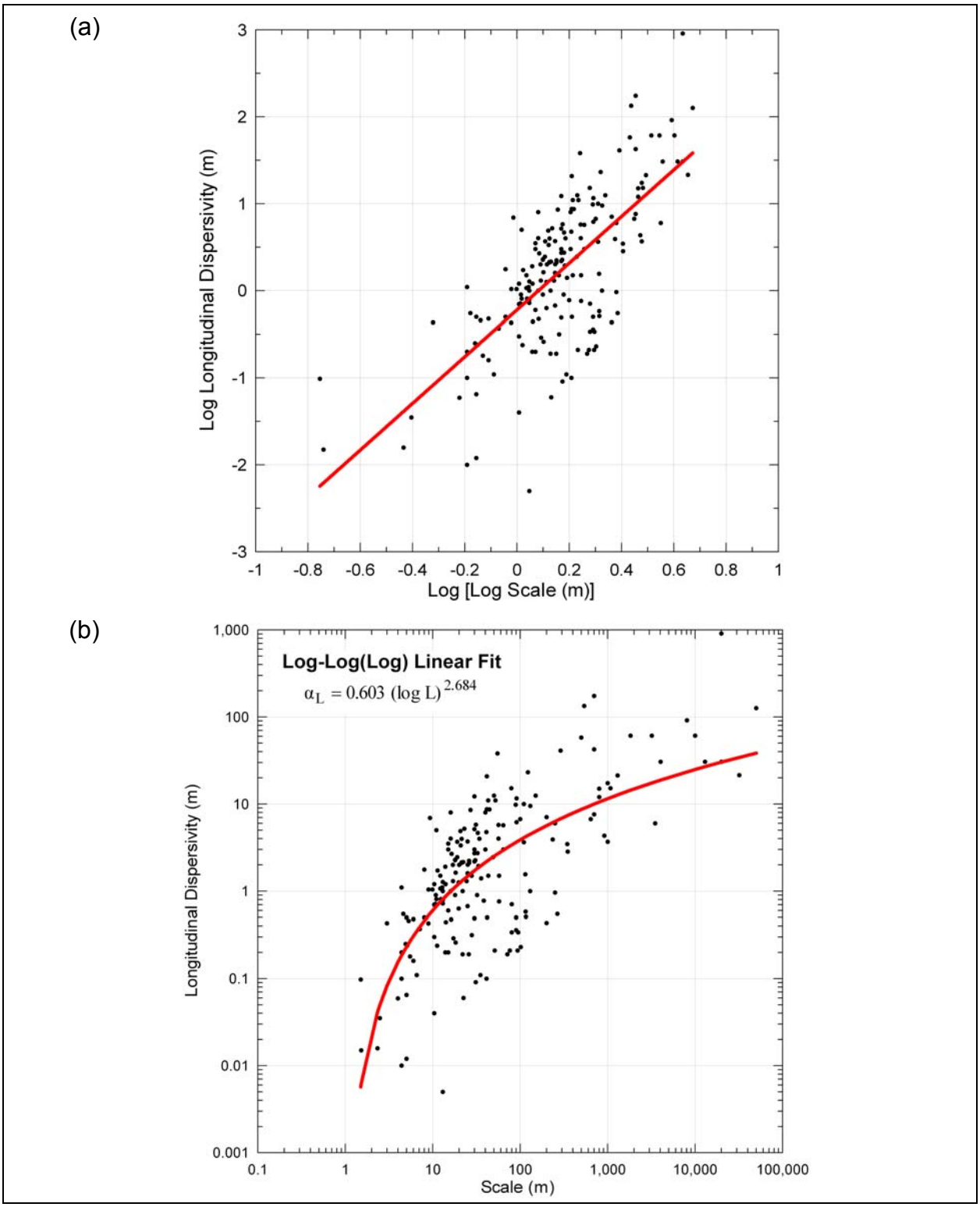

Figure 8-9
(a) Regression Analysis of Log Dispersivity versus Log (Log Scale) and (b) Resultant Dispersivity-Scale Relationship

Table 8-2
Dispersivity Relationships Determined from Regression Analysis

Relationship Type	Equation	Coefficient of Determination (R^2)
Log-log linear	$\alpha_L = 0.114L^{0.706}$	0.48
Log-log piecewise linear (1 line for <300 m scale and 1 line for = 300 m scale)	$\alpha_L = 0.083L^{0.808}$ ($for\ L < 300\,m$) $\alpha_L = 0.411L^{0.529}$ ($for\ L \geq 300\,m$)	0.49
Log-log quadratic	$\alpha_L = 10^{-0.101(\log L)^2 + 1.153(\log L) - 1.337}$	0.50
Log-log asymptotic	$\alpha_L = 39.953\left(1 - \frac{843.251}{L + 843.251}\right)$	0.48
Log-log(log) linear	$\alpha_L = 0.603(\log L)^{2.684}$	0.49

Note: α is longitudinal dispersivity, and L is scale.

All five relationships provide reasonable and similar quality of fit with nearly identical coefficients of determination. Any of these relationships could be used to provide estimates of longitudinal dispersivity for expected transport scales within the RMSM CAU. All of the relationships, except for log-log linear, offer the advantage of being able to capture the behavior of decreasing rate of dispersivity increase for larger transport scales.

The log-log linear relationship is equivalent to the power law shown in Equation (8-2), where coefficient *c* is 0.11 and the scaling exponent m is 0.71. For the piecewise linear relationship, the scaling exponents are 0.81 and 0.53 for scales less than 300 m and greater than or equal to 300 m, respectively. The exponent of 0.53 for the scales greater than or equal to 300 m is relatively consistent with Neuman, who obtained a scaling exponent of about 0.5 when he performed a regression on all data with scales greater than 100 m [7].

8.4 Data Limitations

Dispersivity is not an intrinsic property of the medium in the way that porosity and hydraulic conductivity are thought to be. In order to have a basis for predicting dispersivity from statistical distributions, its dependence on the scale of the measurement and on the type of test and method of analysis must be known. The data available from the NTS area are scarce and mostly consist of quantitative values only for longitudinal dispersivity. None of the NTS tracer tests produced good estimates of transverse dispersivities. The trends in dispersivity with transport distance are compiled from data obtained from locations around the world. As a result, the appropriate longitudinal dispersivity to apply at large scales for the RMSM CAU model has uncertainty associated with the range and distribution of data. This uncertainty can be addressed using sensitivity analyses during the application of the RMSM CAU flow and transport model.

8.5 Summary

As presented in Section 8.3, dispersivity values determined from analysis of transport are scale-dependent, and dispersivity has been characterized as a function of transport distance. The expected distances of contaminant transport *a priori* is the primary basis used to assess the range of dispersivity values appropriate for modeling. Flow modeling is required for assessment of the expected pathways and distances of contaminant transport. Flow model calibration and particle-tracking studies (using initial estimates of effective porosity) will provide insight into expected advective transport distances for contaminants from the underground nuclear test locations.

The value selected for dispersivity is somewhat dependent on the degree to which the heterogeneity of the groundwater system is defined. Because of the large areal and vertical extent, the complex hydrostratigraphic and faulted nature, and the relatively sparse well data for heads and hydraulic properties for calibrating the groundwater flow model within the RMSM CAU, the calibrated groundwater flow model will likely only be moderately constrained. Dispersivity is a modeling parameter that accounts for unmeasured and unspecified variability in the hydraulic properties within the flow and transport model domain. As more of the variability of the groundwater flow regime is modeled explicitly, the appropriate dispersivity to use becomes smaller in magnitude. Longitudinal dispersivities estimated from the derived regression lines for ranges of transport scale (see Section 8.3.5.2) are considered reasonable.

It is recommended that transverse horizontal and vertical dispersivities be selected based on a ratio of longitudinal to transverse horizontal dispersivity of about 3 to 30 and a ratio of longitudinal to transverse vertical dispersivity of about 10 to 800. The transverse vertical dispersivity is typically one to two orders of magnitude smaller than the transverse horizontal dispersivity.

8.6 References

1. Stoller-Navarro Joint Venture. 2004. *The Role of Dispersion in Radionuclide Transport - Data and Modeling Requirements*, S-N/99205-003, Shaw/13052-200. Las Vegas, NV.

2. Freeze, R.A., and J.A. Cherry. 1979. *Groundwater.* Englewood Cliffs, NJ: Prentice Hall.

3. Bear, J. 1972. *Dynamics of Fluids in Porous Media*. New York, NY: Elsevier Publishing Co.

4. Bear, J., and A. Verruijt. 1990. *Modeling Groundwater Flow and Pollution*. Reidel (Dordrecht).

5. Gelhar, L.W., C. Welty, and K.R. Rehfeldt. 1992. "A Critical Review of Data on Field-Scale Dispersion in Aquifers." In *Water Resources Research*, 28: 1955-1972. Washington, DC.

6. Lallemand-Barres, P., and P. Peaudecerf. 1978. *Recherche des relations entre la valeur de la dispersivite macroscopique d'un milieu aquifere, ses autres caracteristiques et les conditions de mesure, etude bibligraphique:* Buleetin, Bureau de Recherches Geologiques et Minieres, Sec. 3/4:227-87.

7. Neuman, S.P. 1990. "Universal Scaling of Hydraulic Conductivities and Dispersivities in Geologic Media." In *Water Resources Research,* Vol. 26(8): 1749-1758. Washington, DC: American Geophysical Union.

8. Neuman, S.P. 1995. "On Advective Transport in Fractal Permeability and Velocity Fields." In *Water Resources Research*, Vol. 31(6): 1455-1460.

9. Neuman, S.P., and V. Di Federico. 2003. "Multifaceted Nature of Hydrogeologic Scaling and Its Interpretation." In *Reviews of Geophysics*, Vol. 41(3): 1014.

10. Pickens, J.F., and G.E. Grisak. 1981. "Scale-Dependent Dispersion in a Stratified Granular Aquifer." In *Water Resources Research,* Vol. 17(4): 1191-1211.

11. Pickens, J.F., and G.E. Grisak. 1981. "Modeling of Scale-Dependent Dispersion in Hydrogeologic Systems." In *Water Resources Research,* Vol. 17(6): 1701-1711.

12. Schulze-Makuch, D. 2005. "Longitudinal Dispersivity Data and Implications for Scaling Behavior." In *Ground Water,* Vol. 43(3): 443-456.

13. Stoller-Navarro Joint Venture. 2005. *Phase II Contaminant Transport Parameters for the Groundwater Flow and Contaminant Transport Model of Corrective Action Unit 98: Frenchman Flat, Nye County, Nevada*, S-N/99205--043. Las Vegas, NV.

14. Stoller Navarro Joint Venture. 2007. *Phase I Contaminant Transport Parameters for the Groundwater Flow and Contaminant Transport Model of Corrective Action Unit 97: Yucca Flat/Climax Mine, Nevada Test Site, Nye County, Nevada*, Revision No. 0, S-N/99205--096. Las Vegas, NV.

15. Sauty, J.P. 1980. "An Analysis of Hydrodispersive Transfer in Aquifers." In *Water Resources Research,* Vol. 16 (1): 145-158. Washington, DC: American Geophysical Union.

16. Burbey, T.J., and S.W. Wheatcraft. 1986. *Tritium and Chlorine-36 Migration from a Nuclear Explosion Cavity,* Publication No. 45050. Las Vegas, NV: Desert Research Institute.

17. Travis, B.J., H.E. Nuttall, S.W. Hodson, and R.S. Rundberg. 1983**.** "Section B: Transport of Tritium the Cambric Cavity Region to RNM-2S: Modeling." In *Laboratory and Field Studies Related to the Hydrology/Radionuclide Migration Project: October 1, 1981 - September 30, 1982,* LA-9691-PR. Los Alamos, NM: Los Alamos National Laboratory.

18. Thompson, J.L. 1988. *Laboratory and Field Studies Related to the Radionuclide Migration Project: October 1, 1986 - September 30, 1987,* LA-11223-PR. Los Alamos, NM: Los Alamos National Laboratory.

19. Ogard, A.E., J.L. Thompson, R.S. Rundberg, K. Wolfsberg, P.W. Kubic, D. Eklmore, and H.W. Bentley. 1988. "Migration of Chlorine-36 and Tritium from an Underground Nuclear Test." In *Radiochim. Acta,* Vol. 44/45: 213-217. Munich, Germany: R. Oldenburg.

20. Welty, C., and L.W. Gelhar. 1989. *Evaluating of Longitudinal Dispersivity from Tracer Test Data*, R89-05, Ralph M. Parsons Laboratory Report. Cambridge, MA: Massachusetts Institute of Technology.

21. Thompson, J.L. 1991. *Laboratory and Field Studies Related to the Hydrology/Radionuclide Migration Project: October 1, 1989 - September 30, 1990*, LA-12100-PR. Los Alamos, NM: Los Alamos National Laboratory.

22. IT Corporation. 1998. *Report and Analysis of the BULLION Forced-Gradient Experiment,* ITLV/13052-042. Las Vegas, NV.

23. Reimus, P.W., and M.J. Haga. 1999. *Analysis of Tracer Responses in the BULLION Forced-Gradient Experiment at Pahute Mesa, Nevada*, LA-13615-MS. Los Alamos, NM: Los Alamos National Laboratory.

24. Moench, A.F. 1989. "Convergent Radial Dispersion: A Laplace Transform Solution for Aquifer Tracer Testing." In *Water Resources Research,* Vol. 25 (3): 439-447. Washington, DC: American Geophysical Union.

25. Bechtel SAIC. 2004. *Saturated Zone In-Situ Testing,* ANL-NBS-HS-000039, Rev. 01, Yucca Mountain Project Analysis Report. Las Vegas, NV.

26. Grove, D.B. 1977. *The Use of Galerkin Finite-Element Methods to Solve Mass-Transport Equations, Water-Resources Investigations* 77-49. U.S. Geological Survey.

27. Leap, D.I., and P.M. Belmonte. 1992. "Influence of Pore Pressure on Apparent Dispersivity of a Fissured Mitic Dolomitic Aquifer." In *Groundwater,* Vol. 30(1): 87-95. Columbus, OH: Groundwater Publishing Company.

28. Stoller-Navarro Joint Venture. 2006. *Well ER-6-1 Tracer Test Analysis: Yucca Flat, Nevada Test Site, Nye County, Nevada*, S-N/99205--084. Las Vegas, NV.

29. Reimus, P.W., Los Alamos National Laboratory. 2006. Personal communication to P. Montazer and I. Farnham (SNJV) regarding dispersion data, 6 June.

30. Moench, A.F. 1995. "Convergent Radial Dispersion in a Double-Porosity Aquifer with Fracture Skin: Analytical Solution and Application to a Field Experiment in Fractured Chalk." In *Water Resources Research,* Vol. 31(8): 1823-1835.

31. Umari, A., J.D. Earle, and M.F. Fahy. 2006. "Analysis of Single-Hole and Cross-Hole Tracer Tests Conducted at the Nye County Early Warning Drilling Program Well Complex, Nye County, Nevada." In *International High-Level Waste Management,* 20 April - 4 May. Las Vegas, NV.

32. Domenico, P.A., and G.A. Robbins. 1985. "The Displacement of Connate Water from Aquifers." In *Geological Society of America Bulletin*, Vol. 96: 328-335.

33. Xu, M., and Y. Eckstein. 1995. "Use of Weighted Least-Squares Method in Evaluation of the Relationship between Dispersivity and Field Scale." In *Ground Water,* Vol. 33, No. 6, pp. 905-908.

9.0 MATRIX DIFFUSION

Matrix diffusion coefficients for solutes in a porous medium are smaller in magnitude than free water diffusion coefficients because of restriction due to the presence of the solid phase of the porous medium. Because porosity data are more readily available than experimentally derived matrix diffusion coefficient data, a relationship could be developed between the ratio of matrix diffusion to free water diffusion coefficients (termed tortuosity) and porosity. Tortuosity is the ratio of the matrix diffusion coefficient to the free water diffusion coefficient. Because no new matrix diffusion information has been produced since the publication of the YFCM TDD, only a brief overview is presented here [1].

9.1 Matrix Diffusion in Contaminant Transport

Solute transport in low-permeability zones is dominated by diffusion. In fractured media, a dual-porosity conceptualization is typically assumed with matrix diffusion between the fractures and the adjacent matrix having the effect of attenuating the concentration and increasing the travel time of aqueous-phase contaminants moving through fractures. This process involves the diffusion of contaminants from groundwater flowing in rock fractures into and out of the relatively stagnant water in the pores of the surrounding rock matrix. The importance of the diffusion of solutes from fractures into the adjacent matrix has been studied and reported extensively in the literature, and has been established as an important process for retarding the transport distance of solutes introduced into fractured geologic systems.

Mass transfer can also occur in unfractured media, including alluvium, by diffusion between the more permeable zones and lower-permeability zones [2]. The low-permeability zones may consist of layers of fine-grained sediments. Diffusion, however, would be expected to be of less importance for alluvium, compared to fractured media, because the ratio of stagnant to flowing water volume in unconsolidated media is usually much smaller than in fractured media. Additionally, the contrast in permeability between the stagnant and flowing zones is typically much less for alluvium than for fractured rocks. For these reasons, matrix diffusion is not expected to be a significant source of reduction in transport distances for alluvium when compared to fractured media.

9.2 Data Sources, Compilation, and Transfer

The NTS diffusion database from the YFCM TDD was used in this study due to the lack of comprehensive data from the RMSM HFM area for all HGUs [1]. All data locations used in quantitative analyses are identified in Appendix E and the associated dataset referenced in Section E.2.0. There are limited data for the NTS area to determine a distribution for matrix diffusion values directly. The data were used to determine functional relationships with other parameters, for which there are more comprehensive data [1]. Representative stochastic values for matrix diffusion

parameters may be determined from laboratory experimentation, field tracer tests, and measurements of porosity and formation factors.

9.3 Data Analysis and Evaluation

The YFCM TDD [1] recommended the empirical tortuosity-porosity relationship based on Archie's equation be used to predict appropriate tortuosity values where no diffusion data exist with the following correlation:

$$\tau = \Phi^{n} \qquad (9\text{-}1)$$

where:
τ = tortuosity
Φ = porosity
n = 1.33, an exponent determined by a regression analysis of the NTS diffusion data

The values of *n* that define the upper and lower 95% confidence intervals are 0.4 and 3.2 for this correlation. Assuming no other phenomena influence the matrix diffusion process, combining the tortuosity with the free water diffusion coefficient for each diffusing species may provide an acceptable value for D_m determined by the equation:

$$D_m = \tau D_o \qquad (9\text{-}2)$$

where:
D_m = matrix diffusion, a property of the rock and the radionuclide
τ = tortuosity, a property of the rock alone
D_o = free water diffusion coefficient a property of the radionuclide alone (and temperature)

Free water diffusion coefficients are temperature-dependent; thus, corrections should be applied in the model for temperature effects because temperatures measured from logging in the UGTA Wells ER-12-4, ER-19-1-1, and ER-12-2 range up to 31, 36, and 47 degrees Celsius (°C), respectively.

The correlation of porosity and tortuosity was used to calculate HGU tortuosity values from the readily available matrix porosity data obtained from the USGS Rock-Property Database [3]. Figure 9-1 presents a box and whisker plot of the tortuosity derived by applying Equation (9-1) to the RMSM HGU matrix porosity data.

There are three broad ranges present on the plot: very low values for the GCU; moderate values for the CA and CCU; and the highest values displayed for the TCU, VTA, WTA, and AA. The AA values are probably not representative as there were no tortuosity data for alluvium rocks in the NTS database. One would expect a very large range for AA as it would be difficult to get a representative measurement due to the extremely varied nature of alluvium. Table 9-1 presents calculated (using Equation [9-1]) tortuosity values from the RMSM sample summary porosity statistics shown in Table 6-2 with the suggested confidence intervals.

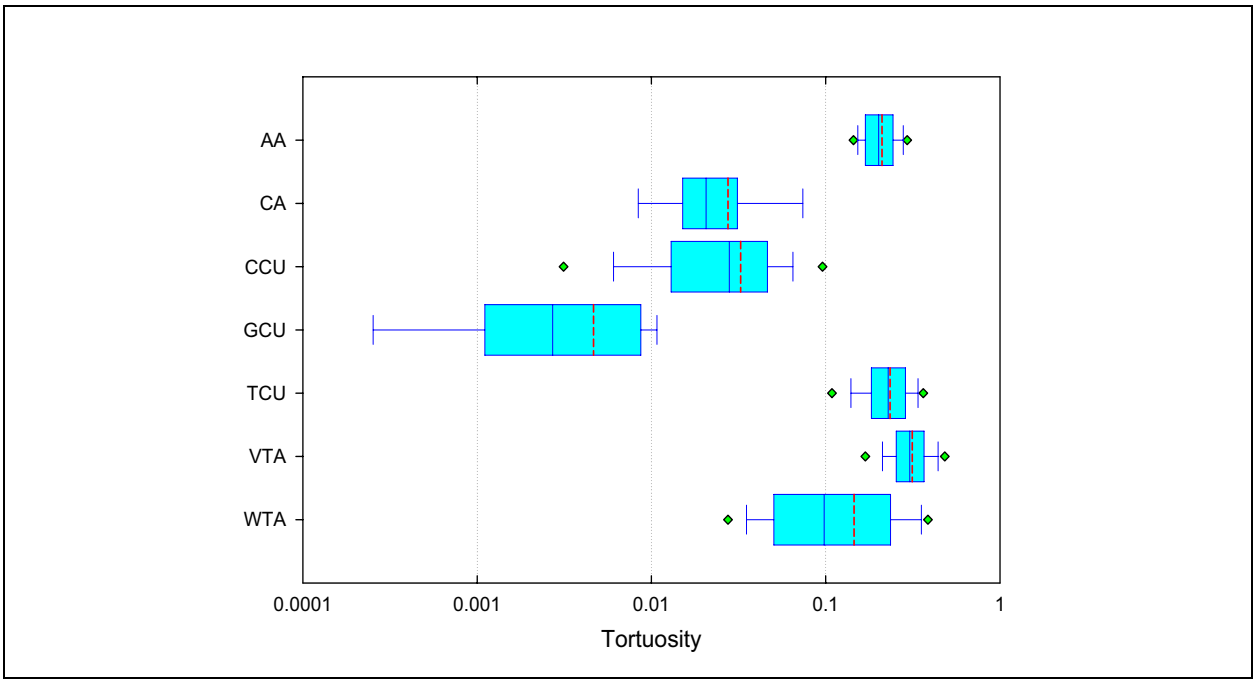

Figure 9-1
RMSM HGU Tortuosity Values Derived from Porosity

MEAN: Red vertical dashed line; MEDIAN: Blue vertical line in box; 1ST QUARTILE: Left box side; 3RD QUARTILE: Right box side; 10TH PERCENTILE: Left whisker; 90TH PERCENTILE: Right whisker; 5TH PERCENTILE: Left green diamond; 95TH PERCENTILE: Right green diamond

The entire dataset of tortuosities ranges over four orders of magnitude. The median tortuosity is 0.072. Even the 75th percentile tortuosity value is low, with 75% of all tortuosities less than 0.15. This suggests that, even for rock with a relatively large porosity, the connectivity is low – the rock pores are connected in a "tortuous" manner. This is supported by the generally low permeabilities, where they were measured and reported for the matrix diffusion experiments. The limited permeability data from the YFCM TDD study show a general trend of increasing tortuosity with increasing permeability as well as more variation in tortuosity for the lower permeability cores. There were no apparent trends of tortuosity with lithology nor tortuosity with depth.

Table 9-1
Tortuosity Calculated from RMSM Porosity Statistics

Unit	Lower 5% Confidence Interval	Mean	Upper 95% Confidence Interval
Hydrogeologic Units			
AA	2.43E-02	2.09E-01	6.25E-01
CA	1.67E-04	2.58E-02	3.33E-01
CCU	2.55E-04	3.08E-02	3.51E-01
GCU	9.92E-07	2.98E-03	1.74E-01
TCU	3.68E-02	2.49E-01	6.59E-01
VTA	6.11E-02	3.08E-01	7.02E-01
WTA	6.67E-03	1.22E-01	5.31E-01
Hydrostratigraphic Units			
AA3	2.43E-02	2.09E-01	6.25E-01
ATCU	1.80E-02	1.84E-01	6.01E-01
BRA	4.10E-03	9.91E-02	4.99E-01
BRCU	3.83E-02	2.54E-01	6.62E-01
LCA3	1.67E-04	2.58E-02	3.33E-01
LCCU1	1.01E-04	2.09E-02	3.12E-01
LTCU	3.78E-02	2.52E-01	6.61E-01
LVTA	8.96E-02	3.62E-01	7.37E-01
MGCU	9.92E-07	2.98E-03	1.74E-01
OSBCU	2.80E-02	2.22E-01	6.36E-01
TM-LVTA	5.98E-02	3.06E-01	7.00E-01
TM-UVTA	6.66E-02	3.20E-01	7.10E-01
TM-WTA	8.17E-03	1.32E-01	5.44E-01
TSA	9.69E-03	1.42E-01	5.56E-01
TUBA	3.24E-03	8.97E-02	4.84E-01
UCCU	3.92E-04	3.69E-02	3.71E-01
UTCU1	4.21E-02	2.64E-01	6.70E-01

9.4 References

1. Stoller-Navarro Joint Venture. 2007. *Phase I Contaminant Transport Parameters for the Groundwater Flow and Contaminant Transport Model of Corrective Action Unit 97: Yucca Flat/Climax Mine, Nevada Test Site, Nye County, Nevada*, Rev. 0, S-N/99205--096. Las Vegas, NV.

2. Stoller-Navarro Joint Venture. 2004. *Letter Report: Analysis of Well ER-2-1 Hydraulic Testing, Yucca Flat FY 2003, Nevada Test Site, Nevada,* DOE/NV--992. Las Vegas, NV.

3. U.S. Geological Survey. 2007. Mercury Core Library & Data Center Rock-Property Information Rock-Property Database. As accessed at http://nevada.usgs.gov/mercury/rock.html on 3 October. Mercury, NV.

10.0 MATRIX SORPTION PARAMETERS

This section presents a summary of the matrix sorption data available in the RMSM CAU. The objective is to accumulate data specific to the RMSM CAU and compare it with prior laboratory and modeling studies from YMP and various NTS CAUs. Because the sorption coefficient for a porous media flow system varies with the mineral composition of the rock and the chemistry of the water, mechanistic modeling studies are used to provide insight into heterogeneity and transferability issues.

10.1 Role of Matrix Sorption in Contaminant Transport

Matrix sorption is a physiochemical process at mineral-water interfaces that controls solute mobility and retardation within the pore spaces of the immobile rock matrix. In general, matrix sorption describes a variety of chemical processes – including surface complexation, ion exchange, and precipitation – that bind contaminants to solids either temporarily or permanently. There are multiple methods for mathematically representing the matrix sorption process in parameterized groundwater transport models. These methods include, but are not limited to:

- Mechanistic pore-scale models representing the sorption process on each immobile mineral grain with thermodynamic relationships for each type of reactive surface
- Mechanistic complexation and exchange models representing average processes on integrated volumes represented with discretized continuum models
- Isotherms seeking to describe or abstract, on a laboratory scale, the integrated behavior of the smaller-scale mechanistic processes

10.1.1 Parameterization

Sorption is treated in the contaminant transport model through an equilibrium distribution coefficient (K_d) approach where the amount of contaminant sorbed to the rock is a function of its concentration in the groundwater. Modeling solute transport using K_d is attractive due to the simplicity with which models are implemented and because the models represent an average behavior, thus decreasing the number of molecular-scale processes that need to be explicitly accounted for in transport models. The K_d value is defined as:

$$K_d = \frac{\text{moles of solute per gram of solid phase}}{\text{moles of solute per milliliter of solution}} \qquad (10\text{-}1)$$

This approach to matrix sorption assumes that the radionuclide has a uniform affinity for the rock surface that is independent of the solute already adsorbed. Another assumption inherent in the use of this parameter is instantaneous equilibrium between the aqueous and sorbed phase. The use of K_d

values in the CAU-scale model requires the assumption of local equilibrium conditions because contact times between radionuclides and rocks may not be the same for the laboratory experiments as the rate of groundwater flow through the reactive rocks in the CAU model. The K_d parameter may be obtained either by direct measurement on aquifer material samples or computed by upscaling mechanistic processes.

10.2 Data Sources and Availability

Measurements of K_d values for several radionuclides on multiple minerals have been collected in support of the UGTA and YMP transport studies. The NTS unclassified radiologic inventory includes a list of 43 source-term radionuclides [1]. For a subset of the radionuclide inventory, matrix sorption parameter values specific to NTS CAUs and the YMP have previously been measured in laboratory studies and estimated through mechanistic models for each radionuclide. However, laboratory experiments and mechanistic model calculations need to be transferred from other sources to adequately describe the entire suite of sorbing radionuclides in the Bowen et al. report [1] (e.g., zirconium [Zr-93] and tin [Sn-121, Sn-126]).

For the RMSM CAU, Desert Research Institute (DRI) conducted the only matrix sorption laboratory measurements for cesium (Cs), strontium (Sr), and lead (Pb) in volcanic rocks [2-4]. Additional matrix sorption parameters measured in other CAUs are summarized in the YFCM TDD [5], where laboratory K_d parameters from the YFCM [6-10] CAU, Frenchman Flat CAU [11-13], Beatty low-level radioactive waste disposal facility [6], and YMP [14-17] are compared graphically using box and whisker plots (see Figures 11-1 and 11-3 through 11-5 in [5]). Furthermore, mechanistic model K_d calculations for samples in YFCM and YMP are compared with the laboratory measurements (see Figures 11-8 through 11-11 in [5]) mentioned above. The K_d values predicted by the mechanistic model are commensurate with the laboratory measurements, providing confidence the mechanistic model values can be appropriately extended to the RMSM groundwater chemistries and mineralogies to supplement the existing RMSM CAU laboratory measurements.

10.3 Data Compilation

Mechanistic modeling approaches explicitly treat the fundamental interactions at the aqueous-aqueous and aqueous-solid interfaces, where processes such as aqueous speciation, surface complexation, ion exchange, precipitation and oxidation/reduction reactions are expressed within a thermodynamic framework. Mineral K_d values are developed from mechanistic models by examining the partitioning of a solute between the aqueous and sorbed phases. The effective K_d values for a given bulk material-radionuclide interaction are computed through the component additivity principle [18], expressed as:

$$K_d = \sum_{i=1}^{n} K_{d,i} \varphi_{m,i} \qquad (10\text{-}2)$$

where:

$K_{d,i}$ = specific K_d for individual mineral i

$\varphi_{m,i}$ = mass fraction of mineral i with respect to the total bulk medium

The K_d values are characterized according to the RMCs present in the RMSM CAU (see the RMSM_HFM.xls workbook in the Appendix\A folder). Mechanistic models were applied to the average groundwater chemistry data representative of the geochemical conditions at each well and tunnel location (see the RMSM_Geochemistry.xls workbook in the Appendix\G folder). Bulk mineral K_d distribution coefficients were computed using the CRUNCH code (an updated version of the GIMRT code [19]) combined with the LLNL surface complexation and ion exchange sorption database [20, 21]. The bulk mineral K_d values are combined with the XRD mineralogy data (see the RMSM_Mineralogy.xls workbook in the Appendix\G folder) through the component additivity principle to give an effective K_d value representative of a given RMC. Further details on the methods and limitations of the mechanistic scaling approach are provided by Zavarin et al. [18].

10.4 Data Analysis and Evaluation

The mineralogy of the RMSM CAU is classified into nine RMCs (see Section 4.2 and the RMSM_HFM.xls workbook). The RMCs were assigned to each XRD mineralogy sample (RMSM_Mineralogy.xls) by matching the corresponding location in the HFM model. The mineralogy data in the RMSM CAU are mainly sampled from the zeolitic, devitrified, and vitric tuffs. Due to limited datasets within the RMSM HFM area, there were not enough samples in the argillic, clastic-confining, and granite-confining units to compute K_d values using the mechanistic model approach. Furthermore, K_d values could not be computed in the vitric tuffs because the water chemistry samples did not satisfy charge balancing criteria. Thus, only K_d values for the devitrified and zeolitic tuffs were computed.

Figures 10-1 and 10-2 illustrate the calculated K_d values of 10 radionuclides in the zeolitic and devitrified tuffs with box and whisker plots. Additional box and whisker plots are shown in the RMSM_Appendix_F.pdf file in the Appendix\F folder. The RMSM CAU mechanistic model K_d values are compared to both direct laboratory measurements and mechanistic model predictions based on laboratory data, which are labeled “Laboratory” and “Mechanistic Model (Laboratory),” respectively. The laboratory measurements for the zeolitic and devitrified tuffs are obtained primarily from the YMP data [14-17] and are described in detail in the YFCM TDD [5].

The mechanistic model provides K_d values for each radionuclide in the zeolitic tuff that are in agreement with the laboratory and mechanistic model predictions of YMP. Discrepancies in the mechanistic model K_d ranges are likely due to differences between the sample mineralogy and water chemistry of RMSM and YMP. However, the general agreement in the zeolitic tuff, which has the largest abundance of mineralogy samples, provides confidence that the mechanistic model provides K_d values consistent with laboratory studies.

For the devitrified tuff (e.g., DMP or WTA HGU) samples, the mechanistic model tends to over-predict the laboratory K_d values. Secondary minerals, zeolites and smectites strongly sorb radionuclides of concern. Cesium (Cs), strontium (Sr), and calcium (Ca) are strongly sorbed by zeolite minerals, while americium (Am), europium (Eu), nickel (Ni), neptunium (Np), plutonium (Pu), samarium (Sm), and uranium (U) are mainly sorbed by smectites. The major minerals in the

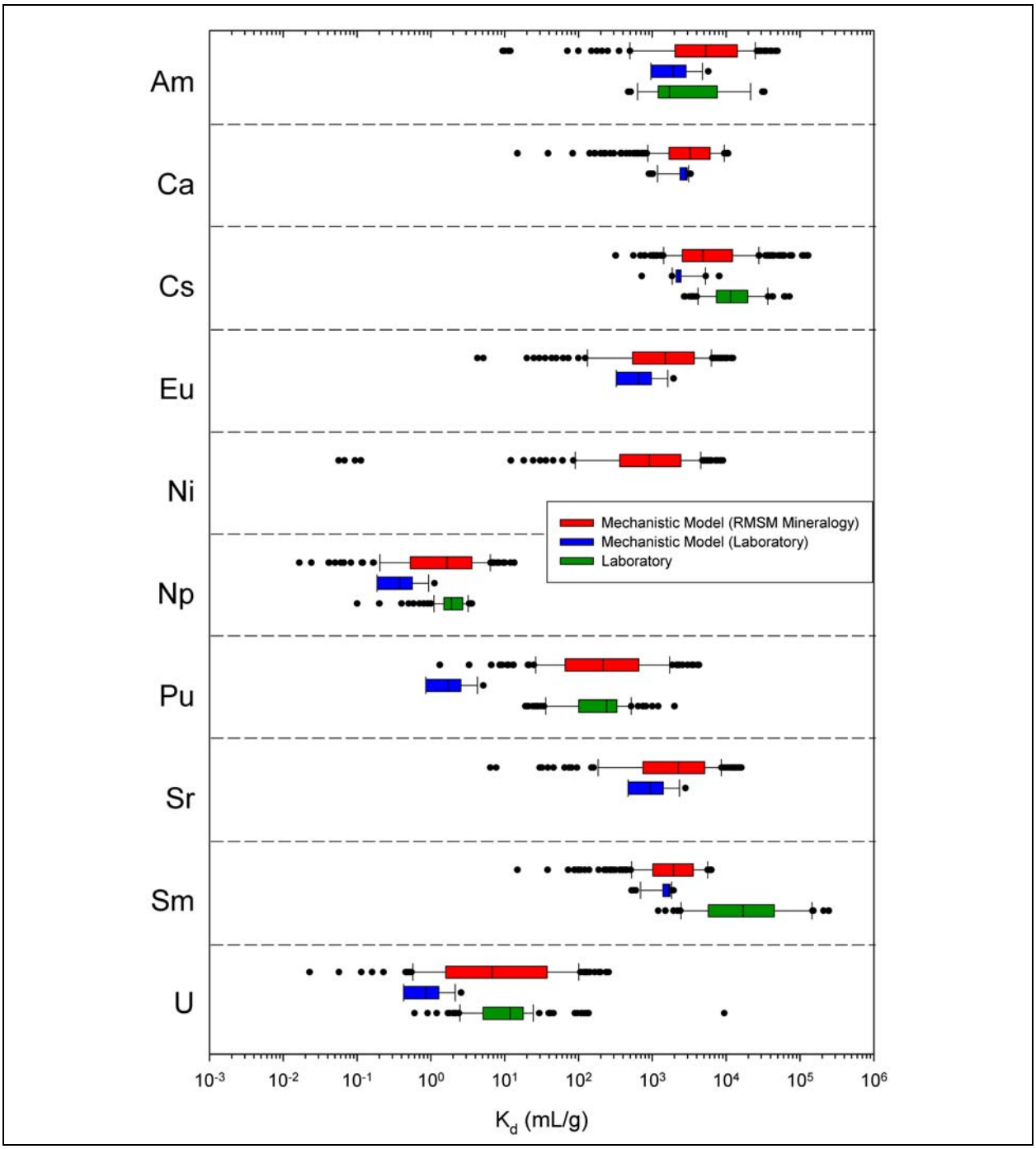

Figure 10-1
Zeolitic RMC K_d Values for Each Radionuclide Obtained from Laboratory and Mechanistic Model Studies

Box and whisker plots provide an integrated presentation of parametric data including the 25th and 75th percentiles (left and right limits of the box), the median (interior crossbar of the box), the data range (left and right limits shown by the whiskers), and outliers (data points beyond the data range). Laboratory data was obtained from measurements at NTS CAUs [5-13] and YMP [14-17]. Mechanistic models using the laboratory mineralogy and water chemistry [5] as input are compared to mechanistic models using RMSM mineralogy and water chemistry.

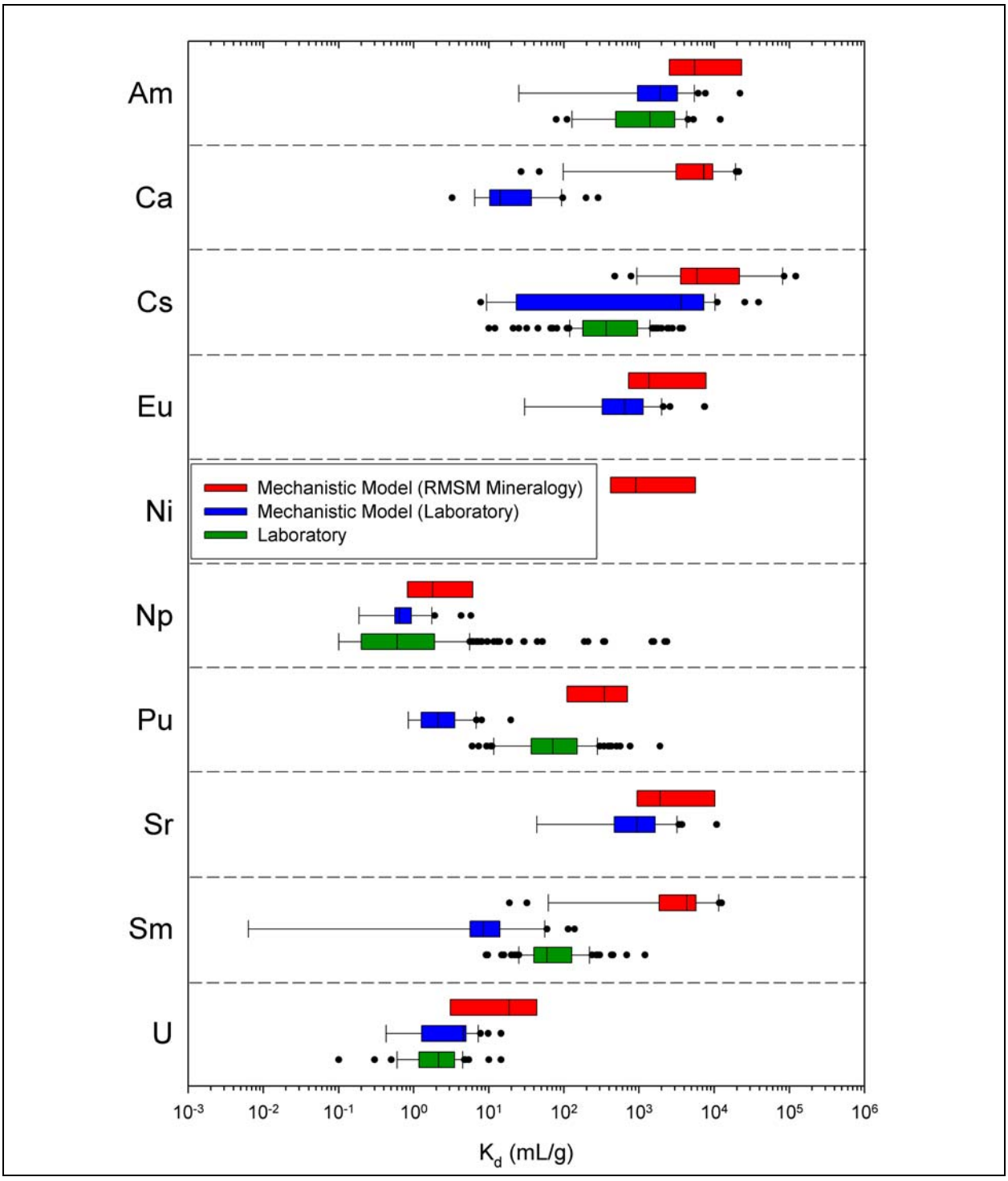

Figure 10-2
Devitrified Mafic-Poor/Rich RMC K_d Values for Each Radionuclide Obtained from Laboratory and Mechanistic Model Studies

Laboratory data was obtained from measurements at NTS CAUs [5-13] and YMP [14-17]. Mechanistic models using the laboratory mineralogy and water chemistry [5] as input are compared to mechanistic models using RMSM mineralogy and water chemistry.

zeolitic tuff are zeolites and smectites, whereas in the vitric tuff, the mineralogy is dominated by feldspar minerals and only minor clays and zeolites. Therefore, efforts to quantify the percentages of secondary minerals, clays and zeolites are much more difficult when the percentages are small. In the devitrified tuff, the zeolite and smectite mineral percentages are diminished, while the felsic material percentages increase. Thus, the accuracy and resolution of the XRD sampling method is critical in detecting relatively smaller zeolite and smectite percentages.

In characterizing the split sample mineralogy, there are numerous XRD methods that have been used, each having its own benefits and drawbacks. For Rainier Mesa, the data consist of "F" and "S" method XRD data in the RMSM_Mineralogy.xls workbook. The "F" method refers to quantitative XRD data obtained from full pattern fitting methods, while the "S" method refers to semi-quantitative estimates. A detailed description of each XRD method is available in the YFCM TDD [5], Appendix D. The "F" data are the most accurate with the highest resolution. However, only a small proportion of the data have been measured with the "F" data. Conversely, the "S" data are plentiful but have poor resolution, especially at low mineral percentages, leading to a significant number of "zero" or "null" values for the mineral percentages. Furthermore, the "S" method data provide, at best, a range of estimated mineral percentages present in a given sample. Histograms of the mineralogy dataset are decomposed into "F" and "S" data in the RMSM_Appendix_G.pdf file in the Appendix\G folder.

Treatment of the measured mineralogical values near or below the detection limits of the respective experiments is a critical component to the mechanistic model calculations. Statistical distributions were computed by neglecting the zero K_d values, which results in K_d values overpredicted in the case of the devitrified tuff (recall, this is not the case in the zeolitic tuff due to the larger zeolite and smectite mineral percentages). Inclusion of the zero values leads to K_d distributions that enhance radionuclide mobility (lower K_d values), while exclusion leads to distributions that favor radionuclide retardation (higher K_d values). The K_d values are given in the RMSM_Matrix Sorption.xls workbook in the Appendix\F folder. To address this issue, LLNL devised a geostatistical method to provide a basis for correcting the mineral percentage to a non-zero value, thus providing a more realistic representation of the true K_d value [22]. These methods will be evaluated when developing the RMSM CAU transport parameters.

10.5 Scaling

Rainier Mesa CAU transport simulations will be conducted over various spatial scales. Scaling considerations for K_d values must address how well measurements conducted at the laboratory scale represents the integrated sorptive behavior of a much larger volume in the CAU-scale model. Factors include representativeness of the samples used for laboratory measurements relative to variability of the formation characterized, and larger-scale longer-term processes that may not be well-characterized in the laboratory. One method for addressing this would be to use the data presented in this report as representative of the small-scale system behavior. Scaling simulations could be designed to identify the effective K_d of a CAU-scale model grid block using multiple realizations of spatially distributed values from this study.

10.6 Limitations

A constraint of the mechanistic modeling approach is that, although a detailed set of reactions may be simulated, parameters for those reactions may not be available, particularly at the CAU scale. For example, a mechanistic transport model requires the concentration of available reactive surface sites (often represented as percent mass of various minerals for which total reactive surface sites are known) be specified. Characterization of surfaces that a solute may come in contact with is generally not known and must be inferred. Further, coatings of reactive mineral sites with other compounds may serve to modify the available reactive surface sites for a given mineral. Another limitation of mechanistic models is that they require large amounts of computer resources due to the complexity and nonlinearity of the processes that they attempt to capture when used in a fully coupled flow and transport model. Although mechanistic models have some limitations in their application for large-scale systems, they remain attractive due to their ability to capture heterogeneity. By doing so, they provide technical credibility to scaled or abstracted methods.

10.7 References

1. Bowen, S.M., D.L. Finnegan, J.L. Thompson, C.M. Miller, P.L. Baca, L.F. Olivas, C.G. Geoffrion, D.K. Smith, W. Goishi, B.K. Esser, J.W. Meadows, N. Namboodiri, and J.F. Wild. 2001. *Nevada Test Site Radionuclide Inventory, 1951-1992*, LA-13859-MS. Los Alamos, NM: Los Alamos National Laboratory.

2. Decker, D.L, C. Papelis, R.L. Hershey, R. Harris, and G. Schmett. 2003. *Temperature Dependence of Sorption Behavior of Lead and Cesium Metal Ions on Western Pahute Mesa and Rainier Mesa Aquifer Rocks*, DOE/NV/13609-21. Reno, NV: Desert Research Institute, Division of Hydrologic Sciences.

3. Papelis, C., and W. Um. 2003. *Evaluation of Cesium, Strontium, and Lead Sorption, Desorption, and Diffusion in Volcanic Tuffs from Frenchman Flat, Nevada Test Site: Microscopic and Spectroscopic Investigations*, DOE/NV/1309-18; Publication No. 45189. Las Vegas, NV: Desert Research Institute.

4. Um, W., and C. Papelis. 2004. "Metal Ion Sorption and Desorption on Zeolitized Tuffs from the Nevada Test Site." In *Environmental Science & Technology*, vol. 38, p. 496-502.

5. Stoller-Navarro Joint Venture. 2007. *Phase I Contaminant Transport Parameters for the Groundwater Flow and Contaminant Transport Model of Corrective Action Unit 97: Yucca Flat/Climax Mine, Nevada Test Site, Nye County, Nevada, Rev. 0*, S-N/99205--096. Las Vegas, NV.

6. Wolfsberg, K., B.P. Bayhurst, S.S. Levy, F.O. Lawrence, S.D. Knight, A.J. Mitchell, A.E. Ogard, and P.L. Wanek. 1983. *Research and Development Related to Sorption of Radionuclides on Soils*, LA-UR-83-800. Los Alamos, NM: Los Alamos National Laboratory.

7. Zavarin, M., S.K. Roberts, T.P. Rose, and D.L. Phinney. 2002. *Validating Mechanistic Sorption Model Parameters and Process for Reactive Transport in Alluvium*, UCRL-ID-149728. Livermore, CA: Lawrence Livermore National Laboratory.

8. Zavarin, M., M.R. Johnson, S.K. Roberts, R. Pletcher, T.P. Rose, A.B. Kersting, G. Eaton, Q. Hu, E. Ramon, J. Walensky, and P. Zhao. 2005. *Radionuclide Transport in Tuff and Carbonate Fractures from Yucca Flat, Nevada Test Site*, UCRL-TR-219836. Livermore, CA: Lawrence Livermore National Laboratory.

9. Ware, S.D., A. Abdel-Fattah, M. Ding, P.W. Reimus, C. Sedlacek, M. Haga, E. Garcia, and S. Chipera. 2005. *Radionuclide Sorption and Transport in Fractured Rocks of Yucca Flat, Nevada Test Site*, LA-UR-05-9279. Los Alamos, NM: Los Alamos National Laboratory.

10. Zavarin, M., S. Roberts, P. Reimus, and M. Johnson. 2007. *Summary of Radionuclide Reactive Transport Experiments in Fractured Tuff and Carbonate Rocks from Yucca Flat, Nevada Test Site*, UCRL-TR-225271. Livermore, CA: Lawrence Livermore National Laboratory.

11. Wolfsberg, K. 1978. *Sorption-Desorption Studies of Nevada Test Site Alluvium and Leaching Studies of Nuclear Test Debris*, LA-7216-MS. Los Alamos, NM: Los Alamos National Laboratory.

12. Wolfsberg, K. 1978. *Sorptive Properties of Alluvium*, Office Memorandum dated 24 October. Los Alamos, NM: Los Alamos National Laboratory.

13. Zavarin, M. 2002. *Matrix Diffusion and Colloid-Facilitated Transport in Fractured Rocks: Model and Parameter Validation*, UCRL-ID-149817. Livermore, CA: Lawrence Livermore National Laboratory.

14. Triay, I.R., A. Meijer, J.L. Conca, K.S. Kung, R.S. Rundberg, E.A. Strietelmeier, C.D. Tait, D.L. Clark, M.P. Neu, and D.E. Hobart. 1997. *Summary and Synthesis Report on Radionuclide Retardation for the Yucca Mountain Site Characterization Project: Yucca Mountain Site Characterization Program Milestone 3784M*, LA-13262-MS, UC-903, and UC-940. Los Alamos, NM: Los Alamos National Laboratory.

15. U.S. Department of Energy, Office of Civilian Radioactive Waste Management, Office of Repository Development. 2001. *Unsaturated Zone and Saturated Zone Transport Properties (U0100)*, ANL-NBS-HS-000019, Rev. 0, ICN 02. Las Vegas, NV.

16. U.S. Department of Energy, Office of Civilian Radioactive Waste Management, Office of Repository Development. 2004. *Site-Scale Saturated Zone Transport*, MDL-NBS-HS-000010, Rev 01, ICN 00. Las Vegas, NV.

17. Yucca Mountain Project. 2007. Technical Data Management Service. As accessed at http://connect.ymp.gov on 13 May.

18. Zavarin, M., S.F. Carle, and R.M. Maxwell. 2004. *Upscaling Radionuclide Retardation - Linking the Surface Complexation and Ion Exchange Mechanistic Approach to a Linear K_d Approach*, UCRL-TR-204713. Livermore, CA: Lawrence Livermore National Laboratory.

19. Steefel, C.I., and S.B. Yabusaki. 1995. *Software for Modeling Multicomponent-Multidimensional Reactive Transport, User Manual and Programmer's Guide*, OS3D/GIMRT. Richland, WA: Pacific Northwest National Laboratory.

20. Zavarin, M., and C.J. Bruton. 2004. *A Non-Electrostatic Surface Complexation Approach to Modeling Radionuclide Migration at the Nevada Test Site: II. Aluminosilicates*, UCRL-TR-208672. 6 June. Livermore, CA: Lawrence Livermore National Laboratory.

21. Zavarin, M., and C.J. Bruton. 2004. *A Non-Electrostatic Surface Complexation Approach to Modeling Radionuclide Migration at the Nevada Test Site: I. Iron Oxides and Calcite*, UCRL-TR-208673. 6 June. Livermore, CA: Lawrence Livermore National Laboratory.

22. Carle, S.F., M. Zavarin, G.A. Pawloski. 2007. Written communication. Subject: *Spatial Variability of Reactive Mineral and Radionuclide K_d Distributions in the Tuff Confining Unit*.

11.0 FRACTURE SORPTION

There have been no new data collected or new method development work completed on fracture sorption since publication of the YFCM TDD [1]. Consequently, this section presents a summary of the fracture sorption section in that document, and addresses application of the data and analysis presented in that document to the RMSM CAU.

11.1 The Role of Fracture Sorption in Contaminant Transport

Fracture sorption is the sorption of radionuclides to fracture surfaces and fracture coating minerals before diffusion into the matrix material where matrix sorption may occur. Similar to matrix sorption, fracture sorption is a physiochemical process at mineral-water interfaces that retards solutes and affects solute mobility within flowing groundwater systems. Fracture sorption is treated separately from matrix sorption because it is parameterized differently.

11.2 Data Types, Sources, and Transfer

The simplest method to represent fracture sorption is to use retardation factors, R, for solutes in fractures. Although closely related, the retardation factor is preferable to K_d because the K_d is based upon a volumetric sample of material, as appropriate for matrix material. In fractures, reactive processes leading to solute retardation are represented per unit length per unit width of fracture rather than per unit volume of rock. A retardation factor is straightforward to apply in transport models.

The use of a fracture retardation factor requires the assumption of local equilibrium. Reactions that are kinetic in nature must be assumed to occur fast enough that the retardation factor adequately captures the process and provides conservative results (i.e., does not overestimate retardation) in CAU-scale simulations. Further, the use of a fixed retardation factor does not allow for changing sorption behavior due to changes in water chemistry or mineral surfaces. The retardation factor can be varied spatially, but does not represent dynamic system changes during the course of a simulation.

11.2.1 Data Types

Data addressing fracture sorption are of two types: empirical data from laboratory experiments and estimates from mechanistic models that compute retardation parameter values from component parameter values. Both types of data characterize fracture sorption according to transport theory. Modeling studies seeking to upscale mechanistic processes to larger-scale retardation factors are

based upon the same processes described for mechanistic models of matrix K_d (Section 10.0). The key components to estimating reactions with fracture coatings are as follows:

- The effective reactive surface area of fracture-coating minerals available to solutes in fractures
- The mineralogic composition of fracture coatings
- The distribution (existence) of fracture-coating minerals in fractures
- Water chemistry
- The sorbing solute

The first three parameters can be used in mechanistic models to estimate effective fracture retardation factors based on specified values for the last two parameters.

A strength of the mechanistic modeling approach is that it specifically represents reactions that control and affect sorption to fracture-coating minerals. Due to the complete representation of all reactions, the mechanistic modeling approach can also describe how groundwater chemistry, such as pH, affects sorption reactions, as well as how sorption reactions may affect groundwater chemistry. The mechanistic approach is not affected by data transferability issues when appropriate CAU-specific parameter values are used for estimating retardation.

A limitation of the mechanistic modeling approach is that appropriate parameter values for the detailed reactions may not be available, particularly at the CAU scale. This is important for estimating fracture retardation factors where spatial variation of fracture-coating materials will have first-order effects on the estimated parameters.

11.2.2 Data Sources

Fracture retardation assessment has been presented in a number of documents within the UGTA Project:

- Estimates of fracture-coating thickness, distribution, mineral content, and availability in conjunction with surface complexation thermodynamic data were used to predict fracture retardation factors ([2], Section 7.0, Appendix F, [3]).
- Estimates of fracture retardation factors were made using mechanistic process models [4].
- Estimates of fracture retardation factors are presented for various rock types on Pahute Mesa [2, 4]. Pahute Mesa volcanic aquifers have reasonably similar water composition to Yucca Flat volcanic aquifers; therefore, for HSUs that crosswalk from Pahute Mesa to Yucca Flat, these data can be used directly (see Table 4-4 of the YFCM HFM for HSU crosswalks) [5].
- Laboratory-scale fracture transport experiments were conducted by LLNL and LANL to determine empirical estimates of fracture retardation factors [6]. Additional information regarding these experiments is provided in original reports [7, 8].

11.2.3 Data Transfer

The data discussed are from the YFCM HFM area and the Central and Western Pahute Mesa CAU. There are no data specific to the RMSM CAU. The general discussions of data transfer presented in the YFCM TDD apply also to use of the data for the RMSM CAU [1]. The empirical data can be transferred respecting equivalent and similar HSUs for Pahute Mesa and Yucca Flat, and for RMSM (Table 4-4). The mechanistic approach is non-CAU specific but becomes specific to the CAU when appropriate CAU-specific parameter values are used in the estimation of retardation.

A quantitative assessment of the sensitivity of transport modeling to the uncertainty in this parameter cannot be provided before the transport model development. The parameter description discusses the importance of this parameter.

11.3 Data Evaluation

The LANL report used a semi-mechanistic approach for estimating fracture retardation factors — coupled with other processes of matrix diffusion, matrix reaction, and colloid-facilitated transport — to determine expected values of fracture retardation factors that were used in predicting radionuclide concentrations in Wells ER-20-5 #1 and ER-20-5 #3 [2]. They found the primary factor controlling fracture retardation is how much of the fracture coating is accessible to solutes migrating in the fracture.

The LLNL reports applied a mechanistic model using thermodynamic reaction databases to predict fracture retardation factors for several regional model HSUs [4, 9]. Diffusion between fractures and matrix material is not explicitly modeled. Rather, this method includes the effect of some diffusion into the matrix near the fracture wall with the increased effective porosity. Thus, the method also combines the effects of sorption to matrix material and fracture minerals with a single set of parameters. The estimated retardation factors from that study are based on the assumption that the primary metal oxide present in the rocks is an iron oxide. The reported range of uncertainty is only related to uncertainty in mineralogic composition of the fracture coatings, not of abundance or accessibility of those minerals to solutes in the fracture water. Increased predicted mobility when colloids are present and compete with immobile reactive minerals for radionuclide sorption was also demonstrated [4].

Both LLNL and LANL conducted laboratory experiments of radionuclide transport through synthetic parallel-plate fractured tuff and carbonate cores [6, 7]. These simplified fracture transport experiments isolated matrix diffusion and sorption effects from all other fracture transport processes (e.g., fracture lining mineral sorption, heterogeneous flow). Additional fracture transport complexity was added by performing induced-fracture LCA flow through experiments (evaluating the effect of aperture heterogeneity) and iron-oxide-coated parallel-plate TCU flow through experiments (evaluating the effect of fracture lining minerals). The tuff and carbonate cores used in the experiments were obtained from the USGS Core Library, Mercury, Nevada. The results of the analyses are estimates of the parameters with the advantage of matching empirical rather than theoretical data.

11.4 Fracture Retardation Factor Summary and Integration

Two approaches have been applied for estimating retardation in fractures due to reactions with fracture-coating minerals account for processes that may affect migration rates and groundwater concentration of reactive radionuclides [2, 4]. However, these approaches are theoretical, and the two approaches yield different results, in some cases because of differences in the conceptual model and the assumptions about processes.

The Wolfsberg et al. approach only considered reactions with the minerals coating the fracture; reactions with matrix minerals are considered in conjunction with the matrix diffusion component of their model [2]. The Zavarin et al. approach included reactions with matrix minerals as well as with fracture-coating minerals, which lead to estimated retardation factors [4]. Another difference between the two approaches is that the Zavarin et al. approach considered ion exchange reactions, which are the primary reactions responsible for retardation of Sr^{2+} and Cs^{+} [4].

For estimates of retardation in fractures based on the analysis and matching of empirical data, matrix sorption accounted for most of the observed retardation of radionuclides in the TCU (unless a radionuclide was transported as a colloid) [6]. Fracture sorption accounted for most of the observed retardation in the LCA. Fracture sorption was shown to play a significant role in the TCU for both U and Np, and was not significant for carbon (C)-14, Sr, Pu, and Cs. In the LCA, fracture sorption was shown to play a significant role for Sr, Cs, Np, and Pu, but was not significant for either C-14 or U.

The fraction sorption parameters determined from the two mechanistic modeling approaches as well as the empirical approach are summarized in Table 11-1. Only the data for the HGUs that are considered to have fracture porosity (LFA, WTA, and CA) are shown. The results can be correlated with HSUs in the RMSM CAU. Considering the mechanistic modeling approaches, the range of uncertainty is largely due to the strictly theoretical nature of the estimation methods. With the exception of Sr^{2+} and Cs^{+}, the empirically-determined retardation factors are generally similar to those developed through the mechanistic modeling approach of Wolfsberg et al. [2]. However, the empirical method results offer the advantage of direct testing and provide results for the LCA.

Table 11-1
Summary of Fracture Retardation Factors

HGUs	Alteration	Ca [a]	Cs [a]	Sr [a]	Am [a]	Eu [a]	Sm [a]	Np [a]	U [a]	Pu(10^{-5}) [a]	Pu(10^{-10}) Pu(10^{-15}) [a, b]	Pu [a, c]	C-14 [a]
LFA [d]	Lava	NA (2,188) NA	(1.04, 1.06) (1,349, 10,965) NA	(1.04, 1.06) (1,318) NA	(163, 231) (98, 115) NA	(163, 231) (95, 120) NA	(163, 231) (129, 145) NA	(1.35, 4.9) (3.7, 13) NA	(1.35, 4.9) (7.1, 35) NA	(9.2, 13) (5.5, 32) NA	(11, 62) (42, 132) NA	NA	NA
WTA [d]	Welded, vitric to devitrified	NA (2,188) NA	(1.01, 1.23) (1,349, 10,965) NA	(1.01, 1.23) (1,318) NA	(63, 837) (98, 115) NA	(63, 837) (95, 120) NA	(63, 837) (129, 145) NA	(1.13, 13.5) (3.7, 13) NA	(1.13, 13.5) (7.1, 35) NA	(2.7, 39) (5.5, 32) NA	(11, 62) (42, 132) NA	NA	NA
CA	Fractured	NA NA NA	NA NA (1.0, 320.0)	NA NA (1.0, 33.0)	NA NA NA	NA NA NA	NA NA NA	NA NA (2.1, ≥ 50)	NA NA (1.0, 3.5)	NA NA NA	NA NA NA	0.00, 50	1.0, 5.0

Source: [5]

[a] Upper range in each cell represents retardation to fracture minerals only [4]. Middle range in each cell represents retardation due to sorption to fracture minerals and matrix minerals [6]. Lower range in each cell represents fracture retardation factors from [8]. Radionuclides shown include analysis of multiple isotopes in some cases.

[b] Retardation factors Pu for oxygen fugacities of 10^{-10} and 10^{-15} [6].

[c] Retardation factors for Pu and C-14 measured from laboratory experiments [8].

[d] The LFA and WTA HGUs are associated with the TMA regional HSU [6].

NA = Not available

11.5 References

1. Stoller-Navarro Joint Venture. 2007. *Phase I Contaminant Transport Parameters for the Groundwater Flow and Contaminant Transport Model of Corrective Action Unit 97: Yucca Flat/Climax Mine, Nevada Test Site, Nye County, Nevada, Revision No.* 0, S-N/99205--096. Las Vegas, NV.

2. Wolfsberg, A., L. Glascoe, G. Lu, A. Olson, P. Lichtner, M. McGraw, T. Cherry, and G. Roemer. 2002. *TYBO/BENHAM Model Analysis of Groundwater Flow and Radionuclide Migration from Underground Nuclear Tests in Southwestern Pahute Mesa, NTS*, LA-13977. Los Alamos, NM: Los Alamos National Laboratory.

3. Pawloski, G.A., A.F.B. Tompson, and S.F. Carle. 2001. *Evaluation of the Hydrologic Source Term from Underground Nuclear Tests on Pahute Mesa at the Nevada Test Site: CHESHIRE Test*, UCRL-ID-147023. Livermore, CA: Lawrence Livermore National Laboratory.

4. Zavarin, M., S.F. Carle, and R.M. Maxwell. 2004. *Upscaling Radionuclide Retardation - Linking the Surface Complexation and Ion Exchange Mechanistic Approach to a Linear K_d Approach*, UCRL-TR-204713. Livermore, CA: Lawrence Livermore National Laboratory.

5. Bechtel Nevada, 2006. *A Hydrostratigraphic Model and Alternatives for the Groundwater Flow and Contaminant Transport Model of Corrective Action Unit 97: Yucca Flat-Climax Mine, Lincoln and Nye Counties, Nevada*, DOE/NV/11718--1119. Las Vegas, NV.

6. Zavarin, M., S. Roberts, P. Reimus, and M. Johnson. 2007. *Summary of Radionuclide Reactive Transport Experiments in Fractured Tuff and Carbonate Rocks from Yucca Flat, Nevada Test Site*, UCRL-TR-225271. Livermore, CA: Lawrence Livermore National Laboratory.

7. Ware, S.D., A. Abdel-Fattah, M. Ding, P.W. Reimus, C. Sedlacek, M. Haga, E. Garcia, and S. Chipera. 2005. *Radionuclide Sorption and Transport in Fractured Rocks of Yucca Flat, Nevada Test Site*, LA-UR-05-9279. Los Alamos, NM: Los Alamos National Laboratory.

8. Zavarin, M., M.R. Johnson, S.K. Roberts, R. Pletcher, T.P. Rose, A.B. Kersting, G. Eaton, Q. Hu, E. Ramon, J. Walensky, and P. Zhao. 2005. *Radionuclide Transport in Tuff and Carbonate Fractures from Yucca Flat, Nevada Test Site*, UCRL-TR-219836. Livermore, CA: Lawrence Livermore National Laboratory.

9. Zavarin, M., S.K. Roberts, T.P. Rose, and D.L. Phinney. 2002. *Validating Mechanistic Sorption Model Parameters and Process for Reactive Transport in Alluvium*, UCRL-ID-149728. Livermore, CA: Lawrence Livermore National Laboratory.

12.0 GEOCHEMISTRY

This section provides a summary of the groundwater chemistry in RMSM sample wells. A geochemical and isotopic evaluation of the RMSM CAU was previously conducted [1]. The main objective of this evaluation is to prepare the data to support the distribution coefficient calculations described in Section 10.0. Thus, the focus is heavily weighted towards the characterization of the average groundwater chemistry in sample wells and the determination of the mineralogy that is associated with each groundwater sample.

12.1 Role of Geochemistry in Contaminant Transport

Groundwater chemistry is important to the prediction of contaminant sorption onto rock surfaces and thus to the prediction of contaminant transport. Dissolved constituents in groundwater influence the extent of molecular-level reactions between contaminants and aquifer materials. Furthermore, groundwater chemistry also provides a means for determining the origin, flow paths, and time scale of groundwater flow and transport independent of estimates based on hydraulic flow analysis.

12.2 Data Compilation

Groundwater chemistry samples from wells, tunnels, and springs within the RMSM HFM boundaries were compiled from the GEOCHEM07.mdb database and are provided in the RMSM_Geochemistry.xls workbook in the Appendix\G folder [2]. The compiled dataset used for the analyses is described as follows:

- The chemical constituents included are calcium (Ca^{2+}), magnesium (Mg^{2+}), sodium (Na^{+}), potassium (K^{+}), chloride (Cl^{-}), sulfate (SO_4^{2+}), bicarbonate (HCO_3^{-}), carbonate (CO_3^{2-}), silica (SiO_2), nitrate (NO_3^{-}), bromide (Br^{-}), phosphate (PO_4^{3-}), and fluoride (F^{-}) ion concentrations. Also included are pH and water temperature.
- Samples were removed if they were inconsistent with historical or regional trends for the reported locations, as noted by the data quality evaluation flags within the GEOCHEM07.mdb database [2].
- The average water chemistry for each well and tunnel is summarized in the RMSM_Geochemistry.xls workbook. Average water chemistries with a major-ion charge balance within ±5% are included in the mechanistic model calculations (Section 10.0). The major ions are Ca^{2+}, Mg^{2+}, Na^{+}, K^{+}, Cl^{-}, SO_4^{2-}, HCO_3^{-}, and CO_3^{2-}.

12.3 Data Analysis and Evaluation

Groundwater samples were collected using different techniques. Samples collected for the UGTA Project wells include both depth-discrete bailed samples and composite groundwater characterization samples. Each groundwater sample listed in Appendix G was assigned a primary HSU and RMC using formation access intervals (FAIs) or discrete bailing depths in the given borehole.

Groundwater samples from 14 wells were considered in this study. Samples from springs and tunnel seeps were not evaluated for the distribution coefficient calculations given that lithology intervals are not well defined and the amount of groundwater samples is limited. The RMSM_Geochemistry.xls workbook summarizes the FAIs, HSUs, and RMCs for each groundwater sample. In addition, the average groundwater chemistry for 14 wells is illustrated on the Piper diagrams in Figures 12-1 and 12-2. Additional Piper diagrams of individual samples, as well as bar plots and stiff diagrams, are presented in the RMSM_Geochemistry.xls workbook.

Evaluation of the dissolved constituents shows there are four main hydrochemical water types, or facies, in NTS groundwater [3-5], which include:

- Na-K-HCO_3 groundwater facies commonly found in volcanic-rock aquifers, where Na^+ plus K^+ constitute at least 60% of the total cation concentration.
- Ca-Mg-HCO_3 facies commonly occurring in carbonate aquifers, where Ca^{2+} plus Mg^{2+} constitute at least 60% of the total cation concentration.
- Ca-Mg-Na-HCO_3 facies assumed to be a mixture of the Na-K-HCO_3 and Ca-Mg-HCO_3 facies [3].
- Ca-Mg-SO_4 facies.

Dissolution of calcite and dolomite is the primary source of Ca^{2+} and Mg^{2+} in carbonate aquifer groundwater. High Na^+ concentrations are typically present in volcanic HSU groundwater from reaction with volcanic glass and feldspar minerals and ion exchange with Ca^{2+} in these highly zeolitized rocks. Bicarbonate is the predominant anionic constituent in the majority of the groundwater and is derived primarily from the dissolution of soil carbon dioxide (CO_2) gas and reaction with carbonate minerals.

12.3.1 Volcanic-Rock Aquifers and Tuff Confining Units

Four wells (Hagestad #1, Test Well #1, Water Well #8, and UE-14b) were completed within the volcanic rock aquifers and tuff confining units, spanning the BRA, TM-WTA, TCA, TSA, ATCU, and UTCU HSUs. As shown in Figure 12-3, each of the volcanic HSU groundwater chemistries are dominated by Na^+, which is consistent with the ion exchange of Ca^{2+} for Na^+ in these highly zeolitized rocks.

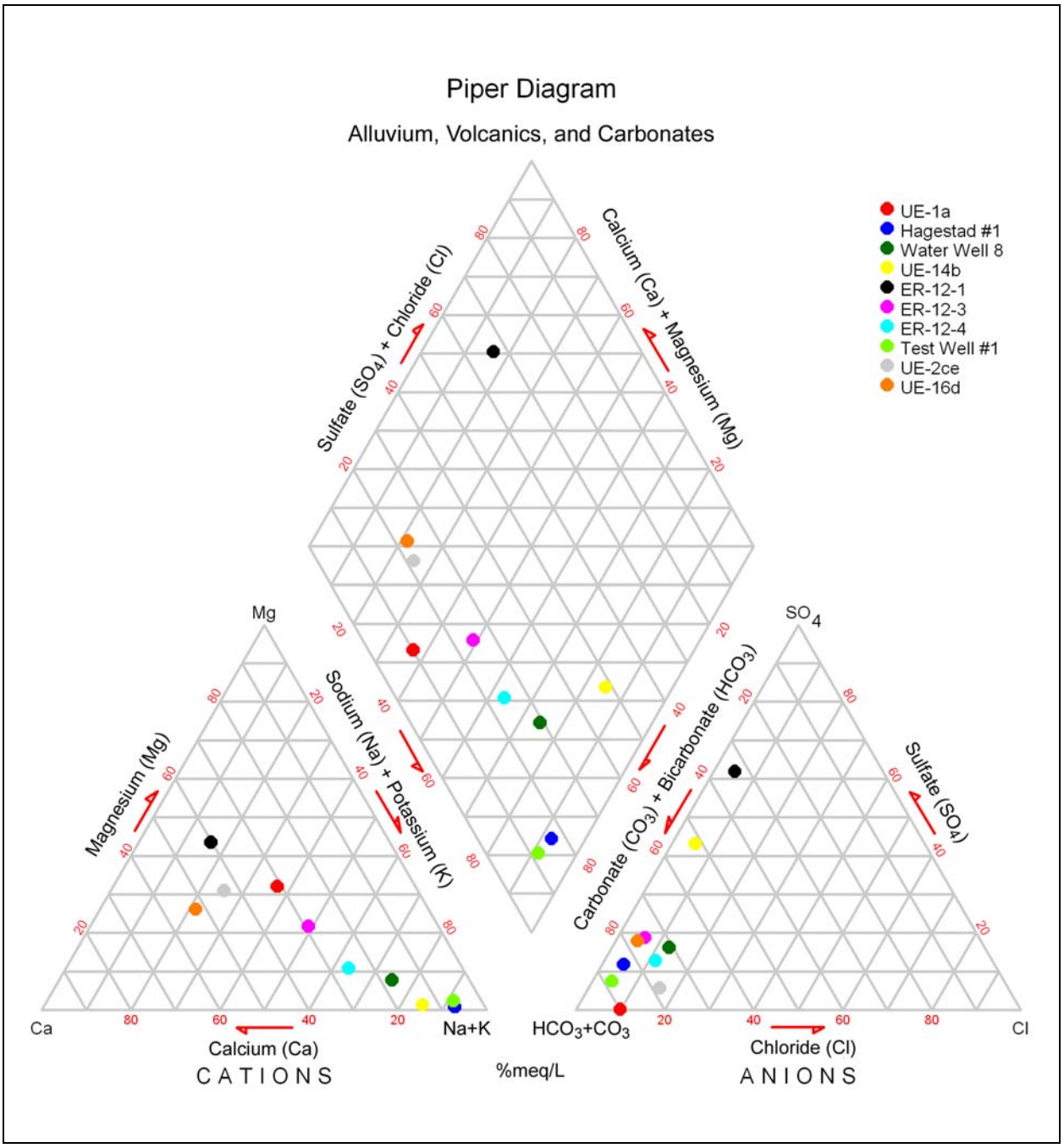

Figure 12-1
Piper Diagram for the Average Sample Chemistry Collected from the Alluvial Aquifer, Volcanic Aquifers, Tuff Confining Units, and Carbonate Aquifers

Piper diagrams consist of three component representations of major-ion chemistry, where cation (i.e., Ca^{2+}, K^{+}, Mg^{2+}, Na^{+}) and anion (i.e., Cl^{-}, SO_4^{2-}, HCO_3^{-}, CO_3^{2-}) data are plotted in separate trilinear diagrams and then projected onto a central diamond-shaped area to show compositional relationships among groundwater samples. They are used to classify the groundwater as a hydrochemical type, where concentrations are expressed in percent milliequivalents per liter.

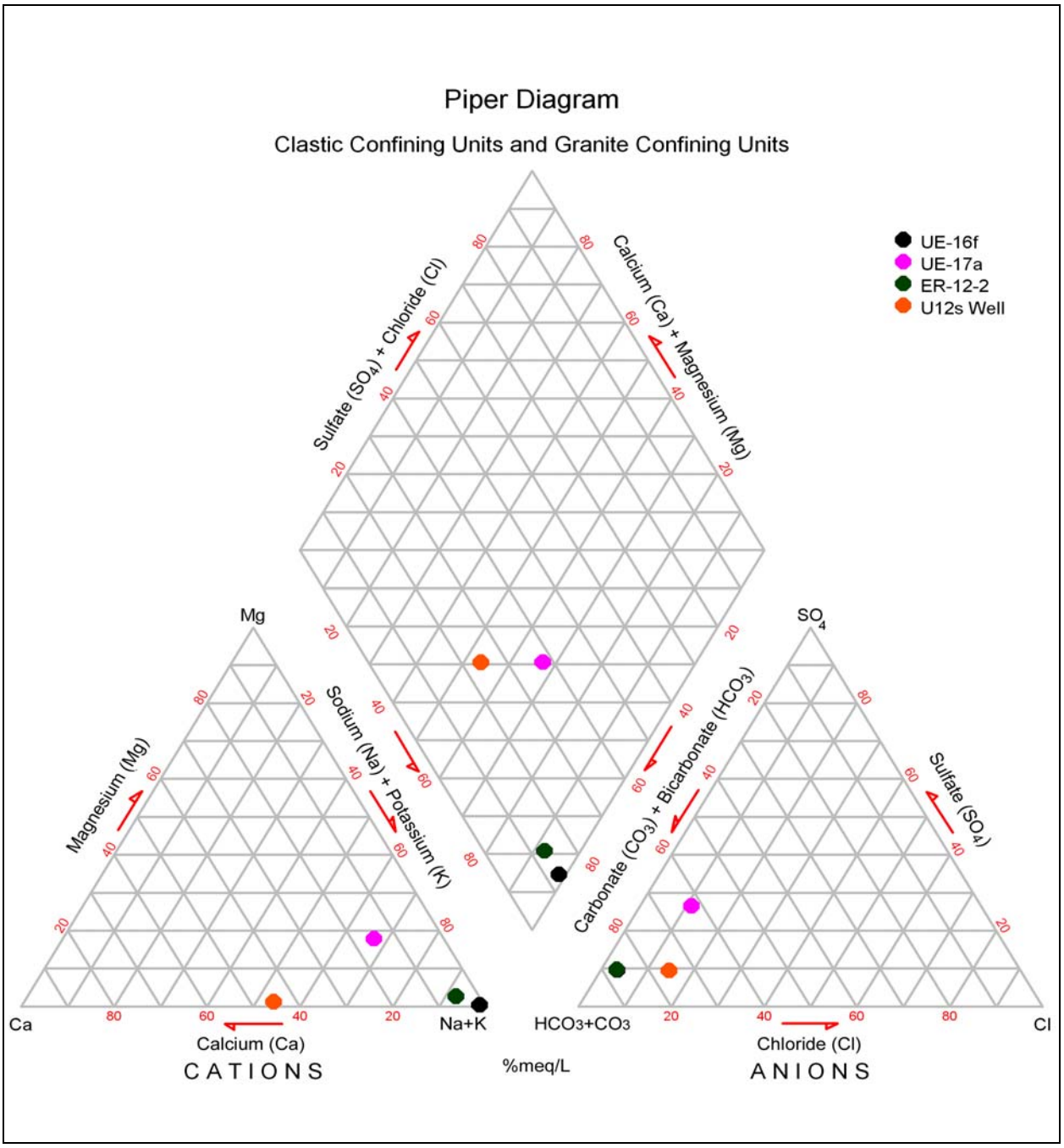

Figure 12-2
Piper Diagram for the Average Sample Chemistry Collected from the Clastic Confining Units and Granite Confining Units

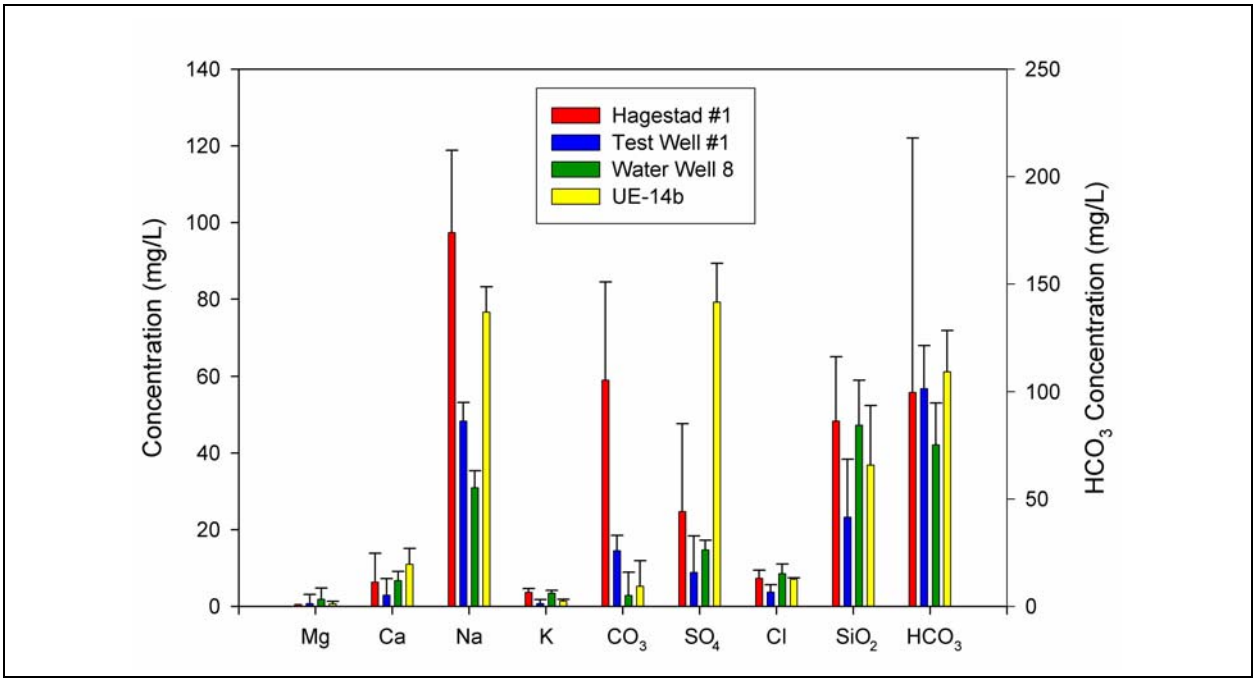

Figure 12-3
Bar Plot for Samples Collected from the Volcanic Aquifers and Tuff Confining Units
The bar plots represent average concentrations that are provided in the RMSM_Geochemistry.xls workbook. HCO_3^- concentrations are plotted on a separate right axis. Error bars (mean ± 1 standard deviation) are presented on the bar plots when multiple samples have been collected.

The Piper diagram shows that the groundwater chemistry of Hagestad #1 and Test Well #1 are each Na-K-HCO_3 type (see Figure 12-2). Significant quantities of the Mg^{2+}, Ca^{2+}, Na^+, SO_4^{2-} and SiO_2 constituents indicate that volcanic groundwater is present at each well (Figure 12-3). The primary HSUs are ATCU for Hagestad #1 and BRA for Test Well #1.

The FAI for UE-14b extends across the TM-WTA, UTCU, and TSA HSUs, where the primary HSU is the TSA. The five groundwater samples collected in UE-14b are representative of volcanic aquifer groundwater. The average water chemistry is presented in Figure 12-1, where large proportions of Na^+ and SO_4^{2-} are present in the groundwater (see Figure 12-3). The primary RMC for UE-14b is DMP representing a high content of quartz and feldspar (> 60%), and low biotite plus hornblende (< 1.5%) (see the RMSM_Geochemistry.xls workbook and Table 4-1).

The FAI for Water Well #8 includes a small portion from the TM-WTA (46 m) and a significantly larger portion from the BRA (566 m). The groundwater chemistry is Na-K-HCO_3 type, where the average pH is neutral at 7.2±0.5. The average water temperature is 25.2±1.4 °C. The RMC in the BRA alternates between DMP and ZEOL at varying depths, indicating the water chemistry is characteristic of both RMCs.

12.3.2 Carbonate Aquifer

Many samples (n = 157) were collected from five wells that sample the carbonate aquifers in the RMSM CAU. Four wells (ER-12-1, ER-12-3, ER-12-4, UE-2ce) were completed within the LCA3, while one well (UE-16d) was completed in the UCA. Overall, the RMC associated with the carbonate aquifers, characterized by greater than 50% carbonate minerals is CC.

Within the LCA3, the groundwater chemistry varies considerably, ranging from Ca-Mg-HCO_3 type, which is typical of groundwater of a carbonate aquifer, to the Na-K-HCO_3 type, which is typical of groundwater of a volcanic-rock aquifer. Different water types are present in wells penetrating the carbonate aquifers (see Figure 12-1) including Na-K-HCO_3-type water (ER-12-3 and ER-12-4) and Ca-Mg-HCO_3-type water (UE-2ce). Groundwater of ER-12-1 is unique relative to all others within the carbonate aquifers. While the FAI does not include continuous LCA3 aquifer units, ER-12-1 samples form a thin sliver of Upper Simonson or Lower Guilmette formation dolostone tectonically sandwiched within Eleana formation clastic rocks. Well ER-12-1 is the only well having less than 50% carbonate plus bicarbonate components, in addition to having extremely high sulfate concentrations (see Figure 12-1). The groundwater chemistry is Ca-Mg-SO_4 type (see the bar plot for the CA in the RMSM_Appendix_G.pdf file). The origins of the high sulfate concentrations are not fully understood, but have been investigated elsewhere [1].

A single well, UE-16d, is completed in the UCA and UCCU. Like groundwater from UE-2ce, chemical analyses from UE-16d allow samples to be classified as Ca-Mg-HCO_3-type water, indicating the likelihood that water from UE-16d is produced from the UCA rather than the UCCU.

12.3.3 Alluvial Aquifer

The UE-1a well was completed in the AA and UCCU of the RMSM geochemistry study area, where the primary HSU is AA. The Piper diagrams in Figure 12-1 and the RMSM_Appendix_G.pdf file show the groundwater chemistry for the two UE-1a samples is Ca-Mg-HCO_3 type. Groundwater in UE-1a has a higher concentration of HCO_3^-, Ca^{2+}, Mg^{2+}, and Cl^- and a lower concentration of SO_4^{2-} and SiO_2. The RMC associated with the AA is VMP, corresponding to a high glass content (> 30%), low clay and zeolite (< 10%, respectively), and low biotite plus hornblende (< 1.5%) (see the RMSM_Geochemistry.xls workbook).

12.3.4 Clastic Confining Units and Granite Confining Units

Three wells within the RMSM geochemistry study area are representative of the UCCU (ER-12-2, UE-16f, UE-17a). The groundwater samples for these wells are the Na-K-HCO_3 type (Figure 12-2). The average water chemistries of ER-12-2 and UE-16f are very similar and cluster together on the Piper diagram. The primary RMC associated with the UCCU is ARG (see the RMSM_Geochemistry.xls workbook). Finally, U-12s is the only well that samples the GCU in the MGCU HSU, where the average water chemistry is mixed type Na-K-Ca-Mg-HCO_3. The primary RMC associated with the MGCU is DMR.

12.4 Limitations

Groundwater data used in this study were sampled and analyzed over a time period from the late 1950s to 2007, and, in many cases, data for a given well are limited to samples collected more than 20 years ago. These older datasets are limited in that the entire parameter suite used for the geochemical investigations is lacking. Geochemical evaluations depend on adequate data coverage, both laterally and vertically, within the study region. Within the RMSM CAU, the wells with the parameter suite necessary to support geochemical characterization are irregularly distributed. This is compounded by sparse groundwater samples from most HSUs, particularly the alluvial and volcanic aquifers. Well samples included in the dataset were often collected as composites, either from wells with single completions that transect multiple HSU boundaries, or from wells with multiple completions that were all pumped simultaneously. Many wells draw from a large vertical cross section of saturated media, possibly resulting in homogenization of the water composition within the borehole [6]. This limits the ability to uniquely define the geochemical characteristics of groundwater within a specific HSU, either locally or regionally, and may have resulted in some of the groundwater mixing that is inferred to have taken place through hydrodynamic processes.

12.5 References

1. Hershey, R.L., J.B. Paces, M. Singleton, E.M. Kwicklis, D.L. Decker, W.M. Fryer, and S. Earman. 2007. Written communication. Subject: *Geochemical and Isotopic Evaluation of Groundwater Movement in Corrective Action Unit 99: Rainier Mesa and Shoshone Mountain, Nevada Test Site*. Las Vegas, NV.

2. Stoller-Navarro Joint Venture. 2007. *Comprehensive Water Quality Database for Groundwater in the Vicinity of the Nevada Test Site, Geochem07.mdb*, S-N/99205--059-Rev. 1. Las Vegas, NV.

3. Schoff, S.L., and J.E. Moore. 1964. *Chemistry and Movement of Ground Water, Nevada Test Site*, Report TEI-838, p. 75. Denver, CO: U.S. Geological Survey.

4. Blankennagel, R.K., and J.E. Weir, Jr. 1973. *Geohydrology of the Eastern Part of Pahute Mesa, Nevada Test Site, Nye County, Nevada*, Professional Paper 712-B. Washington, DC: U.S. Geological Survey.

5. Winograd, I.J., and W. Thordarson. 1975. *Hydrogeologic and Hydrochemical Framework, South-Central Great Basin, Nevada-California, with Special Reference to the Nevada Test Site*, USGS-PP-712-C. Denver, CO: U.S. Geological Survey.

6. Fenelon, J.M. 2005. *Analysis of Ground-Water Levels and Associated Trends in Yucca Flat, Nevada Test Site, Nye County, Nevada, 1951-2003*, Scientific Investigations Report 2005-5175. Carson City, NV: U.S. Geological Survey.

13.0 COLLOID-FACILITATED TRANSPORT

Because colloid data specific to the RMSM CAU are limited, transfer of data from other UGTA CAUs (Frenchman Flat, Pahute Mesa, and RMSM) and from the YMP was necessary. The NTS-wide information for colloids in groundwater has not changed, and a summary of that information and the analysis conducted for the YFCM TDD is presented in this section [1]. These data are transferred to RMSM by way of the HGU identified for the source formation of the analyzed samples. There is no data to specifically support the applicability of the data to RMSM for samples from other CAUs, and there is no established basis otherwise for estimating colloid content for groundwater. The only new information on colloids available since publication of the YFCM TDD is specifically for samples from N- and T-Tunnels in Rainier Mesa. This new information is discussed separately in Section 13.8 because the hydrologic situation within the tunnels is distinct from groundwater.

13.1 Role of Colloids in Contaminant Transport

Colloids are small particles (< 1 micrometer [μm]) that can facilitate the migration of contaminants in groundwater flow systems. Colloids facilitate the transport of strongly sorbing contaminants by providing mobile particles onto which the contaminants can sorb and be transported by the groundwater rather than being sorbed on immobile solids. Some contaminants may occur as colloid particles (intrinsic colloids), which may also travel as mobile particles. Generally one of the two following conditions must be met for colloid-facilitated transport to be significant:

- Colloids remain mobile over relatively long distance and time scales, AND radionuclides are irreversibly or nearly irreversibly sorbed to the colloids, OR
- The product of the surface-area-based radionuclide partition coefficient onto colloids and the mobile colloid surface area is comparable to or greater than the product of the surface-area-based radionuclide partition coefficient onto immobile surfaces and the immobile surface area.

Colloids facilitate mobility of attached radionuclides or as intrinsic colloids, but the magnitude of radionuclide transport by colloids is unknown. The amount would be a strong function of colloid mineralogy, concentration and size, colloid transport parameters, radionuclide sorption/desorption behavior and chemistry of the radionuclide. The process of association of source term radionuclides with colloids has not been studied, and the potential magnitude of radionuclide association with colloids is unquantified. The sensitivity of transport predictions to colloid-facilitated transport has not been determined, but could be significant, particularly in terms of dose.

13.2 Dataset Summary

Data for characterization of colloid-facilitated transport are organized into five categories: (1) colloid mineralogy, (2) colloid concentration and size data, (3) colloid transport parameters, (4) radionuclide distribution coefficients and sorption rates, and (5) radionuclide associations with colloids at source locations near cavities.

Data were compiled from all available sources for NTS-specific data and YMP data, and the locations and sources for all data are identified in Figure 13-1. Additional data were transferred and included in the analysis only where necessary to support general characterization of a parameter. Data on colloids are sparse, and the parameters are characterized in general.

13.3 Colloid Mineralogy

Mineralogy of colloids is important because the sorption, desorption, and distribution parameters for colloids within the groundwater system are dependent upon mineralogy. The colloidal mineralogy is primarily composed of clays and zeolites that are also present as fracture lining minerals in the host rocks and identified as colloids in groundwater samples collected at the NTS.

Mineralogy of colloids is reported for colloids filtered from groundwater samples taken from volcanic tuffs from Pahute Mesa and from Rainier Mesa U-12e, U-12t, and U-12n Tunnels. No mineralogy data were compiled for samples from other applicable characterization groups (CGs). Note: The CGs are the same as HGUs except that several types of volcanic aquifer HGUs (WTA, VTA, and LFA) are grouped into the VA CG. These are composited because there is often operational compositing in collection of the samples and insufficient supporting data to distinguish differences between these HGUs.

Data were transferred from Pahute Mesa to supplement available RMSM CAU-specific data. In general:

- The colloids in the NTS groundwater samples are mineralogically similar, although the actual abundance of each mineral varies from aquifer to aquifer.
- The colloidal material is composed primarily of clays and zeolites. The colloid minerals mimic the minor, host rock minerals from which they originated, and most likely represent the fracture lining minerals.
- Refractory colloids generated at the time of nuclear test detonations or resulting from alteration of the resulting melt glass (probably mostly clays) cannot be ruled out as a potentially significant contributor to colloid-facilitated transport at the NTS.

13.4 Colloid Concentrations and Size Distributions

Colloid concentration and size distribution data affect the colloid-facilitated carrying capacity of groundwater. Colloid concentration and size data are available for 45 different wells/completion

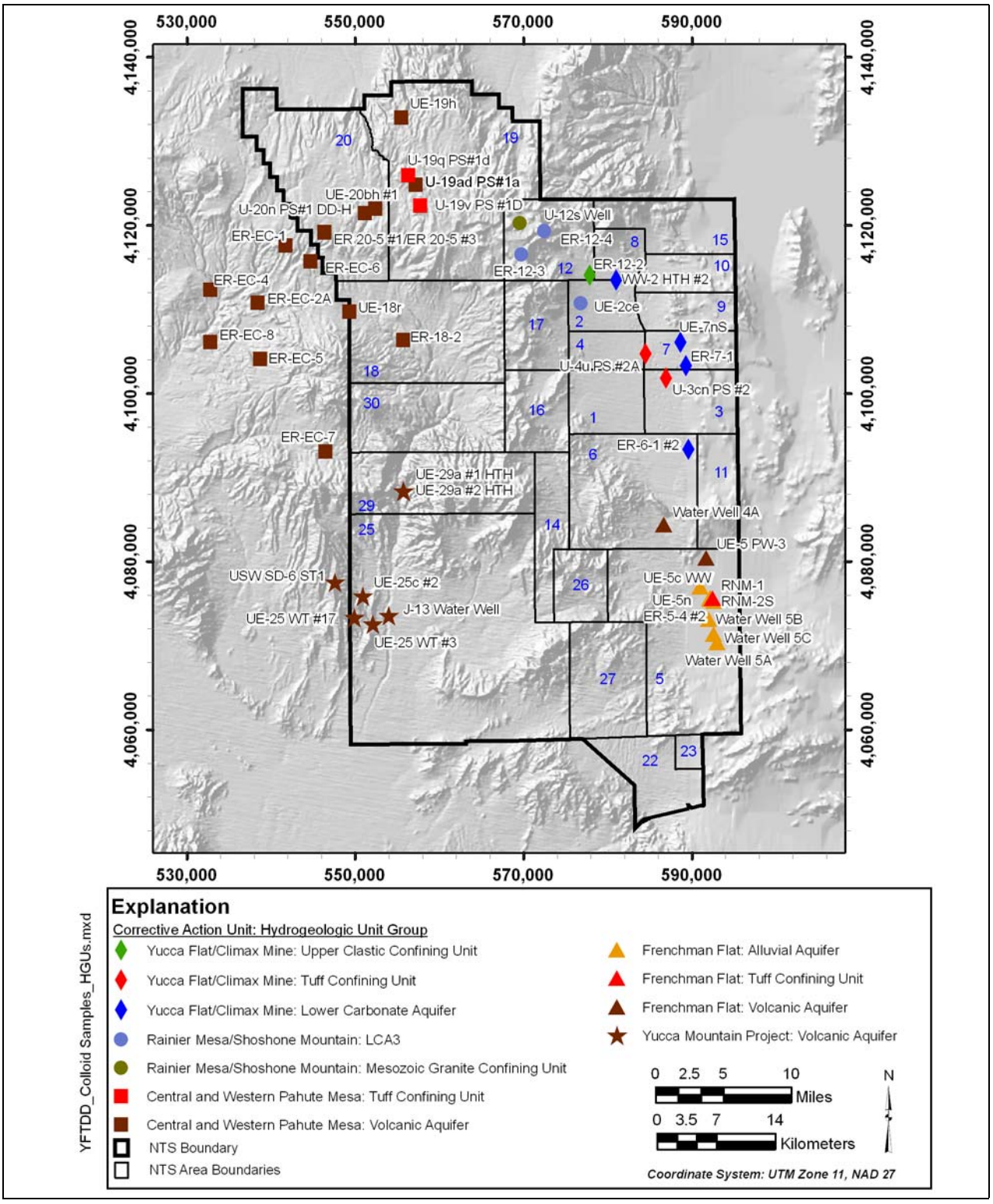

Figure 13-1
Location Map for Colloid Samples

intervals in the NTS area, variously located in all four CAUs (including ER wells downgradient of Pahute Mesa) and the YMP area. Section 13.5 of the YFCM TDD discusses the nature of these analyses as well as limitations of the analysis method and the representativeness of colloid data from analysis of pumped samples. The data include samples from seven different HGU-based CGs. See Tables 13-1 and 13-2, and Figure 13-1 of the YFCM TDD [1] for complete information. Table 13-1 lists the wells that have data and sample IDs for the selected sample analyses. Figure 13-1 shows the locations of these wells with different symbols for each CAU and with color codes for the CGs to which the sample is assigned. There are data for only four locations in RMSM, three of which are for the LCA3 HGU and one for the GCU HGU. Complete colloid concentration and size data for all well samples listed in Table 13-1 are provided in Appendix H.

Table 13-1
Representative Colloid Samples
(Page 1 of 2)

SITE_ID	MASTER_ID	Sample ID	CAU	Sampled HSU [a]	CG [b]
UE-2ce	370831116080701	14390.71	RMSM	LCA3	LCA3
ER-12-3	371142116125102	14236.71			
ER-12-4	371311116105902	14240.7			
U-12s Well	371342116125102	14402.7		MGCU	GCU
U-3cn PS #2	370338116011901	14377.71	YFCM	LTCU	TCU
U-4u PS #2A	370513116025101	14384.7			
ER-12-2	371019116072101	14231.7		UCCU	UCCU
ER-6-1 #2	365901115593501	14250.7		LCA	LCA
ER-7-1	370424115594301	14251.7			
UE-7nS	370556116000900	14391.7			
Water Well 2 (USGS HTH #2) 3,422 ft, uncased	370958116051512	14399.72			
Water Well 5A	364635115572901	7445.74	FF	AA	AA
Water Well 5C	364708115574401	7447.73			
Water Well 5B	364805115580801	7446.72			
UE-5n	364915115574101	14396.7			
RNM-2S	364922115580101	14395.7			
RNM-1	364928115580101	14394.7			
UE-5c Water Well	365011115584702	7443.74		AA/LTCU	
UE-5 PW-3	365201115581601	7442.73		TM-WTA	VA
Water Well 4A	365412116013901	7444.74			
ER-5-4 #2	364927115574801	14247.7		LTCU	TCU

Table 13-1
Representative Colloid Samples
(Page 2 of 2)

SITE_ID	MASTER_ID	Sample ID	CAU	Sampled HSU [a]	CG [b]
ER-EC-7	365910116284401	7435.7	PMOV	FCCM	VA
ER-EC-5	370504116335201	7433.7		TMCM	
ER-EC-8	370610116375301	7465.72		FCCM/TMCM	
ER-18-2	370615116222401	7430.7		TMCM	
UE-18r	370806116264001	6629.7			
ER-EC-2A (1,635-4,973 ft)	370852116340501	7466.7		FCCM/TMCM	
ER-EC-4	370935116375301	7432.72		TMA/FCCM/TCVA	
ER-EC-6 (1,581-5,000 ft)	371120116294801	7468.7		BA/UPCU/TCA/LPCU/ TSA/CHCU/CFCM	
ER-EC-1	371223116314701	7469.7			
ER-20-5 #3	371311116283801	14246.71		CHZCM	
ER-20-5 #1	371312116283801	5164.7		TSA/CHZCM	
U-20n PS#1 DD-H (3,025 ft)	371425116252401	5187.7		CHZCM	
UE-20bh #1	371442116243301	6627.7			
U-19ad PS 1A	371613116211701	14361.7		PLFA	
UE-19h	372034116222501	7470.7		BRA	
U-19v PS #1D	371453116205700	14366.71, 14366.72 [c]		BFCU	TCU
U-19q PS#1d	371649116215401	5246.7			TCU
UE-25 WT #3	364757116245801	7453.7	YMP	TM-LVTA/TM-WTA/ UTCU/TSA/LVTA	VA
UE-25 WT #17	364822116262601	7455.7			
J-13 Water Well	364828116234001	7459.7		TSA	
UE-25c #2	364947116254401	7471.71		CHVTA/YMCFCM	
UE-29a #1 HTH	365629116222601	4922.7		PCM	
UE-29a #2 HTH	365629116222602	4925.7		YMCFCM	
USW SD-6 ST1	365040116275901	7461.7		Unknown	

[a] HSU for respective geologic model; see geologic model documentation for key
[b] Characterization groups
[c] Duplicate samples

Data were transferred from CAUs other than RMSM and the YMP area because of a lack of data specific to RMSM area sufficient to define either colloid concentration or size distributions.

The combined data, identified in Table 13-1, were used to determine an empirical cumulative distribution function (ECDF) of colloid concentration in general. Figure 13-2 shows the log-normal distribution of the composited concentration data; the distribution has a mean of 7.73 and a standard deviation of 1.45 $\log_{10}$ colloids/mL. There are only sufficient data to define an ECDF for the AA and VA CGs. For both of these CGs, the CG-specific data would define an ECDF with a somewhat narrower range than the composite ECDF. There are insufficient data to determine a specific ECDF for any CG for the RMSM CAU. Note the limitation of the analysis method to only determine

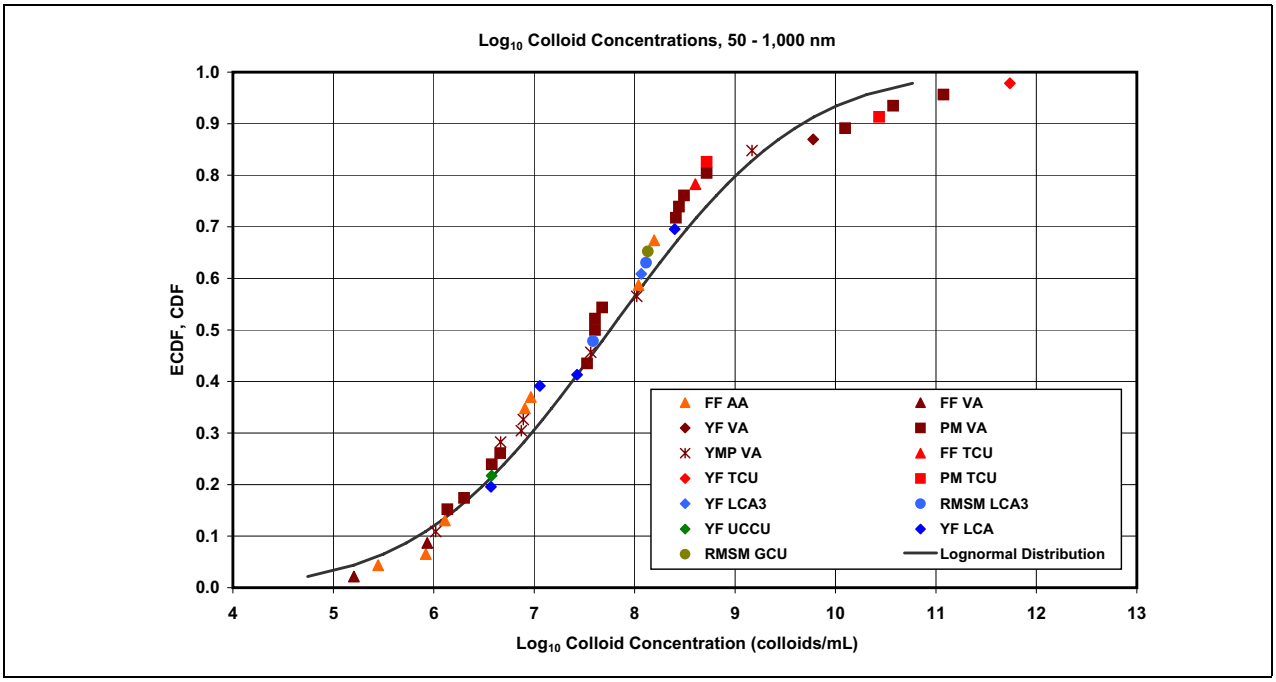

Figure 13-2
Cumulative Distribution Function of Log_{10} Colloid Concentrations for All NTS Data

colloids > 50 nm affects the size data and consequently the distribution of the size data. Also note Figure 13-2 shows the concentration distribution by number of colloids, not by mass or surface area.

The analyses of colloid size distributions were also conducted using the composite data for the same reasons as for concentration distributions. Figure 13-3 shows the lognormal distributions determined for each CG. The parameters for the lognormal distributions are given in Table 13-2. Further information is provided in Section 13.5.4 of the YFCM TDD [1].

Scaling of the results of the data analysis to the CAU scale are addressed in Section 13.5.6 of the YFCM TDD.

13.5 Colloid Transport Parameters

Colloid-facilitated transport is subject to retardation and attenuation resulting from reversible attachment and detachment of colloids from immobile surfaces by physical and/or chemical processes and irreversible removal as a result of size exclusion in pore throats, physical attachment to rough surfaces, coagulation, and settling.

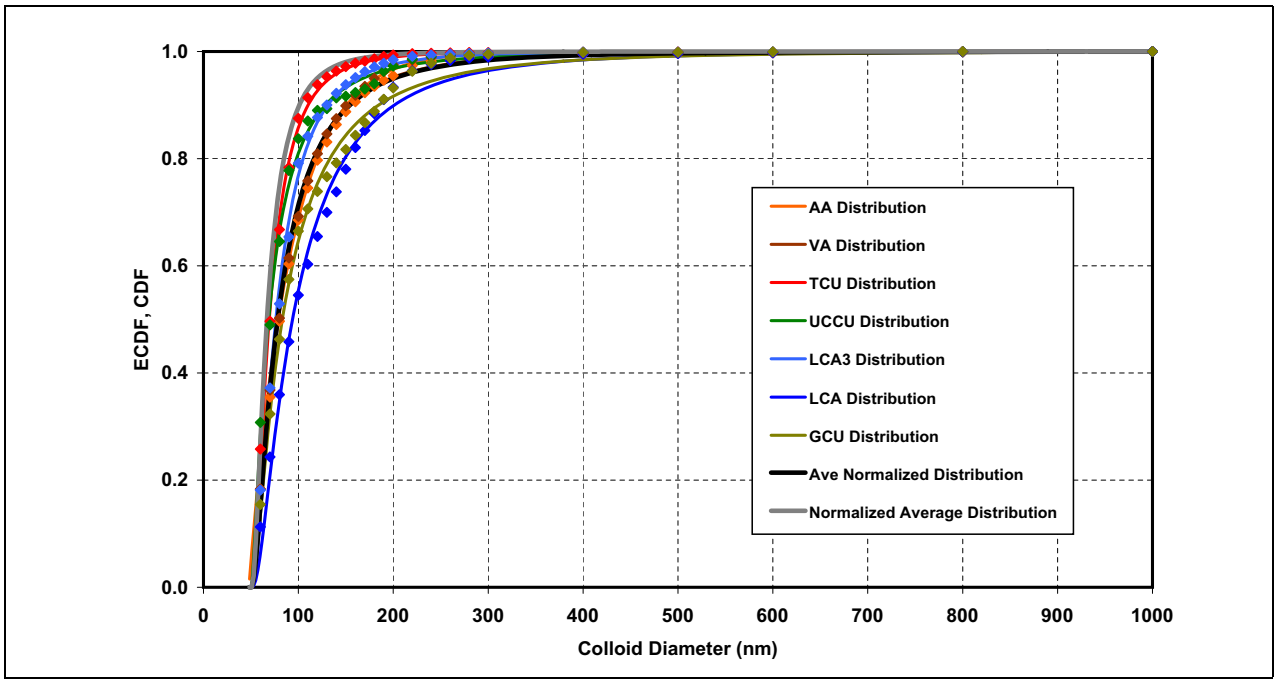

Figure 13-3
Cumulative Distribution Function of Colloid Diameter
for All NTS Data and Characterization Groups

Table 13-2
Summary of Colloid Concentrations (Log_{10}) and Size Distributions
for Characterization Groups

CG	RMSM Colloid Samples				NTS Area Samples				Size Distributions [a]	
	Samples	Log_{10} colloids/mL			Samples	Log_{10} colloids/mL			Mean	SD
		Max	Mean [b]	Min		Min	Max	Mean [b]	nm	
AA	--	--	--	--	7	5.45	8.20	6.80	100	68
VA					24	5.20	11.08	7.67	97	61
TCU					5	8.61	11.74	9.85	79	31
LCA3	3	7.59	8.11	7.92	3	7.59	8.11	7.92	120	87
UCCU	--	--	--	--	1	--	--	6.58	89	42
LCA					4	6.57	8.40	7.36	85	55
GCU	1			8.13	1	--	--	8.13	110	92
All HGUs	4	7.59	8.11	7.97	45	5.21	11.74	7.76	98	65

[a] All distributions lognormal, +shift = 50 nanometers (nm)
[b] Mean of the Log_{10} concentration (geometric mean)

Colloid transport parameters are determined by interpretation of tracer transport experiments, either at the laboratory scale or the field scale. Few tracer transport experiments have been conducted at the field scale, and only a limited number have been performed at the laboratory scale. No tracer transport experiments have been run in rocks from the RMSM CAU, so data were transferred from field-scale and laboratory-scale experiments conducted in rock from within the YFCM (LCA CG) and the PMOV (VA CG) HFMs as well as YMP area (AA CG). For use in characterization of filtration rate constants for alluvium, data for the field scale were transferred from a foreign site based on a description of the test media consistent with NTS alluvium. Most transport parameters were determined for either colloid surrogates (carboxylate-modified latex [CML] microspheres or bacteriophages) or artificial colloids (refined clay minerals or silica of appropriate size range), not natural colloids. Almost no data exist for tracer transport experiments using natural colloids.

13.5.1 Parameterization

Colloid transport parameters are not physical measurements of properties, but parameters of the transport model used for interpretation of the transport experiments. Consequently, specification of the parameters is dependent upon the theory on which the model is based, and the parameters can change with changes in the theory and their values as a function of interpretation of the experiment [1]. The transport parameters specified here are taken from the source documents, as specified, and are the result of the transport theory used for interpretation (see Section 13.5.1 of the YFCM TDD). The parameters from the sources are consistent because they are all based on the same interpretation theory and have been determined by the same researchers. Tests are interpreted by fitting filtration rate constants and retardation factors to simulate the tracer breakthrough. Detachment rates are calculated from the interpretation. The transport parameters addressed are filtration rate constant and retardation factor.

13.5.2 Filtration Parameters

Plots of ECDFs for the AA CG and VA CG laboratory and field filtration rate constants are shown in Figures 13-4 and 13-5. Plots of the filtration rate constants as a function of time show the filtration rate constants decrease with mean residence time, particularly for field-scale data [1].

Two values for filtration rate for one field experiment in the LCA are in Table 13-6, and the results of a laboratory fracture flow experiment on LCA core are in Table 13-7 of the YFCM TDD.

Detachment rates were estimated from analyses of the Yucca Mountain C-hole tracer tests in the Bullfrog and Prow Pass formations (VA CG) [2]. The colloid detachment rate constants are 0.00015 and 0.00025 1/cm-hr (upper bound) for the Prow Pass tuff, and 0.0002 and 1.08 1/cm-hr for the Bullfrog tuff.

13.5.3 Retardation Factor

The ECDFs for colloid transport retardation factors for alluvium (Figure 13-6) and fractured volcanics (Figure 13-7) were determined combining both laboratory-scale and field-scale data.

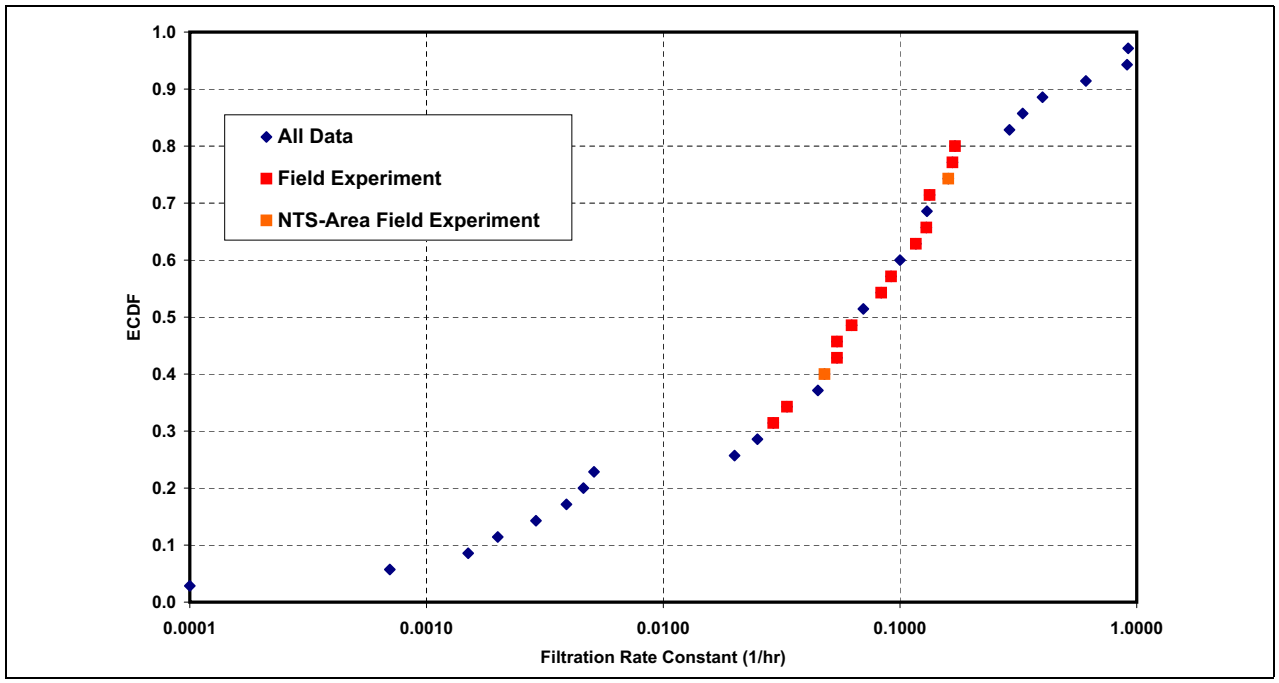

Figure 13-4
Cumulative Probability Distribution of Colloid Filtration Rate Constants for Alluvium

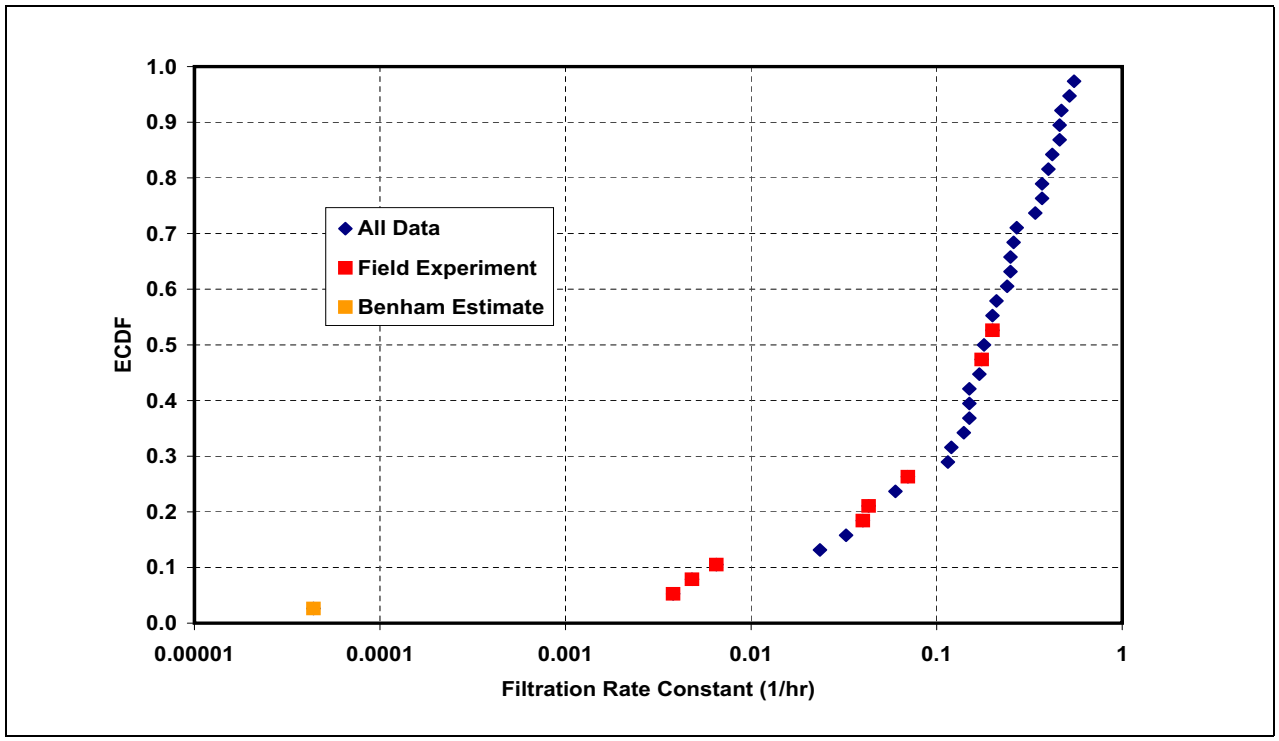

Figure 13-5
Cumulative Probability Distribution of Colloid Filtration Rate Constants for Volcanics

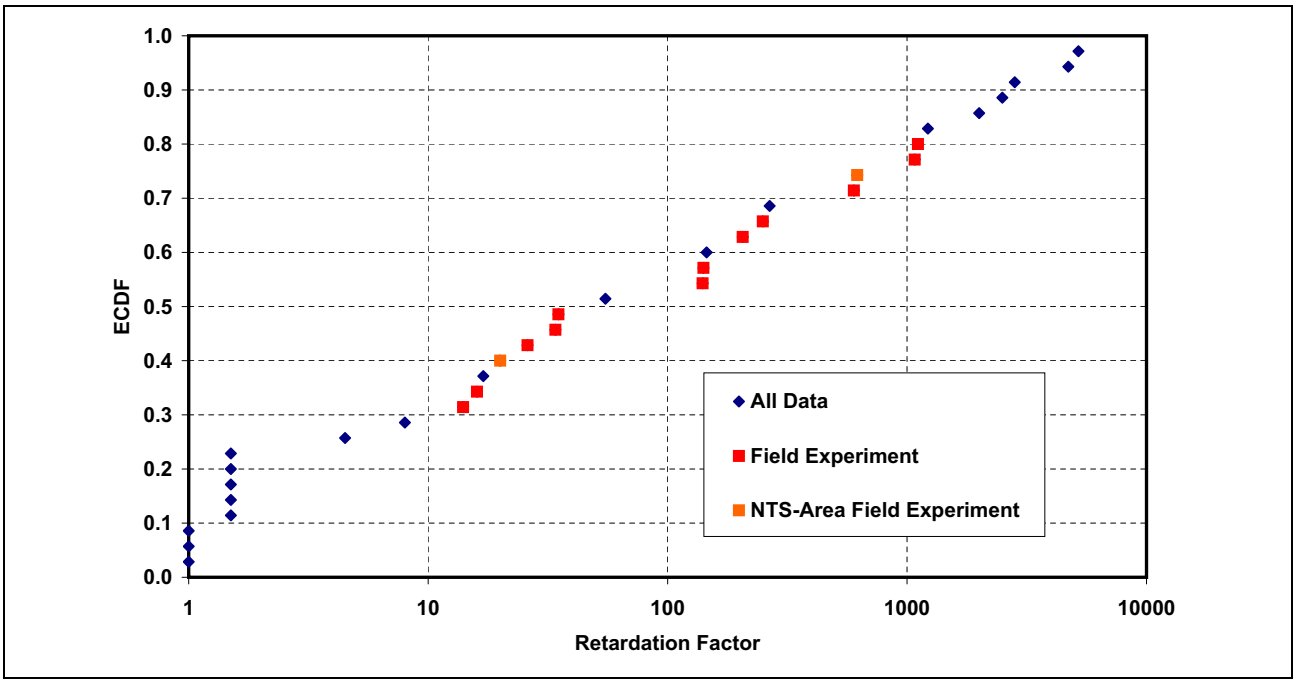

Figure 13-6
Cumulative Probability Distribution of Colloid Retardation Factors for Alluvium

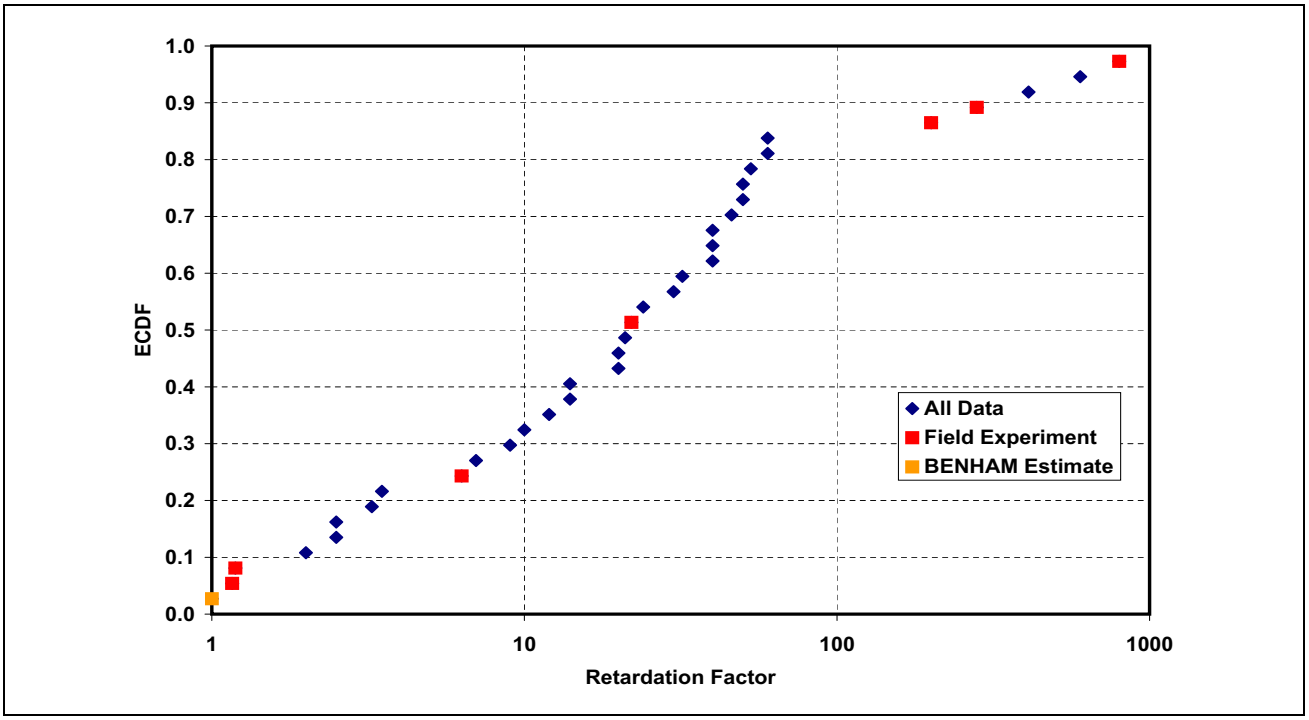

Figure 13-7
Cumulative Probability Distribution of Colloid Retardation Factors for Fractured Volcanic Rocks

13.5.4 Additional Filtration and Retardation Data

Additional data for filtration and retardation rates, not included in the ECDFs, were reported for interpretations of laboratory-scale reactive transport experiments in which radionuclides apparently migrated as or sorbed to colloids [1]. These parameter values were determined using different interpretation assumptions from the data used for the ECDFs and were not combined because the basis for the values may not be consistent. See Sections 13.6.2.1 and 13.6.2.3 of the YFCM TDD [1] for complete discussion.

13.5.5 Scaling

There may be scale dependence of colloid filtration rate constants and retardation factors. However, most data are from laboratory studies or field tests at scales much smaller than the CAU scale. Rather than an explicit scale dependence, there may be wide distribution of filtration rate constants associated with colloid transport in a fracture flow system.

13.5.6 Limitations

There are few field-scale transport experiments, and they involve surrogates for colloids rather than the radionuclides of concern. The data are derived from interpretations of transport experiments and are dependent upon the interpretation theory and method, which is not standardized.

13.6 Radionuclide Associations with Colloids

Association of radionuclides with colloids in groundwater samples directly demonstrates the potential for colloid-facilitated transport of radionuclides [3, 4]. However, there have only been several analyses of groundwater samples that distinguish radionuclides associated with colloids from the complete radionuclide content. The available data provide information on several radionuclides for samples from several locations for only a few CGs. Data are available for the RMSM CAU (TCU CG) as well as the Pahute Mesa (VA CG), Yucca Flat (LCA CG), and Frenchman Flat (AA CG).

13.7 Actinide Distribution Coefficients and Sorption Rates onto Colloids

Actinide distribution coefficients (K_d) values, sorption (k_f, forward) rates, and desorption (k_d, reverse) rates onto colloids have been measured in the laboratory (batch and fracture transport experiments) for some radionuclides and for some colloid types, for UGTA and YMP.

13.7.1 Distribution Coefficients

See Section 13.8.1.1 of the YFCM TDD [1] for complete discussion for distribution coefficients. Figure 13-8 displays the ranges for K_d determined from batch experiments conducted for YMP, with extended ranges for some species based on additional work conducted for UGTA. The text

summarizes detailed observations of radionuclide sorption behavior during the experiments. These laboratory experiments were not specific to RMSM but involved selected colloid material, radionuclides, and YMP-specific water composition. Another set of experiments were conducted for UGTA for Pu(IV) and Pu(V) sorption onto seven colloid types (of which three are the same as the previous experiments). The results are shown on Figure 13-9 and agree well with the previous experiments where the experiments overlap.

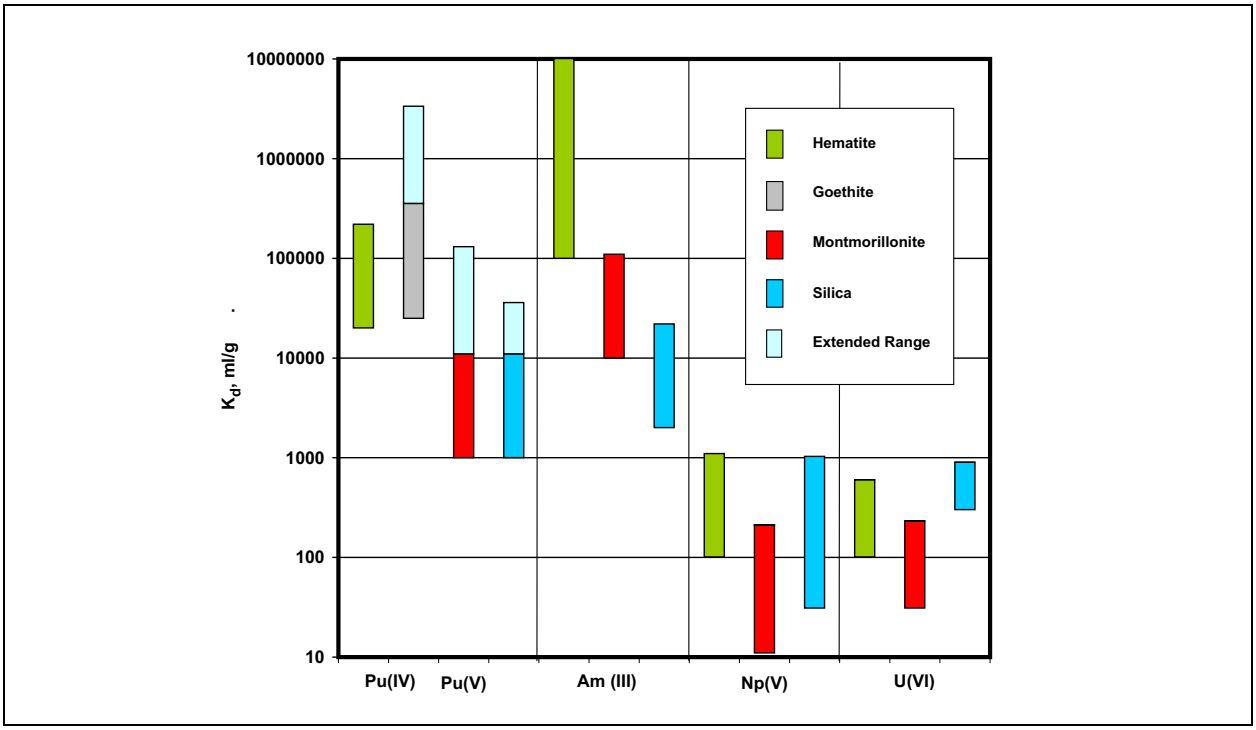

Figure 13-8
Ranges of K_d Values Measured for Actinide Sorption onto Colloids
Source: [5]

13.7.2 Sorption/Desorption

Table 13-8 of the YFCM TDD, summarizes the results of various laboratory (batch and fracture transport) experiments for k_f (sorption rate constant) and k_b (desorption rate constant).

A detailed discussion of sorption and desorption onto colloids during various experiments is presented in Sections 13.8.1.2 and 13.8.1.3 of the YFCM TDD [1]. These laboratory experiments were not specific to RMSM but involved selected colloid material, radionuclides, and Pahute Mesa and YMP-specific water composition (volcanic aquifer). Data limitations are discussed in detail in Section 13.8.2 of the YFCM TDD [1].

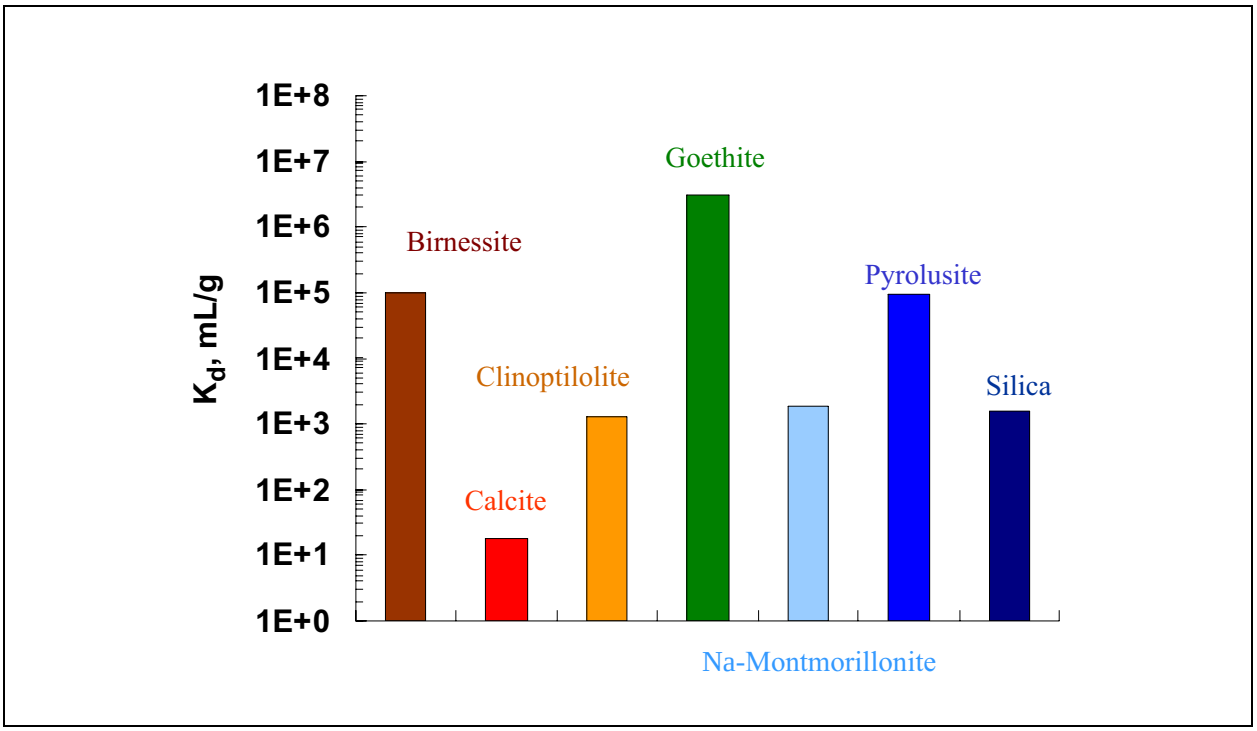

Figure 13-9
Distribution Coefficient Calculated for Pu^{+5} Sorbed onto Various Mineral Colloids
Source: [5]

13.7.3 Scaling

A significant scaling issue is the application of data for laboratory experiments with short time scales to the potential transport times *in situ*. Another scaling factor is the difference between transport in fractures with sorbing facture surfaces versus laboratory experiment results for colloid sorption within a non-reactive container. More detailed information on scaling matters is in Section 13.8.3 of the YFCM TDD [1].

13.8 Colloid Data for N- and T-Tunnels

Colloid data for samples from N- and T- Tunnels are in a recent LANL letter report detailing analyses of samples of water impounded behind the portal seals of N- and T-Tunnels [6]. The basic results are listed in Table 13-1 of the letter report. Additional information on these sample results can be found in the letter report. This information is applicable to the environment within the tunnels.

13.9 Summary

This section summarizes the available data for colloid-facilitated transport for NTS CAUs (including YMP). There is insufficient information available to characterize the concentration, size distribution or mineralogy of colloids for the range of formations within specific CAUs, and the total dataset only

provides substantial information for a few generalized formation types (CGs). The data are most complete for alluvium and fractured volcanic rocks (in general), and there is a limited dataset for fractured carbonate rocks. There are only miscellaneous data for other rock types. The data have been analyzed to the extent possible to characterize the information, and does not necessarily provide appropriate parameter values for transport modeling. Colloid transport parameters are reported as the data sources reported, and may only be appropriate within the context of the theory and transport model used for interpretation.

13.10 References

1. Stoller-Navarro Joint Venture. 2007. *Phase I Contaminant Transport Parameters for the Groundwater Flow and Contaminant Transport Model of Corrective Action Unit 97: Yucca Flat/Climax Mine, Nevada Test Site, Nye County, Nevada*, Revision No. 0, S-N/99205--096. Las Vegas, NV.

2. Bechtel SAIC. 2004. *Saturated Zone Colloid Transport*, Rev. 2, ANL-NBS-HS-000031. Los Alamos, NM: Los Alamos National Laboratory.

3. Kersting, A.B., D. W. Efurd, D. L. Finnegan, D. J. Rokop, D. K. Smith, and J. L. Thompson. 1999. "Migration of Plutonium in Groundwater at the Nevada Test Site." In *Nature* 397, 56-59.

4. Kersting, A.B., and P.W. Reimus, eds. 2003. *Colloid-Facilitated Transport of Low-Solubility Radionuclides*: *A Field, Experimental, and Modeling Investigation*, UCRL-ID-149688. Livermore, CA: Lawrence Livermore National Laboratory.

5. Novikov, A.P., S.N. Kalmykov, S. Utsunomiya, R.C. Ewing, F. Horreard, A. Merkulov, S.B. Clark, V.V. Tkachev, B.F. Myasoedov. 2006. *Colloid Transport of Plutonium in the Far-Field of the Mayak Production Association, Russia*.

6. Roback, R.C., A.I. Abdel-Fattah, C. Jones, and B. Martinez. 2007. *REDOX Measurements and Colloid Concentration and Size Distribution Analyses of Groundwater Samples from Rainier Mesa Tunnels U-12n and U-12t*, LA-UR-07-6962. Los Alamos National Laboratory, Earth and Environmental Sciences.

Appendix A

Hydrostratigraphic Framework Model

A.1.0 INTRODUCTION

Supporting information for the RMSM HFM is provided in the Appendix\A folder on the accompanying DVD. The supporting information includes tables outlining the HSU, HGU, RMC, and RMU systems; geologic cross sections; and geologic block diagrams.

A.2.0 DATASET SUMMARY

An Excel workbook file, RMSM_HFM.xls, contains four worksheets described in Table A.2-1. The workbook outlines the HSUs, HGUs, RMCs and RMUs in the HFM and shows the relationships between the different classification systems.

Table A.2-1
RMSM_HFM.xls
(Page 1 of 2)

Sheet	Sheet Description	Column Name	Column Description
RMSM_HSUs	Hydrostratigraphic Units of the RMSM HFM Model	Hydrostratigraphic Unit	Hydrostratigraphic unit name (the HSU code given in parentheses)
		Dominant Hydrogeologic Units	HGU codes that are dominant in the HSU
		Typical Lithologies	Description of the lithologies composing the HSU
		Stratigraphic Unit Map Symbol(s)	Stratigraphic units included in the HSU
		Hydrologic Significance	Description of the significant characteristics of each HSU
RMSM_HGUs	Hydrogeologic Units of the RMSM Model Area	Hydrogeologic Unit	Hydrogeologic unit name (the HSU code given in parentheses)
		Typical Lithologies	Description of the lithologies composing the HGU
		Hydrologic Significance	Description of the significant characteristics of each HGU

Table A.2-1
RMSM_HFM.xls
(Page 2 of 2)

Sheet	Sheet Description	Column Name	Column Description
RMSM_RMCs	Reactive Mineral Categories for the RMSM Model	Reactive Mineral Category	Reactive Mineral Category name (the HSU code given in parentheses)
		Typical Lithologies	Description of the lithologies composing the RMC
		Major Alteration	Description of the alterations within the RMC
		Reactive Minerals Present in Significant Quantities	Description of minerals composing the RMC
		UGTA Criteria	General RMC mineral percentage cutoff criteria
RMSM_HSUs_RMCs	Hydrostatigraphic and Reactive Mineral Categories of the RMSM Model	Hydrostratigraphic Unit	Hydrostratigraphic unit name
		HSU Symbol	The HSU code
		Dominant HGUs	HGU codes that are dominant in the HSU
		Reactive Mineral Unit	Description of the lithologies composing the HSU
		Dominant RMCs	RMC codes that are dominant in the HSU
		Typical Stratigraphic Units	Stratigraphic codes that are dominate in the HSU

An Excel workbook file, RMSM_HSU_Mineralogy.xls, contains statistics of XRD analyses of mineralogy samples in the RMSM HFM by HSU. The mean, standard deviation, and minimum and maximum percentage are given for each reactive mineral for the samples in the HSU.

An Adobe portable document format (pdf) file, RMSM_HFM_Figures.pdf, contains block diagrams and cross sections of the HFM model.

Appendix B

Matrix Porosity

B.1.0 INTRODUCTION

Matrix porosity data from laboratory measurements of borehole core samples are in the Appendix\B folder on the accompanying DVD.

B.2.0 DATASET SUMMARY

An Excel workbook file, RM_Matrix_Porosity_Data.xls, contains three worksheets described in Table B.2-1.

Table B.2-1
RM_Matrix_Porosity_Data.xls
(Page 1 of 2)

Sheet	Sheet Description	Column Name	Column Description
Matrix_Porosity_Data	RMSM matrix porosity data from the USGS Rock-Property Database (10/03/2007)	BIN Site Type	Borehole Index Number, Site Name, Site Type
		HSU	Hydrostratigraphic Unit Name
		HGU	Hydrogeologic Unit Name
		Interval	Sampled interval in meters
		Porosity	Porosity in percent
HGU_Porosity_by_Site	RMSM Average HGU porosities by location	BIN Site	Borehole Index Number, Site Name
		AA	Alluvial Aquifer
		CA	Carbonate Aquifer
		CCU	Clastic Confining Unit
		GCU	Granite Confining Unit
		TCU	Tuff Confining Unit
		VTA	Vitric-Tuff Aquifer
		WTA	Welded-Tuff Aquifer
		None	HGU not assigned
HSU_Porosity_by_Site	RMSM Average HSU porosities by location	BIN Site	Borehole Index Number, Site Name
		AA3	Alluvial Aquifer
		ATCU	Argillic Tuff Confining Unit
		BRA	Belted Range Aquifer
		BRCU	Belted Range Confining Unit
		LCA3	Lower Carbonate Aquifer Thrust
		LCCU1	Lower Clastic Confining Unit Thrust
		LTCU	Lower Tuff Confining Unit
		LVTA	Lower Vitric Tuff-Aquifer
		LVTA1	Lower Vitric-Tuff Aquifer 1
		LVTA2	Lower Vitric-Tuff Aquifer 2
		MGCU	Mesozoic Granite Confining Unit

Table B.2-1
RM_Matrix_Porosity_Data.xls
(Page 2 of 2)

Sheet	Sheet Description	Column Name	Column Description
HSU_Porosity_by_Site	RMSM Average HSU porosities by location	OSBCU	Oak Springs Butte Confining Unit
		RVA	Redrock Valley Aquifer
		SWA	Stockade Wash Aquifer
		TMLVTA	Timber Mountain Lower Vitric-Tuff Aquifer
		TMUVTA	Timber Mountain Upper Vitric-Tuff Aquifer
		TMWTA	Timber Mountain Welded-Tuff Aquifer
		TSA	Topopah Spring Aquifer
		TUBA	Tub Spring Aquifer
		UCCU	Upper Clastic Confining Unit
		UTCU	Upper Tuff Confining Unit
		UTCU1	Upper Tuff Confining Unit 1
		None	HSU not assigned

An Adobe pdf file, RM_Matrix_Porosity.pdf, has the following figures:

- Linear regression analysis of HGU porosity as a function of depth
- Porosity histograms by HSU and HGU
- Porosity CDF plots by HSU and HGU
- Box and whisker plots by HSU and HGU

Appendix C

Effective Porosity

C.1.0 INTRODUCTION

Supporting information for the RMSM Effective Porosity is provided in the Appendix\C folder on the accompanying DVD. The supporting information includes table and graphs outlining available information on effective porosity.

C.2.0 DATASET SUMMARY

An Excel workbook file, RMSM_Effective_Porosity.xls, contains several worksheets with tables outlining effective porosity data for HGUs in the RMSM model. Summary worksheets are described in Table C.2-1, and supporting worksheets are described Table C.2-2.

Table C.2-1
RMSM Effective Porosity Summary Worksheets
(Page 1 of 2)

Sheet	Sheet Description	Column Name	Column Description
Aquifer HGU Summary	Summary of Recommended Distributions for the Effective Porosity of the Fractured Aquifer HGUs for the Yucca Flat/Climax Mine CAU-Scale Model	HGU	Hydrogeological Unit
		Lower Bound	Lower 5% Confidence Interval
		Upper Bound	Upper 95% Confidence Interval
		Mode (Peak)	Most Frequent Value
		Distribution	Distribution type
WTA Summary	Summary of Estimated Effective Porosity Ranges for the WTA HGU and Recommended Range for the Yucca Flat/Climax Mine CAU-Scale Model	Source	Source of analysis
		Effective Porosity (fraction) Minimum	Effective Porosity (fraction) Minimum
		Effective Porosity (fraction) Maximum	Effective Porosity (fraction) Maximum
		Location	Location/Locality of estimate
		Method	Method used to obtain estimate
		DDE_F	Data Documentation Evaluation Flag
LFA Summary	Summary of Estimated Effective Porosity Ranges for the Lava-Flow Aquifer and Recommended Range for the Yucca Flat/Climax Mine CAU-Scale Model	Source	Source of analysis
		Effective Porosity (fraction) Minimum	Effective Porosity (fraction) Minimum
		Effective Porosity (fraction) Maximum	Effective Porosity (fraction) Maximum
		Location	Location/Locality of estimate
		Method	Method used to obtain estimate
		DDE_F	Data Documentation Evaluation Flag

Table C.2-1
RMSM Effective Porosity Summary Worksheets
(Page 2 of 2)

Sheet	Sheet Description	Column Name	Column Description
CA Summary	Summary of Estimated Effective Porosity Ranges for the Carbonate Aquifer and Recommended Range for the Yucca Flat/Climax Mine CAU-Scale Model	Source	Source of analysis
		Effective Porosity (fraction) Minimum	Effective Porosity (fraction) Minimum
		Effective Porosity (fraction) Maximum	Effective Porosity (fraction) Maximum
		Location	Location/Locality of estimate
		Method	Method used to obtain estimate
		DDE_F	Data Documentation Evaluation Flag

Table C.2-2
RMSM Effective Porosity Supporting Worksheets

Sheet	Sheet Description
WTA-1	Effective Porosities Determined from Tracer Testing at the C-holes Complex
WTA-2	Effective Porosities from Welded-Tuff Air-Permeability and Gas Tracer Tests (after [1])
WTA-3	Estimate of Fracture Porosity of the Tuffs Penetrated by Test Well USW H-4 (from [2])
WTA-4	Fracture Porosities Calculated for the Welded-Tuff Aquifers from Hydraulic Conductivity and Fracture Spacing Using Equation (8-10)
WTA-5	Calculated Fracture Porosities for the Welded-Tuff Aquifer (after [3])
WTA-6	Effective Porosity Estimates for Welded Tuff in the Basin and Range Province (after [4])
WTA-7	Fracture Porosities Used by [5] for the Welded-Tuff Aquifer
LFA-1	Estimate of Effective Porosity for the BULLION Forced-Gradient Experiment Based on Plug Flow Calculations (after [6])
LFA-2	Effective Porosities from the Numerical Model Calibration to Tracer Recovery During the BULLION Forced-Gradient Experiment [6]
LFA-3	Effective Porosities from the Analysis of the BULLION Forced-Gradient Experiment [7]
LFA-4	Fracture Porosities Calculated for Lava-Flow Aquifers from Hydraulic Conductivity and Fracture Spacing Using Equation (8-10)
LFA-5	Fracture Porosities Used by [5] for a Lava-Flow Aquifer
CA-1	Summary of Effective Porosities Determined Using the Breakthrough Curves from the ER-6-1 Well Cluster Tracer Test
CA-2	Calculated Porosities for the Two-Well Recirculating Tracer Tests Conducted at the Amargosa Tracer Site Assuming Plug Flow
CA-3	Summary of Fracture Porosities Determined for the Culebra Dolomite at the Waste Isolation Pilot Plant Site
CA-4	Fracture Porosities Calculated for Wells ER-6-1#2 and ER-7-1 Using Hydraulic Conductivity and Fracture Spacing (Equation [8-10])
CA-5	Calculated Fracture Porosities for Boreholes ER-6-1#2 and ER-7-1 Using Fracture Spacing and Aperture Calculations
CA-6	Effective Porosity Estimates for Carbonate Rocks in the Basin and Range Province (after [4])
Equations	List of Selected Equations Used in Calculations

C.3.0 REFERENCES

1. Freifeld, B.M. 2001. *Estimation of Fracture Porosity in an Unsaturated Fractured Welded Tuff Using Gas Tracer Testing.* Department of Civil and Environmental Engineering, University of California, Berkeley, Ph. D. dissertation.

2. Erickson, J.R., and R.K. Waddell. 1985. "Identification and Characterization of Hydrologic Properties of Fractured Tuff Using Hydraulic and Tracer Tests -- Test Well USW H-4, Yucca Mountain, Nye County, Nevada," In *Water-Resources Investigations Report* 85-4066. U.S. Geological Survey.

3. U.S. Department of Energy, Nevada Operations Office. 1997. *Regional Groundwater Flow and Tritium Transport Modeling and Risk Assessment of the Underground Test Area, Nevada Test Site, Nevada*, DOE/NV--477. Las Vegas, NV.

4. Bedinger, M.S., K.A. Sargent, W.H. Langer, F.B. Sherman, J.E. Reed, and B.T. Brady. 1989. *Studies of Geology and Hydrology in the Basin and Range Province, Southwestern United States, for Isolation of High-Level Radioactive Waste – Basis of Characterization Evaluation,* Professional Paper 1370-A. U.S. Geological Survey.

5. Wolfsberg, A., L. Glascoe, G. Lu, A. Olson, P. Lichtner, M. McGraw, T. Cherry, and G. Roemer. 2002. *TYBO/BENHAM Model Analysis of Groundwater Flow and Radionuclide Migration from Underground Nuclear Tests in Southwestern Pahute Mesa, NTS*, LA-13977. Los Alamos, NM: Los Alamos National Laboratory.

6. IT Corporation. 1998. *Report and Analysis of the BULLION Forced-Gradient Experiment,* ITLV/13052-042. Las Vegas, NV.

7. Reimus, P.W., and M.J. Haga. 1999. *Analysis of Tracer Responses in the BULLION Forced-Gradient Experiment at Pahute Mesa, Nevada,* LA-13615-MS. Los Alamos, NM: Los Alamos National Laboratory.

Appendix D

Dispersivity

D.1.0 INTRODUCTION

Dispersivity data compiled from literature are provided in the Appendix\D folder on the accompanying DVD.

D.2.0 DATASET SUMMARY

An Excel workbook file, RMSM_Dispersivity_Data.xls, contains 33 worksheets described in Table D.2-1.

Table D.2-1
Dispersivity_Data.xls

Sheet	Sheet Description	Column Name	Column Description
Dispersivity Data	Dispersivity data compiled from literature, used for general analysis	Site_Name	Name of site where the test was conducted
		Rock_Types	Rock-type category per NTS HGUs
		Aquifer_Material	Description of the type of rock/material in which the test was conducted
		Minimum_Scale_of_Test (m)	Minimum scale of the test
		Maximum_Scale_of_Test (m)	Maximum scale of the test
		Average_Scale_of_Test (m)	Average scale of the test
		Dispersivity_Longitudinal_Min (m)	Minimum longitudinal dispersivity
		Dispersivity_ Longitudinal_ Intermediate (m)	Intermediate longitudinal dispersivity
		Dispersivity_Longitudinal_Max (m)	Maximum longitudinal dispersivity
		Dispersivity_Longitudinal_Geomean (m)	Geometric mean of longitudinal dispersivity
		Percent of Scale	Dispersivity/scale of test
		Dispersivity_Transverse (m)	Transverse dispersivity
		Dispersivity_Vertical (m)	Vertical dispersivity
		DDE_F	Assigned DDE_F level
		Author_ Reliability	Author_ Reliability
		Author_ Reliability_Unified	Author_ Reliability_Unified
		Data Value ID	Description of data value derivation (if applicable)
		Data_Source	Data_Source
DDE_F levels	Explanation of Data Documentation levels	Data Documentation Evaluation	Explanation and descriptions of DDE_F levels
Reference Citations	Citations for all data sources (literature references)	Reference ID	ID for reference used in the 'Dispersivity Data' worksheet
		Reference Citation	Citation for reference

Appendix E

Matrix Diffusion

E.1.0 INTRODUCTION

The matrix diffusion dataset from the YFCM TDD [1] is in the Appendix\E folder on the accompanying DVD.

E.2.0 DATASET SUMMARY

An Excel workbook file, RM_Matrix_Diffusion_Data.xls, contains the following data as described in Table E.2-1.

Table E.2-1
Rainier Mesa Matrix Diffusion Data
(Page 1 of 3)

Sheet	Sheet Description	Column Name	Column Description
Matrix_Diffusion_Dataset	NTS Matrix Diffusion Data	SampleID	The number of data entry
		Sample number	The name of the well, unique sample numbers, and typically the depth in feet
		Location	Yucca Flat (YF), Yucca Mountain (YM), Rainier Mesa (RM), or Pahute Mesa (PM)
		Porosity	The fraction of void space within the rock, the void volume divided by the bulk volume
		Effective Porosity	The fraction of void space within the rock that is interconnected and available for fluid flow (only two references reported effective porosity [2, 3]
		HSU	Hydrostratigraphic unit for this sample
		Lithology	The type of rock: quartz, carbonate, tuff, zeolitic tuff, or granite/crystalline
		Depth (m)	The depth below ground surface of the well core from which the rock sample was obtained
		Entry Date	The date that the matrix diffusion data were added to this dataset (or substantially modified or updated)
		Diffusion coef (m2/s)	Experimentally derived diffusion coefficient, in m^2/s
		Derived diffusion	Matrix diffusion coefficient that is not reported directly in the reference source, but rather calculated or derived from the reported tortuosity and the free water diffusion coefficient using Equation (10-2)

Table E.2-1
Rainier Mesa Matrix Diffusion Data
(Page 2 of 3)

Sheet	Sheet Description	Column Name	Column Description
Matrix_Diffusion_Dataset	NTS Matrix Diffusion Data	Chemical species	Tracer chemical used in the diffusion cell experiment
		Species adj diffusion coeff (to tritiated water) m2/s	Experimentally derived diffusion coefficient, in m^2/s, adjusted from the actual tracer species used in the measurement to a tritiated water basis, to achieve a consistent tracer basis for the entire dataset of measurements
		Original source	Reference source reporting the diffusion coefficient measurement
		Source page #, Table #	Page and table number, where available, from original source reporting diffusion coefficient measurement and other raw data
		Tortuosity	The bulk measure of the constrictivity and tortuous nature of the interconnected pore space through which diffusion is occurring; in the form presented in Equation (10-2), tortuosity should always have a magnitude greater than zero and less than one
		Derived tortuosity	Tortuosity that is not reported directly in the reference source, but rather calculated or derived from the reported matrix diffusion coefficient and the free water diffusion coefficient using Equation (10-2)
		Permeability(m2)	A measure of the ability of a porous material to transmit fluids; related to the constrictivity or tortuosity of the rock
		Temp(°C)	Temperature at which matrix diffusion was measured (rarely reported)
		Diffus measur method	Lab diffusion cell experiment (DCE); diffusion wafer experiment (DWE); method other than diffusion cell exp, such as x-ray or neutron imaging, electrical conductivity, batch experiments, using pulverized particles, etc. (nonDEC); unknown (UnK)
		Frac in sample?	Fractures present in sample ?
		Sample thickness, cm	Thickness of sample in centimeters
		M1a meas method factor	Multiplier Factor for measurement method
		M1b frac meas factor	Multiplier Factor for presence of coated fracture surfaces
		M1c sample thick factor	Multiplier Factor for representative sample thickness

Table E.2-1
Rainier Mesa Matrix Diffusion Data
(Page 3 of 3)

Sheet	Sheet Description	Column Name	Column Description
Matrix_Diffusion_Dataset	NTS Matrix Diffusion Data	M1 meas meth	Measurement Method Factor: = M1a x M1b x M1c
		M2a test series meth	Multiplier Factor for the quality of the test series experimental method and calibration
		M2b1 indiv meas meth	Multiplier Factor for authors evaluation of the quality of the test series experimental method and calibration
		M2b2 indiv meas meth	Multiplier Factor for authors evaluation of the quality of the test series experimental method and calibration. Also, if calculated matrix diffusivity is greater than free water diffusivity, experimental problems are indicated and M2b2 = 0
		M2b test series meth	Test Series Method Factor: = M2b1 x M2b2
		M2 data anal meth	Data Reduction and Analysis Method Factor: = M2a x M2b
		M3 doc qual	Quality of the Documentation Factor
		M Total Multiplier	Total Multiplier: = M1 x M2 x M3
		Total Score	Total Score: = W x M
		Multiplier comments	Notes concerning multiplier factors
		Comments	General notes on the sample

E.3.0 REFERENCES

1. Stoller Navarro Joint Venture. 2007. *Phase I Contaminant Transport Parameters for the Groundwater Flow and Contaminant Transport Model of Corrective Action Unit 97: Yucca Flat/Climax Mine, Nevada Test Site, Nye County, Nevada,* Revision No. 0, S-N/99205--096. Las Vegas, NV.

2. Hershey, R.L., W. Howcroft, and P.W. Reimus. 2003. *Laboratory Experiments to Evaluate Diffusion of ^{14}C into Nevada Test Site Carbonate Aquifer Matrix*, Publication No. 45180. Las Vegas, NV: Desert Research Institute.

3. Walter, G.R. 1982. *Theoretical and Experimental Determination of Matrix Diffusion and Related Solute Transport Properties of Fractured Tuffs from the Nevada Test Site*, LA-9471-MS, UC-70. Los Alamos, NM: Los Alamos National Laboratory.

Appendix F

Matrix Sorption

F.1.0 INTRODUCTION

The matrix sorption distribution coefficient dataset, developed from the mechanistic model and mineralogy and groundwater chemistry data from the RMSM CAU, contains K_d data for each RMC. A total of 12 K_d estimates for the CC, 20 for the DMP, 8 for the SC, and 396 for the ZEOL RMCs are obtained for a total of 10 radionuclides (Am, Ca, Cs, Eu, Ni, Np, Pu, Sm, Sr, and U). The matrix sorption dataset is provided in the Appendix\F folder on the accompanying DVD.

F.2.0 DATASET SUMMARY

An Excel workbook file, RMSM_MatrixSorption.xls, contains one worksheet described in Table F.2-1.

Table F.2-1
RMSM_MatrixSorption.xls

Sheet	Sheet Description	Column Name	Column Description
RMSM_Kds	RMSM K_d values computed through mechanistic model calculations	SplitID	Unique sample identification number that links the K_d value to a specific XRD sample split
		RMC_Code	Reactive mineral category assigned to the XRD sample split, and thus to the K_d
		Water_Chemistry	Groundwater chemistry sample used for the K_d calculation
		Am Kd	Am K_d for the specified water chemistry and mineralogy sample, mL/g
		Ca41 Kd	Ca41 K_d for the specified water chemistry and mineralogy sample, mL/g
		Cs Kd	Cs K_d for the specified water chemistry and mineralogy sample, mL/g
		Eu Kd	Eu K_d for the specified water chemistry and mineralogy sample, mL/g
		Ni Kd	Ni K_d for the specified water chemistry and mineralogy sample, mL/g
		Np Kd	Np K_d for the specified water chemistry and mineralogy sample, mL/g
		Pu Kd	Pu K_d for the specified water chemistry and mineralogy sample, mL/g
		Sm Kd	Sm K_d for the specified water chemistry and mineralogy sample, mL/g
		Sr Kd	Sr K_d for the specified water chemistry and mineralogy sample, mL/g
		U Kd	U K_d for the specified water chemistry and mineralogy sample, mL/g

An Adobe pdf file, RMSM_Appendix_F.pdf, has the following figures:

Geochemistry Figures

- Box and whisker plots comparing laboratory data with the mechanistic model K_d values
- Box and whisker plots comparing the radionuclide K_d values in various RMCs

Appendix G

Geochemistry and Mineralogy

G.1.0 INTRODUCTION

The geochemistry dataset included in this appendix contains parameters from the GEOCHEM07.mdb database [1]. The compilation contains representative major (Ca^{2+}, Na^{+}, Mg^{2+}, K_{+}, Cl^{-}, SO_4^{2-}, HCO_3^{-}, and SiO_2) and minor (CO_3^{2-}, NO_3^{-}, Br^{-}, PO_4^{3-}, and F^{-}) solute data for groundwater representative of the wells and tunnels within the RMSM HFM boundaries. In addition, mineralogy samples were characterized through XRD analysis methods and reported within the Petrographic, Geochemical, and Geophysical (PGG) database [2]. The mineralogy compilation provides the relative mineral abundance present within the RMSM wells and tunnels. The geochemistry and mineralogy datasets are provided in the Appendix\G folder on the accompanying DVD.

G.2.0 DATASET SUMMARY

An Excel workbook file, RMSM_Geochemistry.xls, contains three worksheets described in Table G.2-1.

Table G.2-1
RMSM_Geochemistry.xls
(Page 1 of 3)

Sheet	Sheet Description	Column Name	Column Description
RMSM_Geochem_Dataset	RMSM geochemistry data for all samples	Master_ID	Location ID, indicating the completion status of the well at the time of sampling, as reported in the GEOCHEM07.mdb database
		SITE_ID	Sample location name as reported in the GEOCHEM07.mdb database
		SAMPLE_ID	Unique identifier for the sample in the GEOCHEM07.mdb database
		S_Date2	Sample collection date
		Br (mg/L)	Concentration of bromine, mg/L
		Ca (mg/L)	Concentration of calcium, mg/L
		Cl (mg/L)	Concentration of chlorine, mg/L
		CO3 (mg/L)	Concentration of carbonate, mg/L
		F (mg/L)	Concentration of florine, mg/L
		HCO3 (mg/L)	Concentration of bicarbonate ion, mg/L
		K (mg/L)	Concentration of potassium, mg/L
		Mg (mg/L)	Concentration of magnesium, mg/L
		Na (mg/L)	Concentration of sodium, mg/L
		NO3 (mg/L)	Concentration of nitrate ion, mg/L
		pH (pH units)	pH of the system in pH units

Table G.2-1
RMSM_Geochemistry.xls
(Page 2 of 3)

Sheet	Sheet Description	Column Name		Column Description
RMSM_Geochem_Dataset	RMSM geochemistry data for all samples	SiO2 (mg/L)		Concentration of silicon oxide, mg/L
		SO4 (mg/L)		Concentration of sulfate ion, mg/L
		Water Temperature (°C)		Groundwater temperature in °C
RMSM_Geochem_Averages	RMSM average geochemistry data for each well	Common Name		Common name of the well
		Number of Samples		Total number of samples in a given well
		FAI (m)	Top Elevation	Top elevation of the formation access interval, meters above sea level
			Bottom Elevation	Bottom elevation of the formation access interval, meters above sea level
		pH	Mean	Mean pH of the system in pH units
			SD	Standard deviation of the pH in pH units
		T (°C)	Mean	Mean groundwater temperature in °C
			SD	Standard deviation of the groundwater temperature in °C
		Ca (mg/L)	Mean	Mean concentration of calcium ion, mg/L
			SD	Standard deviation of calcium concentration, mg/L
		Mg (mg/L)	Mean	Mean concentration of magnesium, mg/L
			SD	Standard deviation of magnesium concentration, mg/L
		K (mg/L)	Mean	Mean concentration of potassium ion, mg/L
			SD	Standard deviation of potassium ion, concentration, mg/L
		Na (pH units)	Mean	Mean concentration of sodium ion, mg/L
			SD	Standard deviation of sodium concentration, mg/L
		Cl (mg/L)	Mean	Mean concentration of chlorine ion, mg/L
			SD	Standard deviation of chlorine concentration, mg/L
		CO3 (mg/L)	Mean	Mean concentration of carbonate ion, mg/L
			SD	Standard deviation of carbonate concentration, mg/L
		HCO3 (mg/L)	Mean	Mean concentration of bicarbonate ion, mg/L
			SD	Standard deviation of bicarbonate concentration, mg/L
		SO4 (mg/L)	Mean	Mean concentration of sulfate ion, mg/L
			SD	Standard deviation of sulfate concentration, mg/L

Table G.2-1
RMSM_Geochemistry.xls
(Page 3 of 3)

Sheet	Sheet Description	Column Name		Column Description
RMSM_Geochem_Averages	RMSM average geochemistry data for each well	Br (mg/L)	Mean	Mean concentration of bromine ion, mg/L
			SD	Standard deviation of bromine concentration, mg/L
		F (mg/L)	Mean	Mean concentration of fluorine ion, mg/L
			SD	Standard deviation of fluorine concentration, mg/L
		NO3 (mg/L)	Mean	Mean concentration of nitrate ion, mg/L
			SD	Standard deviation of nitrate ion, concentration, mg/L
		Charge Balance		Charge balance error of the average groundwater chemistries
RMSM_HSU_RMC	RMSM HSU and RMC well depth intervals	Common Name		Common name of the well
		Number of Samples		Total number of samples in a given well
		Top Elevation		Top elevation of the HSU/RMC interval, meters above sea level
		Bottom Elevation		Bottom elevation of the HSU/RMC interval, meters above sea level
		HSU		Hydrostratigraphic Unit
		RMC		Reactive Mineral Category

An Excel workbook file, RMSM_Mineralogy.xls, contains three worksheets described in Table G.2-2.

Table G.2-2
RMSM_Mineralogy.xls
(Page 1 of 4)

Sheet	Sheet Description	Column Name	Column Description
RMSM_Mineralogy_Dataset	RMSM mineralogy data for all samples	Location_Id	Identifier of a specific location on the surface or within a tunnel
		SampleId	Unique identifier of a sample taken from a specific location
		SplitId	Unique identifier of a split sample taken from a specific location
		Utm_e	Easting, in meters, for location in Zone 11 of UTM projection, 1927 NAD
		Utm_n	Northing, in meters, for location in Zone 11 of UTM projection, 1927 NAD
		SamType	This code translates into the type of sample analyzed by XRD (see Code Translations worksheet)
		SampleDepth_U	Uppermost bound for the sample depth, in meters beneath the ground surface

Table G.2-2
RMSM_Mineralogy.xls
(Page 2 of 4)

Sheet	Sheet Description	Column Name	Column Description
RMSM_Mineralogy_Dataset	RMSM mineralogy data for all samples	SampleDepth_L	Lowermost bound for the sample depth in meters beneath the surface
		SamElev_Av	Average sample elevation, in meters above mean sea level
		Altn	Alteration code (see Code Translations worksheet)
		mAlt	Minor alteration code (see Code Translations worksheet)
		Strat_Unit	Stratigraphic unit associated with the sample split (see Code Translations worksheet)
		Strat_T_Elev	Elevation, in meters, for the top of the stratigraphic unit assigned in the Strat Unit column
		Strat_B_Elev	Elevation, in meters, for the base of the stratigraphic unit assigned in the Strat Unit column
		Strat_Above	Stratigraphic unit above the sampled unit
		Strat_Below	Stratigraphic unit below the sampled unit
		LithCode	Lithology associated with the XRD split (see Code Translations worksheet)
		HSU_Code	The hydrostatrigraphic unit, as defined in the HSU TABLE
		RMC_Code	The reactive mineral category, as defined in the RMC TABLE
		AA	Adularia mineral percentage
		AB	Albite mineral percentage
		AM	Amphibole mineral percentage
		AN	Anorthite mineral percentage
		AP	Apatite mineral percentage
		BT	Biotite mineral percentage
		BY	Bytownite mineral percentage
		CC	Total calcite mineral percentage
		CH	Chlorite mineral percentage
		CR	Cristobalite mineral percentage
		CX	Clinopyroxene mineral percentage
		CY	Clay mineral percentage
		DM	Dolomite mineral percentage
		FL	Fluorite mineral percentage
		FS	The total felsic mineral percentage
		GL	Total glass percentage
		GY	Gypsum mineral percentage
		HL	Halite mineral percentage
		HM	Total hematite mineral percentage

Table G.2-2
RMSM_Mineralogy.xls
(Page 3 of 4)

Sheet	Sheet Description	Column Name	Column Description
RMSM_Mineralogy_Dataset	RMSM mineralogy data for all samples	HN	Hornblende mineral percentage
		KA	Kaolinite mineral percentage
		KF	Alkali feldspar percentage
		MI	Total mica mineral percentage
		MT	Magnetite mineral percentage
		MU	Muscovite percentage
		O1	Percentage of other minerals that are unspecified in the XRD results
		OL	Olivine mineral percentage
		OP	Opal mineral percentage
		OR	Orthoclase mineral percentage
		PL	Plagioclase mineral percentage
		PY	Pyrite mineral percentage
		QZ	Quartz mineral percentage
		SD	Sanidine mineral percentage
		SM	Total smectite mineral percentage
		TR	Tridymite mineral percentage
		WW	The total of all mineral abundances
		ZA	Analcime percentage
		ZC	Clinoptilolite percentage
		ZE	Total zeolite mineral percentage
		ZH	Chabazite percentage
		ZM	Mordenite percentage
		Comments	Comments that amplify information from an XRD analysis
		XRD_Meth	Code that indicates the XRD methodology used (see Code Translations worksheet)
		XRD_Analyst	The analyst that performed the XRD analysis
RMSM_Mineralogy_Summary	Summary of the RMSM mineralogy dataset. This includes only data where the total mineral abundance (WW) is at least 90%	SplitID	Unique identifier of a split sample taken from a specific location
		RMC_Code	The reactive mineral category, as defined in the RMC TABLE
		XRD_Method	Code that indicates the XRD methodology used (see Code Translations worksheet)
		CC	Total calcite mineral percentage
		HM	Total hematite mineral percentage
		MI	Total mica mineral percentage
		SM	Total smectite mineral percentage
		ZE	Total zeolite mineral percentage

Table G.2-2
RMSM_Mineralogy.xls
(Page 4 of 4)

Sheet	Sheet Description	Column Name	Column Description
Code Translations	Translates the lithology, alteration, stratigraphic, sample type and XRD method codes used in the RMSM_Mineralogy_Dataset and RMSM_Mineralogy_Summary worksheets	LithCode	Lithology Code
		Lith_Name	Lithology Name
		Alt_Code	Alteration Code
		Alt_Name	Alteration Name
		Strat_Unit	Stratigraphic Unit
		Strat_Name	Stratigraphic Name
		SAM_TYPE_CODE	Sample Type Code
		SAM_TYPE_NAME	Sample Type Name
		XRD_Code	XRD Code
		Description	Full description of XRD method

An Adobe pdf file, RMSM_Appendix_G.pdf, has the following figures:

Geochemistry Figures

- Piper diagram example
- Piper diagrams of the average water chemistry in each well
- Piper diagrams of every water sample for a given well
- Bar plots of the water chemistry of each well by HGU
- Stiff diagrams of the average water chemistry in each well

Mineralogy Figures

- Mineralogy histograms by HSU
- Mineralogy histograms by RMC
- Mineralogy histograms by RMC, comparing Full Spectrum (F) and Semiquantitative (S) XRD data

G.3.0 REFERENCES

1. Stoller-Navarro Joint Venture. 2007. *Comprehensive Water Quality Database for Groundwater in the Vicinity of the Nevada Test Site, Geochem07.mdb,* S-N/99205--059-Rev. 1. Las Vegas, NV.

2. Warren, R.G., D.A. Sawyer, F.M. Byers, Jr., and J.C. Cole. 2003. *A Petrographical, Geochemical and Geophysical Database and Framework for the Southwestern Nevada Volcanic Field.* Los Alamos National Laboratory Report LA-UR-03-1503.

Appendix H

Colloid-Facilitated Transport

H.1.0 INTRODUCTION

Dispersivity data compiled from literature are in the Appendix\H folder on the accompanying DVD.

H.2.0 DATASET SUMMARY

An Excel workbook file, RM_Colloid_Data.xls, contains six worksheets described in Table H.2-1.

Table H.2-1
M_Colloid_Data.xls
(Page 1 of 3)

Sheet	Sheet Description	Column Name	Column Description
Colloid Size, Concentration Data	Selected representative colloid sample analysis results	MASTER_ID	Draft Geochem_07 Database data ID
		SITE_ID	Site name
		Sample_ID	Sample identification number
		Sample_Date	Sample date
		50 - 60 nm	Number of colloids in bin (size range) per mL
		60 -70 nm	
		70 - 80 nm	
		80 -90 nm	
		90 - 100 nm	
		100 -110 nm	
		110 - 120 nm	
		120 - 130 nm	
		130 - 140 nm	
		140 - 150 nm	
		150 - 160 nm	
		160 - 170 nm	
		170 - 180 nm	
		180 - 190 nm	
		190 - 200 nm	
		>200 nm	
		200 - 220 nm	

Table H.2-1
M_Colloid_Data.xls
(Page 2 of 3)

Sheet	Sheet Description	Column Name	Column Description
Colloid Size, Concentration Data	Selected representative colloid sample analysis results	220 - 240 nm	Number of colloids in bin (size range) per mL
		240 - 260 nm	
		260 - 280 nm	
		280 - 300 nm	
		300 - 400 nm	
		400 - 500 nm	
		500 - 600 nm	
		600 - 800 nm	
		800 - 1000 nm	
		>1000 nm	
		Total, 50 - 200 nm	Total number of colloids in size range
		Total, 200 - 1000 nm	
		Total, 50 - >1000 nm	
Alluvium Transport	Alluvium transport parameter data	Laboratory Column Experiments	Experiment ID
		Residence Time (hours)	Residence time during experiment
		Filtration Rate Constant (kfilt, 1/hour)	Calculated filtration rate constant
		Retardation Factor (Rcol)	Calculated retardation factor
		Colloid (or Analog)	Colloid (or analog) used in experiment
		Source	Source of data
Volcanics Transport	Volcanics transport parameter data	Site Name	Site ID
		Mean Residence Time (hour)	Residence time during experiment
		Filtration Rate Constant (kfilt, 1/hour)	Calculated detachment rate constant
		Detachment Rate Constant (kdet, 1/cm-hour)	Calculated filtration rate constant
		Retardation Factor (Rcol)	Calculated retardation factor
		Colloid Type	Colloid (or analog) used in experiment
		Source	Source of data
Carbonate Transport	Carbonate transport parameter data	Site Name	Site ID
		Mean Residence Time (hour)	Residence time during experiment
		Filtration Rate Constant (kfilt, 1/hour)	Calculated detachment rate constant
		Detachment Rate Constant (kdet, 1/cm-hour)	Calculated filtration rate constant
		Retardation Factor (Rcol)	Calculated retardation factor
		Colloid Type	Colloid (or analog) used in experiment
		Source	Source of data

Table H.2-1
M_Colloid_Data.xls
(Page 3 of 3)

Sheet	Sheet Description	Column Name	Column Description
Sorption, Desorption	Sorption, desorption data	Colloid	Colloid used in experiment
		Actinide	Actinide used in experiment
		Batch kf (hr-1)	Batch kf determined
		Batch kb (hr-1)	Batch kb determined
		Fracture kf (hr-1)	Fracture kf determined
		Fracture kb (hr-1)	Fracture kb determined
Kd ranges	Kd data	Colloid	Colloid used in experiment
		Actinide	Actinide used in experiment
		Lower Kd Bound, mL/g	Lower Kd Bound determined
		Upper Kd Bound, mL/g	Upper Kd Bound determined
		UGTA Extension, mL/g	UGTA Extension determined

Appendix I

Comments from Nevada Division of Environmental Protection

(2 Pages)

NEVADA ENVIRONMENTAL RESTORATION PROJECT
DOCUMENT REVIEW SHEET

1. Document Title/Number: Phase I Contaminant Transport Parameters for the Groundwater Flow and Contaminant Transport Model of Corrective Action Unit 99; Rainier Mesa/Shoshone Mountain, Nye County, Nevada;	2. Document Date: May 2008
3. Revision Number: Rev. 0	4. Originator/Organization: John Hand (702) 295-1870
5. Responsible DOE NNSA/NSO Subproject Mgr.: Bill Wilborn	6. Date Comments Due: April 7, 2008
7. Review Criteria: Complete Document	
8. Reviewer/Organization Phone No.: State of Nevada; Mr. John J. Jones (702-486-2850)	9. Reviewer's Signature:
10. Comment Responses transmitted via email from NDEP to Bill Wilborn on April 8, 2008	**11. Comment Response Date: 4/30/08**

12. Comment Number/Location	13. Type[a]	14. Comment	15. Comment Response	16. Accept
1. Page 5-5, Section 5.2.1.3, second paragraph, first sentence		Please provide the value for gpm.	Text will be changed to (< 3.8 lpm [1 gpm]).	Accept, see comment response.
2. Page 6-5, Table 6-2		The SD for data sets RVA, SWA, TSA and Tuba Hydrostratigraphic Units (HSUs) are not appropriate because there are not sufficient data points to calculate a meaningful SD. Therefore, the given SDs, as well as the CVs, should be removed from the table for the specified HSUs.	Table will be revised.	Accept, see comment response.
3. Page 8-19, Figure 8-9		Please provide an R^2 value on Figure 8-9 (a) for the regression.	R^2 values for each regression are provided in Table 8-2. The table will be modified to identify the figure that each entry line refers to.	Accept, see comment response.
4. Page 9-3, Figure 9-1		The whiskerplot for GCU HGU is incomplete as the left whisker is missing. Also, the 5th and 95th percentiles are missing for both the CA and GCU HGUs. All information should be plotted.	At least nine distinct data points are required to compute the 5th, 10th, 90th and 95th percentiles. Also, there may be no data points beyond the 10th and 90th percentiles.	Accept, see comment response.
5. Page 13-16, first full paragraph, second sentence		Figure 13-3 on Page 3-17 is not a lognormal plot as indicated in the sentence on Page 13-6. This needs to be corrected.	The text states that Figure 13-3 shows the lognormal distributions, not that the plot is lognormal. The statement is correct.	Reject, see comment response.
6. Page 13-9,		Figure 13-5 appears to be exactly the same as Figure 13-3 on Page 13-7. Figure 13-5 is not a plot of filtration rate constants because the horizontal axis shows colloid diameter.	The correct figure will be included in the final report.	Accept, see comment response.
7. Page 13-13, Section 13.8, first paragraph, second sentence		The letter report referenced (Roback et al, 2007, LA-UR-07-6962) is not included on the DVD in the references section.	The reference will be included on the DVD.	Accept, see comment response.
8. Appendix B, Plots of porosity versus depth on the DVD		The line fits for the CA, CCU, GCU, TCU and WTA HSUs are not reasonable. Please explain the reason for conducting this analysis. Also, the R^2 should be presented on the plots.	To support the statement in section 6.4 that there was no apparent reduction in porosity with depth, the plots were included in the appendix. There is no reason to provide the R^2 values as the plots demonstrate no correlation.	Reject, see comment response

[a]Comment Types: M = Mandatory, S = Suggested.

12. Comment Number/Location	13. Type[a]	14. Comment	15. Comment Response	16. Accept
9. Appendix B, Porosity Histograms on the DVD		A legend for the colors on the porosity histograms should be included.	They grade from cold colors (purple) representing the mean to hot colors (red) at 2 Standard Deviations from the mean. Since the histograms are annotated with the Standard Deviations from the mean the coloring is only a visual guide and as such legends are not necessary.	Reject, see comment response
10. Appendix B, CDF Plots on the DVD		The HSUs for which data are presented should be indicated on the plots.	The figures will be revised.	Accept, see comment response.
11. Appendix B, Box and Whisker Plots on the DVD		The plots for the CA, GCU, LCA3, LCCU, MGCU, TMUVTA and TSA HSUs are not complete as there are missing whiskers and/or missing 5th and/or 95th percentiles. All plots should be completed.	See comment response #4.	Accept, see comment response.
12. Appendix F, Box Plots on the DVD		Why is there less information presented for the DMP Kds for Am, Eu, Ni, Np, Pu, Sm and U as compared to the ZEOL when the caption(s) state the same information should be presented for both DMP and ZEOL RMC's?	See comment response #4.	Accept, see comment response.
13. General Comment		The NDEP is aware that the current document has been developed under the newly revised RMSM CAU investigation plan to develop a model to indicate where best to collect new data, rather than develop a contaminant boundary. Due to the fact that the data for the RMSM CAU is sparse, large amounts of data must be transferred from other areas. With the transfer of data comes the requirement that quality assurance and quality control (QA/QC) procedures for the data transfer be strictly followed. The RMSM document does follow QA/QC procedures, but adherence to the procedures is ill-defined or weak at times. The NDEP understands that the lack of site-specific data and a change in modeling plans can produce some weak data links and confusing data control. Therefore, it is recommended that in future transfers of data, a stricter and clearer adherence to the procedures be followed.	Application of QA/QC procedures is documented in general in Table 3-1. Much of the data evaluated and analyzed in this document is maintained within large-scale databases for the entire project (all CAUs). Many aspects of data evaluation and qualification are handled in the creation and population of these databases, and details of QA/QC evaluations can be found in the documentation associated with those databases. Specific information for specialized QA/QC evaluations for this CAU is provided in the individual sections within discussions of data analysis. Different types of data used to characterize different parameters require different and often specialized considerations for QA/QC evaluations. The generalized prescriptions of the UGTA QAPP and the Data Transferability TBD cannot generally be applied in the simple form they have been described, and have been adapted. In some cases, an entirely different approach has been taken for specific, well-considered reasons. The QA/QC controlling documents cited allow for these variations. It must also be recognized that the data documents only present compilation and characterization-level analysis of data for model parameters in general. During modeling, more specialized parameter characterization may be developed to better relate the data to the specific model conceptualization, and more detailed QA/QC would be applied at the point that the required considerations are identified.	Accept, see comment response.

[a]Comment Types: M = Mandatory, S = Suggested.

Plate

Plate 1
Rainier Mesa/Shoshone Mountain Hydrostratigraphic Area and Corrective Action Sites

Explanation

- RMSM Wells
- RMSM Corrective Action Sites
- NTS Boundary
- NTS Area Boundaries
- RMSM Tunnels
- RMSM HFM Boundary
- PMOV HFM Boundary
- YFCM HFM Boundary
- UGTA CAUs

0 1.25 2.5 5 Miles

0 1.25 2.5 5 7.5 Kilometers

N

Coordinate System: UTM, NAD27, Zone 11, Meters

P:\UGTA Common\Rainier_Mesa_Shoshone_Mountain\GIS\HDD_and_TDD_Plate.mxd

DVD Containing This Document, Supporting Datasets, and Selected References

DISTRIBUTION

	Copies
Tim Murphy State of Nevada Nevada Division of Environmental Protection 2030 E. Flamingo Road, Suite 230 Las Vegas, NV 89119-0818	2 Hard copies w/DVDs
W.R. Wilborn Environmental Restoration Division U.S. Department of Energy National Nuclear Security Administration Nevada Site Office P.O. Box 98518, M/S 505 Las Vegas, NV 89193-8518	2 Hard copies w/DVDs
K.C. Thompson Environmental Restoration Division U.S. Department of Energy National Nuclear Security Administration Nevada Site Office P.O. Box 98518, M/S 505 Las Vegas, NV 89193-8518	1 DVD
Alicia Tauber Environmental Management Records U.S. Department of Energy National Nuclear Security Administration Nevada Site Office P.O. Box 98518, M/S 505 Las Vegas, NV 89193-8518	1 Hard copy w/DVD
U.S. Department of Energy National Nuclear Security Administration Nevada Site Office Technical Library P.O. Box 62 Oak Ridge, TN 37831-0062	1 DVD

	Copies
U.S. Department of Energy Office of Scientific and Technical Information P.O. Box 62 Oak Ridge, TN 37831-0062	1 DVD
Southern Nevada Public Reading Facility c/o Nuclear Testing Archive P.O. Box 98521, M/S NLV 400 Las Vegas, NV 89193-8521	2 DVDs
Manager, Northern Nevada FFACO Public Reading Facility ATTN: Kathryn Etcheverria c/o Nevada State Library & Archives 100 N Stewart Street Carson City, NV 89701-4285	2 DVDs
Celeste Sandoval Nye County Nuclear Waste Repository Project Office 1210 E. Basin Road, Suite #6 Pahrump, Nevada 89060	1 Hard copy w/DVD
Naomi Becker Los Alamos National Laboratory, M/S T003 Bikini Atoll Rd., SM30 Los Alamos, NM 87545	1 DVD
Gayle Pawloski Lawrence Livermore National Laboratory 7000 East Avenue, L-231 Livermore, CA 94550-9234	1 DVD
Mavrik Zavarin Lawrence Livermore National Laboratory 7000 East Avenue, L-231 Livermore, CA 94550-9234	1 DVD
Bonnie Thompson U.S. Geological Survey Water Resources Division 160 North Stephanie Street Henderson, NV 89074	1 DVD

	Copies
Chuck E. Russell Desert Research Institute 755 E. Flamingo Las Vegas, NV 89119	1 DVD
Ken Ortego National Security Technologies, LLC P.O. Box 98521, M/S NLV 082 Las Vegas, NV 89193-8521	1 DVD
Sam Marutzky Stoller-Navarro Joint Venture 7710 W. Cheyenne, Bldg. 3 Las Vegas, NV 89129	1 Hard copy w/DVD
Greg Ruskauff Stoller-Navarro Joint Venture 7710 W. Cheyenne, Bldg. 3 Las Vegas, NV 89129	1 DVD
Bill Fryer Stoller-Navarro Joint Venture 105 Technology Drive, Suite 190 Broomfield, CO 80021	1 DVD
John Hand Stoller-Navarro Joint Venture 7710 W. Cheyenne, Bldg. 3 Las Vegas, NV 89129	1 DVD
Nathan Bryant Stoller-Navarro Joint Venture 7710 W. Cheyenne, Bldg. 3 Las Vegas, NV 89129	1 DVD
Stoller-Navarro Joint Venture Central Files 7710 W. Cheyenne, Bldg. 3 Las Vegas, NV 89129	1 Hard copy w/DVD